Spring 1-1-2011

Measurement of Atmospheric Volatile Organic Compounds from Urban, Industrial and Biogenic Sources by Proton-Transfer Ion Trap Mass Spectrometry

Daniel M. Bon
University of Colorado at Boulder, dan3db@gmail.com

MEASUREMENT OF ATMOSPHERIC VOLATILE ORGANIC COMPOUNDS FROM URBAN, INDUSTRIAL AND BIOGENIC SOURCES BY PROTON-TRANSFER ION TRAP MASS SPECTROMETRY

by

DANIEL M. BON

B.A., Carleton College, 1990

M.S., Western Washington University, 1999

A thesis submitted to the

Faculty of the Graduate School of the

University of Colorado in partial fulfillment

of the requirement for the degree of

Doctor of Philosophy

Department of Chemistry and Biochemistry

2011

This thesis entitled:
Measurement of Atmospheric Volatile Organic Compounds from Urban, Industrial and Biogenic Sources by Proton-Transfer Ion Trap Mass Spectrometry

written by Daniel M. Bon
has been approved for the Department of Chemistry and Biochemistry

_____
Dr. Joost de Gouw

_____
Dr. Ray Fall

*Date*_____

The final copy of this thesis has been examined by the signatories, and we find that both the content and the form meet acceptable presentation standards of scholarly work in the above mentioned discipline.

Bon, Daniel M., (Ph.D., Chemistry)
Measurement of Atmospheric Volatile Organic Compounds from Urban, Industrial and Biogenic Sources by Proton-Transfer Ion Trap Mass Spectrometry

Thesis directed by Dr. Joost de Gouw

Abstract

Volatile organic compounds (VOCs) are released into the atmosphere through a variety of processes. An understanding of the chemistry of VOCs is critical because of their role in air pollution and climate, but their diversity challenges even modern analytical methods. In this work, I present VOC measurements made by Proton-Transfer-Reaction Ion Trap Mass Spectrometry (PIT-MS) in air impacted by different emission sources: biogenic, urban, industrial and biomass burning. The main goal of these studies was to use the PIT-MS instrument's high time resolution, full mass scan capability and capacity for collision-induced dissociation (CID) to quantify complex VOC mixtures.

CID was successfully used to identify VOCs and to separate isomeric and isobaric VOCs in biogenic emissions and biomass burning plumes. Comparison of PIT-MS results with other VOC measurement methods, the use of gas chromatography with PIT-MS and CID were all used to characterize the specificity of methods that use proton transfer by H_3O^+ ions in all four field environments. The results revealed many limitations to common PTR signal attributions.

Results from these studies demonstrate the usefulness of the PIT-MS instrument to characterize complex VOC mixtures. In Mexico City, three major sources of VOC emissions were identified: vehicular traffic, liquid propane gas

(LPG) usage and chemical formation. VOC emissions relative to carbon monoxide (CO) are about a factor of 2 larger in Mexico City than in the United States. In Houston, TX, PIT-MS measurements were used to evaluate an industrial emissions inventory. The complexity of measured VOCs in industrial plumes is significantly larger than described in the inventory and for many VOCs, emission fluxes inferred from the measurements are significantly higher than those listed in the inventory. Results from these campaigns could inform future inventories and help inform policy decisions.

Taken together, PIT-MS instrument is shown to be useful in providing routine, online VOC measurements with clear scientific merit. At the same time, the PIT-MS is successfully used to probe and extend the analytical abilities of proton-transfer-reaction based instruments for atmospheric measurements.

DEDICATION

To my daughter, Emily Welsh-Bon and my parents, David and Carol Bon.

ACKNOWLEDGEMENTS

This work could not have been completed without the help of an army of people who offered their support along the way. I am especially grateful to my parents for all of their love and support throughout my graduate studies. I am also eternally grateful to my daughter Emily who, thankfully, could not comprehend all the recent demands on my time and energy, but put up with them anyway. Emily, your understanding, patience and tolerance were way beyond your years. Your ebullience and energy kept me going in the toughest of spots. Congratulations to you on getting your kindergarten diploma the same week I defended this dissertation.

I am also grateful to the countless friends in California, Colorado and elsewhere who supported and encouraged me over the years. There are far too many to list, but I could not have finished without their help. Special thanks to the legion of folks who helped ease my child-rearing responsibilities and who provided much needed sanity breaks. Special thanks to Kelly and Joe Stroker, Rebecca Perry, and Elizabeth Wright who provided friendship to both Emily and me and who generously opened their homes to us on so many occasions.

I would also like to thank Troy Thornberry, Paola Massoli and Jessica Gilman who offered friendship, professional encouragement and served as sounding boards for ideas. You all inspired me and pointed me toward the light at the end of the tunnel: life after graduate school.

I am indebted to both Ray Fall and Joost de Gouw for providing funding, advice and encouragement throughout my graduate studies. Thanks to you both for

your patience, constructive feedback and ideas and for all the time you spent reading my work and listening to my ideas. I am particularly grateful to Joost for the weekly meetings and the countless hours he made available in his busy schedule to help me navigate the final year of my graduate studies.

None of the work presented here could have been done without supporting atmospheric measurements provided by colleagues and collaborators. I would like to thank everyone at the Chemical Sciences Division at the NOAA Earth System Research Laboratory in Boulder. I would also like to thank Carsten Warneke the builder of the PIT-MS instrument for his contributions to my education. Thanks also to the other members of my dissertation committee for their support.

This work would not have been possible without generous funding from the US EPA STAR program, NOAA and the National Science Foundation. This work was financially supported by the National Science Foundation under grant ATM-0516610. This publication was partially developed under a STAR Research Assistance Agreement No. FP-9163901-0 awarded by the U.S. Environmental Protection Agency. It has not been formally reviewed by the EPA. The views expressed in this dissertation are solely those of its author. The EPA does not endorse any products or commercial services mentioned in this publication.

CONTENTS

TABLES

FIGURES

CHAPTER I

VOLATILE ORGANIC COMPOUNDS IN THE EARTH'S ATMOSPHERE

1. Introduction

Volatile organic compounds (VOCs) are released into the atmosphere by a variety of natural and anthropogenic processes and these volatiles are of great interest to atmospheric scientists. Recent estimates of the global emission of VOCs into the atmosphere range from about 1200 to 1600 TgC yr^{-1} (Goldstein and Galbally, 2007;Olivier et al., 2005;Reimann and Lewis, 2007;Williams and Koppmann, 2007;Yokelson et al., 2008). This is a very large amount of organic carbon, much of which is chemically reactive. Major sources of atmospheric VOCs include vegetative emission, biomass burning, and the use of fossil fuels. Other sources of atmospheric VOCs include the ocean, soils, natural hydrocarbon seeps, industry, and solvent usage, among others. VOC diversity is staggering—thousands of different organic compounds have been observed in the atmosphere (Williams and Koppmann, 2007). Measuring and speciating this mixture has been and remains a challenge to analytical methods.

2. Sources of Atmospheric VOCs

On a global scale, VOC emissions are dominated by biogenic sources. Isoprene, a highly reactive 5-carbon diene, is emitted by a wide variety of plants. This single compound is thought to account for about 65% of biogenic emissions

and 40% of total VOC emissions (Guenther et al., 1995;Guenther et al., 2006;Williams and Koppmann, 2007). Plants also emit large quantities of VOCs such as alcohols (e.g. methanol and ethanol), ketones (e.g. acetone), and a variety of terpenoid compounds assembled biochemically from isoprene units, among others. Biogenic VOCs are emitted from both natural vegetation and agricultural crops. A recent review provides a thorough exploration of the variety of biogenic VOCs emitted, their biochemical origins and functions and their atmospheric fates (Steiner and Goldstein, 2007).

A second major source of atmospheric VOCs on a global scale is emission from biomass burning, both natural and as the result of human activity. Biomass burning is thought to account for about 10% of global VOC emissions (Reimann and Lewis, 2007). However, recent estimates suggest the contribution from biomass burning could be much larger, up to 500 TgC/year (Yokelson et al., 2008). Smoke from wildfires and agricultural burning can have dramatic effects on human health and air quality on local and regional scales. The intermittent nature of fires, their variable intensity, and the diversity of fuels burned complicate our understanding of their effects at all scales from local to global. VOC emission factors for biomass burning have been summarized in the literature(Andreae and Merlet, 2001). More recent work in a laboratory setting focuses on refining VOC emission factors by vegetation type and geographic region (McMeeking et al., 2009;Warneke et al., 2011).

Anthropogenic VOC emissions are often dominant at local and regional scales near areas of high population density. All stages of fossil fuel usage, from drilling,

refining and combustion, contribute significantly to anthropogenic emissions (Reimann and Lewis, 2007;Olivier et al., 2005). Vehicular traffic has been the target of emission controls for both diesel and gasoline engines but remains a major source of VOCs in cities. Other major sources of VOCs in cities are fuel evaporation (gasoline and liquid propane gas), industrial facilities and refineries. Smaller scale and more variable VOC emissions are observed from painting, road construction, and dry cleaning in urban settings (Reimann and Lewis, 2007).

3. Atmospheric Chemistry of Volatile Organic Compounds

VOCs are removed from the atmosphere through a variety of physical and chemical mechanisms including oxidation, photolysis, wet and dry deposition and the condensation of VOCs onto particles. Chemical removal (oxidation) of most atmospheric VOCs is driven primarily by the hydroxyl radical (OH•), which is formed photochemically. The atmospheric residence time of VOCs is often expressed as a function of their chemical lifetimes with respect to the OH radical. Other oxidants such as the nitrate and chlorine radicals, and ozone can be important local sinks for some VOCs under the right conditions.

Important products of the atmospheric oxidation of volatile hydrocarbons include alkyl nitrates, peroxy acetyl nitrates (PANs) and oxygenated VOCs. Lower molecular weight hydrocarbons can be formed when carbon-carbon bonds are broken by, for example, the oxidation of unsaturated VOCs by ozone (Finlayson-Pitts and Pitts, 2000). Oxidized VOCs containing one or more oxygen atoms are generally more polar and less volatile than their parent compounds and can

contribute to the formation of secondary organic aerosol (Goldstein and Galbally, 2007). The contribution of atmospheric VOCs to aerosol formation is a topic of great current interest, and is further discussed below.

4. Direct and Indirect Health Effects of VOCs

The sources and sinks of atmospheric VOCs and their chemistry are important because of the role VOCs play in air pollution and climate. Air pollution is of growing international concern and is estimated to contribute to approximately 2 million premature deaths per year worldwide (World Health Organization, 2008). As primary pollutants, many VOCs are hazardous and are regulated in both indoor and outdoor air in the United States (Finlayson-Pitts and Pitts, 2000). The toxicity of some VOCs has been studied (Finlayson-Pitts, 1997), though our knowledge of the cumulative health effects and toxicology of VOCs exposure is limited by the huge variety of VOCs emitted.

In and around heavily populated urban areas, VOCs released as a result of fossil fuel use are significant contributors to the formation of photochemical smog and ground-level ozone. Ozone, formed by photochemical reactions involving VOCs and nitrogen oxides (NO_x), has direct adverse effects on human health and can also damage both agricultural crops and natural vegetation (Finlayson-Pitts, 1997;Krupa et al., 2001).

Urban VOCs can also contribute to formation of particulate pollution which can have adverse affects on human health (Brunekreef and Forsberg, 2005;van Zelm et al., 2008). Mechanisms of secondary organic aerosol (SOA) formation from urban

VOCs are not well understood and current atmospheric models appear to underestimate SOA production from anthropogenic sources by an order of magnitude (de Gouw et al., 2005;Hallquist et al., 2009;Volkamer et al., 2006;de Gouw and Jimenez, 2009).

The effects of anthropogenic VOC emissions are not limited to urban areas. Emissions from cities can be transported downwind to rural areas and secondary pollutants continue to form during transport. Thus, the health effects of urban particulate pollution are also not confined to city limits. The effects of ozone produced in urban areas on agricultural crops and forests are observed at a considerable downwind distance from metropolitan areas.

In addition, anthropogenic VOCs have an indirect effect on climate through their contribution to an increase in particulate pollution and tropospheric ozone, an important greenhouse gas (Collins et al., 2002;Shindell et al., 2009;Solomon et al., 2007). Organic aerosols scatter radiation and have a cooling effect on climate. There is also considerable evidence of intercontinental transport of ozone and organic aerosol from, for example, Asia to North America.

5. Measurement of Atmospheric VOCs

Atmospheric VOCs are measured through a variety of analytical techniques including gas chromatography, mass spectrometry and through the use of a variety of optical methods. Air samples can be collected in flasks or in adsorbent cartridges and analyzed for VOCs in the laboratory or VOCs can be measured directly by

instruments designed specifically for continuous operation at a remote ground site, on ships or research aircraft.

For the purposes of this work, VOCs were quantified using field-portable gas chromatographs (GC) and mass spectrometers (MS). Gas chromatography systems with flame-ionization detectors (GC-FID) were used for measurements of light alkanes and alkenes. GC systems were also coupled with hard (electron impact) and soft (proton-transfer reaction) ionization methods and detected using mass spectrometry (GC-MS). These methods will be described in more detail in chapters 2 and 3.

The focus of the studies presented here is on the characterization and use of a custom-built field portable proton-transfer reaction ion trap mass spectrometer (PIT-MS) developed at NOAA for the quantification of VOCs. To this end, field measurements were made in a wide range of environments with vastly different VOC compositions. In 2005 and 2007, biogenic VOCs were measured near the Blodgett forest research station in the foothills of the Sierra Nevada Mountains of northern California. In 2006, VOC measurements were made in both in a densely populated urban environment (Mexico City) and in a highly industrialized part of Houston, Texas. Laboratory-based VOC measurements were made both at the NOAA facility in Boulder, Colorado and at the U.S. Forest Service's Fire Sciences Laboratory in Missoula, Montana.

This thesis presents the potential of PIT-MS methodology to address the on-line analysis of complex VOC mixtures in air samples in both remote and urban settings.

CHAPTER 2

PROTON-TRANSFER-REACTION ION TRAP MASS SPECTROMETRY

1. Introduction

The term chemical ionization mass spectrometry (CIMS) describes the use of a variety of ion-molecule reactions to achieve highly selective and efficient ionization of target compounds. CIMS techniques have been widely employed recently for the sensitive and fast detection (1 Hz or faster) of atmospheric trace gases at ambient concentrations down to a few parts per trillion by volume (pptv) and below (Huey, 2007). CIMS instruments use ionized atoms or molecules (e.g. CH_5^+, SF_5^-, I^-, H_3O^+) as reagent ions to ionize target molecules and the subsequent detection of the product ions by mass spectrometry. CIMS instruments have been used to measure a variety of gas-phase compounds including inorganic and organic acids, ammonia and even atmospheric radicals (Green et al., 2006;Huey, 2007;Veres et al., 2008;Field, 1990;St Clair et al., 2010).

2. The Proton-Transfer Reaction (PTR) ionization method

One type of CIMS instrument that has been widely used to measure VOCs is the proton-transfer reaction mass spectrometry (PTR-MS) instrument (Ionicon Analytik). The PTR-MS instrument uses a specific chemical ionization method for VOCs that enables the detection of many atmospherically important VOCs with sampling rates similar to those in other CIMS instruments. Commercial PTR-MS

instruments are typically equipped with quadrupole mass spectrometers for detection of protonated product ions, although recent instruments operate with time of flight (TOF) mass spectrometers as the detector (Lindinger et al., 1998;Graus et al., 2010).

The proton-transfer reaction (PTR) ionization method uses hydronium reagent ions (H_3O^+) produced in a hollow cathode electrical discharge ion source to selectively ionize VOCs. VOCs with a proton affinity greater than that of water (691 kJ/mol) can be ionized by proton-transfer from H_3O^+:

$$H_3O^+ + R \longleftrightarrow RH^+ + H_2O \quad \text{(equation 2.1)}$$

Where R is the VOC. The amount of VOC in an air sample that is ionized by proton-transfer is given by:

$$\left[RH^+\right] \approx \left[H_3O^+\right] k \left[R\right] \Delta t \qquad \text{(equation 2.2)}$$

where k is reaction rate constant for equation 2.1 and Δt is the residence time in the drift reactor (de Gouw and Warneke, 2007), discussed in more detail below. For many common atmospheric VOCs, reaction (1) occurs at the thermal collision rate (k_c) (Lindinger et al., 1998;Warneke et al., 2001;de Gouw and Warneke, 2007). Under normal operating conditions, the rate of the reverse reaction (1) is negligible.

VOCs that can undergo proton transfer with hydronium include most oxygenates and aromatics, some unsaturated hydrocarbons (e.g. isoprene) and

nitrogen-containing hydrocarbons. Ionization is "soft", i.e. in many cases, the parent VOC ion is observed with minimal fragmentation. Collisional ionization of VOCs occurs in a drift tube reactor assembly to avoid extensive clustering of hydronium and product ions with water molecules. At the end of the drift tube, ions are extracted into the mass spectrometer by way of an electric field established by a series of electrostatic lenses.

The ion chemistry involved and its application to the detection of atmospheric VOCs is discussed in greater detail elsewhere (de Gouw and Warneke, 2007). The method and its various applications is reviewed by Blake et al. (Blake et al., 2009).

3. Ion Source and Drift Tube

Schematics of the hollow cathode ion source used in PTR-MS are shown in Figures 2.1 and 2.2. A constant flow of water vapor in the range of 5-10 cm^3 min^{-1} (sccm) is introduced into the source where it is ionized by electrical discharge. The source is very efficient at producing hydronium (H_3O^+) ions, which are extracted into an intermediate chamber, prior to injection into the drift tube reactor (Figure 1). The hydronium ion (H_3O^+) and its water clusters (H_3O^+)•(H_20)$_n$ (n=1, 2, 3) generated in the ion source and drift tube are referred to collectively as primary, or reagent, ions, while protonated VOCs are referred to as product ions.

Sample air is pumped continuously through the drift tube, where ions are exposed to an electric field. The combined effect of the ion acceleration between

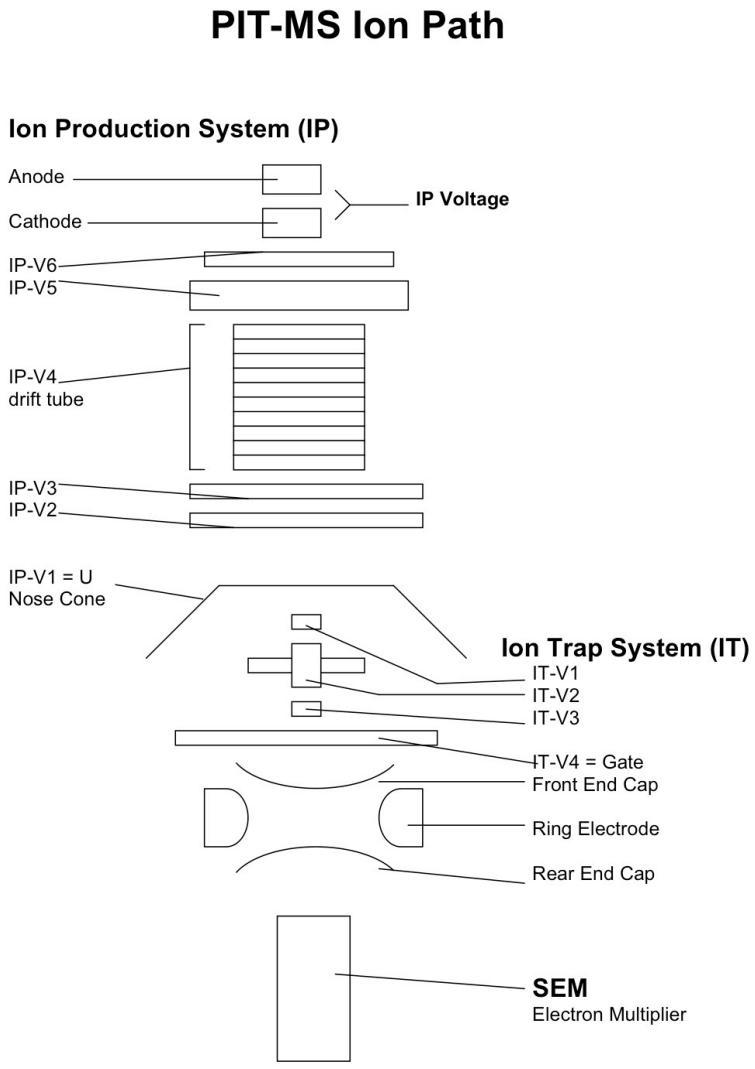

Figure 2.1. PIT-MS ion path diagram showing ion production and extraction elements (IP) and ion trap elements (IT). This instrument configuration was used between 2004 and 2006. After 2006 a resistive glass drift tube was used for the drift tube and IP-V2 and IP-V3 elements were removed.

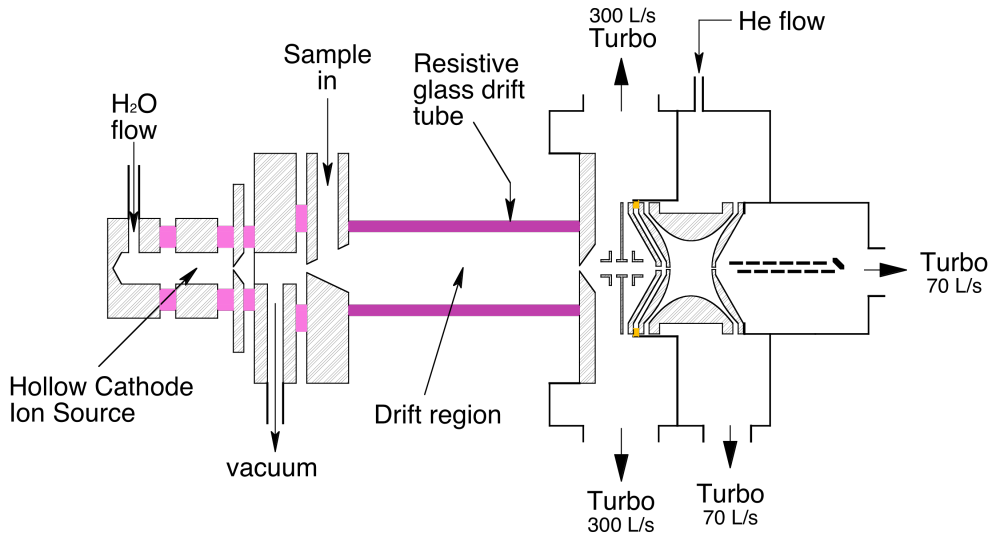

Figure 2.2. PIT-MS instrument schematic showing gas inlet and pumping schemes as well as the ion production, extraction and trapping elements. The configuration pictured here shows the instrument as it was configured from 2007 on with the resistive glass drift tube.

collisions and the loss of energy during collisions, leads to an average drift velocity of ~1000 m/s. Primary ions traveling through the PTR-MS drift tube react by proton transfer with VOCs in the sample stream.

As an air sample flows through the drift tube region of the PIT-MS instrument, VOCs in the stream are ionized by H_3O^+ ions and efficiently transported downstream by a voltage applied across the drift tube. Ions are extracted through an orifice at the end of the drift tube and into the ion trap mass spectrometer. Non-ionized sample air and excess water also pass through the orifice and are pumped away by turbo-molecular pumps (Varian, Inc.).

In equation 2.2 above, we saw that the efficiency of ionization of VOCs depends on the reaction rate constant, the concentration of primary ions and VOCs in the drift tube and on the drift tube residence time which is given by:

$$\Delta t = \frac{L}{\mu_0 N_0}(E/N)^{-1} \qquad (2.3)$$

where L is the length of the drift tube reactor, E is the electrical field, μ_0 is the reduced ion mobility, N is number density of the gas in the drift tube and N_0 is gas number density at STP (1 atm, 273.15K) (de Gouw and Warneke, 2007). Instrument sensitivity is defined in PTR-MS as the signal, RH^+ from 1ppbv of a VOC normalized to 10^6 H_3O^+ sec^{-1} (ncps/ppbv).

The potential, E, applied along the drift tube is set so that a value of E/N (electrical field/number density) of ~120 Td (1 Td= $1x10^{-17}$ V cm^2) is maintained in

the drift region. At E/N values of ~120 Td, a balance is achieved between residence time and ion kinetic energy, which sharply reduces hydronium•water cluster ($(H_3O^+)•(H_20)_n$) formation, greatly simplifying the interpretation of mass spectra. The effects of E/N settings on relative abundance of hydronium ion•water clusters in the drift region is described in more detail elsewhere (de Gouw and Warneke, 2007). Certain VOCs (e.g. benzene, toluene) react differently with the hydronium and hydronium ion•water clusters, instrument sensitivity to these compounds is affected slightly by the E/N value used (Warneke et al., 2001).

4. The Proton-Transfer Reaction Ion trap Mass Spectrometer

NOAA scientists have used Proton-Transfer Reaction Ion Trap Mass Spectrometry (PIT-MS) to develop a custom-built, field-portable chemical ionization mass spectrometer designed for high time resolution quantification of atmospheric VOCs. The PIT-MS instrument uses a hydronium (H_3O^+) ion source and drift-tube reactor similar to that of a commercial PTR-MS instrument but is equipped with an ion trap mass spectrometer instead of a quadrupole mass filter (Warneke et al., 2005a;Warneke et al., 2005b). The advantages of PIT-MS over PTR-MS are discussed below.

Two different PIT-MS drift tube configurations were used to collect the data presented in this thesis. In the first design, the drift tube was constructed of steel rings separated by Teflon spacers (Figure 2.1). The steel rings are connected by resistors so that a uniform potential can be applied across the drift tube. In the second configuration (Figure 2.2), the steel and Teflon rings are replaced by a

resistive glass tube (Burle Industries, Inc.). This second design was developed for an aerosol PTR-ion trap instrument described elsewhere (Thornberry et al., 2009) and effectively minimized the surfaces inside the drift tube to reduce memory effects. Other improvements that were implemented in the later instrument involved a re-design of the different pumping in the instrument and a reduction in the number of orifices ions have to pass through in order to improve instrument sensitivity. Modifications made to the PIT-MS instrument to improve sensitivity are detailed elsewhere (Warneke et al., 2011).

4.1 Advantages of PIT-MS

An ion trap mass spectrometer has several potential advantages over the quadrupole mass spectrometer used in the commercial PTR-MS instrument. The first advantage is an increased duty cycle. Unlike a quadrupole mass filter, which permits ions of one single mass at a time and discards all other ions, an ion trap mass spectrometer collects ions regardless of their mass and can produce a full range mass scan in a short amount of time, much shorter than the time to accumulate ions. (Warneke et al., 2005a;Prazeller et al., 2003). The PIT-MS instrument produces a mass spectrum (m/z 30-220) each trapping cycle (0.5 – 10 s). In contrast, a quadrupole PTR-MS instrument typically scans 10-15 masses with a dwell time of about 1 s per mass. The PTR-MS instrument is about an order of magnitude more sensitive than the PIT-MS at a given m/z for a 1 s measurement

(Warneke et al., 2011). However, this advantage is lost if a full mass scan is required.

Another advantage of the PIT-MS instrument is that the detection efficiency of an ion trap increases at higher masses. In comparison, the quadrupole mass filter in the PTR-MS instrument has its highest detection efficiency at about 70 amu (Warneke et al., 2011). This advantage is potentially important for the measurement of atmospheric VOCs where lower volatility, higher mass compounds may play a role in the formation of secondary organic aerosol (Goldstein and Galbally, 2007;de Gouw et al., 2011;de Gouw and Jimenez, 2009).

The PIT-MS instrument is also capable of collision-induced dissociation (CID) measurements. In CID, ions of a single m/z ratio are selective trapped and then accelerated inside the ion trap, causing them to fragment in distinctive patterns based on molecular structure. CID has the potential to resolve isobaric compounds (compounds with the same molecular mass, but different structures) at least in some cases. The utility of CID in resolving the isobaric problem in PTR-MS was first reported by Lindinger (1998). The ability of an ion trap PTR instrument to perform CID has been demonstrated in the first ion trap instrument equipped with a proton-transfer source and drift tube (Prazeller et al., 2003) and also in a laboratory setting using the NOAA PIT-MS instrument (Warneke et al., 2005a). More recently a linear ion trap has been shown to resolve, in a field setting, two important oxidation products of isoprene (Mielke et al., 2010). The CID capability of the PIT-MS

instrument is described in more detail below. The use of PIT-MS for CID for biogenic field measurements is discussed in Chapter 6.

4.2 PIT-MS Gas Inlet

The gas inlet of the PIT-MS (Figure 2.3) is constructed of 1/8 inch Teflon tubing to minimize surface adherence of VOCs. A diaphragm pump pulls a continuous flow of ambient air through the gas inlet at a typical flow rate of ~150 sccm. Flow rates are controlled manually by way of a Teflon needle restriction valve. To provide instrumental background measurements, the sample can be diverted through a platinum catalyst maintained at 350°C to effectively remove VOCs from the sample flow (Warneke et al., 2003). Gas from a calibration standard can be introduced downstream of the catalytic converter to provide instrument calibrations. A sample PIT-MS data collection sequence is shown in Figure 2.5. The figure shows examples of the primary ion, background (catalyst), ambient and calibration measurements needed in the field for VOC measurement using the PIT-MS instrument.

The PIT-MS inlet pressure is held constant (~80 millibar) by a pressure controller. Sample flow in excess of about ~20 sccm is diverted through the pressure controller, metered and vented through the diaphragm pump. This set-up controls the drift tube pressure to 2.4 mbar within a few percent. Longer term drifts in the drift tube pressure are adjusted for automatically by the control software.

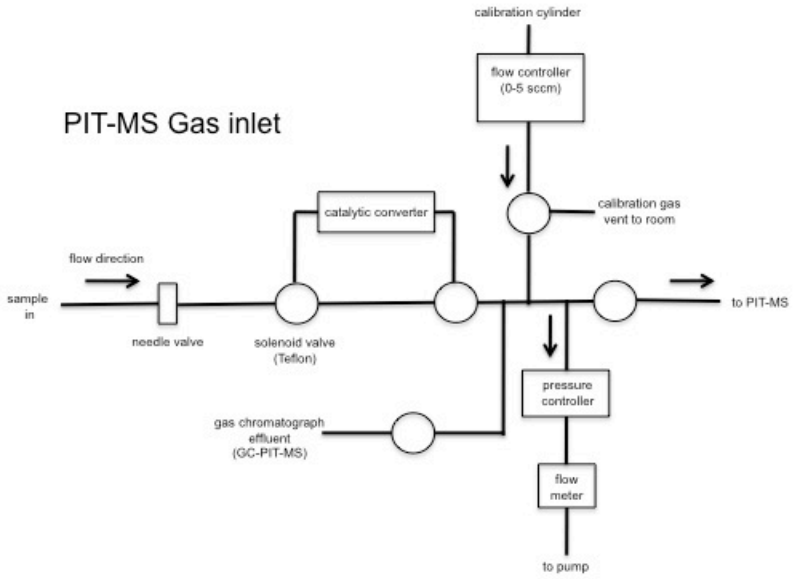

Figure 2.3. Schematic diagram of the gas inlet system used with the PIT-MS instrument. The scheme also shows how the sample flow can be diverted to the catalytic converter.

4.3 Ion Trap Mass Spectrometer

Ions exiting the drift tube are collected in a quadrupole ion trap (IT). A detailed description of the ion trap mass spectrometer used in the PIT-MS instrument can be found elsewhere (Warneke et al., 2005a;Lovejoy and Wilson, 1998;Curtius et al., 2001) and only a brief summary will be presented here.

After ions are extracted from the drift tube reactor, four electrostatic ion lenses guide the ions into the ion trap (Figure 1, IT-V1 to IT-V4). The fourth lens, the "gate", is used to allow or block ions from entering the IT. A pressure of 1×10^{-3} mbar is maintained inside the trap by adding helium. The helium is used for collisional cooling of ions in the trap and also provides a buffer gas when the ion trap is used in collision induced dissociation (CID) mode. The interior of the ion trap has hyperbolic geometry with a radius (r_o) of 1 cm. This geometry is achieved using a combination of a circular ring electrode and two end cap electrodes. A radio frequency (f = 1 MHz) power supply (RM Jordan Co.) is used to generate the voltage applied to the ring electrode to produce the field needed for ion trapping. A National Instruments PCI board is used to generate the sinusoidal and filtered noise field (FNF) waveforms applied to the end caps and to control the amplitude of the RF voltage applied to the ring electrode. The filtered noise field (FNF) is applied to the end cap electrodes to allow selective exclusion of ions by mass to charge ratio (m/z). Furthermore, a sinusoidal waveform (AC) voltage (f=0.5-1 kHz) is applied to the end caps to allow axial modulation of ions in the trap to improve mass resolution.

Figure 2.4 shows a typical control sequence used in the ion trap for the gate (ions on/off), RF and FNF voltages. A positive voltage applied to an electrostatic lens (gate) allows ions to enter the ion trap, while a negative voltage on the same lens stops ion trapping. Ions enter the trap through an orifice in the front endcap and are trapped by the RF field established inside the ion trap. A FNF voltage applied to the end cap electrodes during filling (trapping) is used to exclude ions below or above a certain m/z threshold. For example, during product ion scans, primary ions are excluded from the ion trap by the FNF waveform voltage to avoid space charge effects observed when the ion trap is over-filled.

Regular primary ion scans are needed to correct for changes in the output of the ion source, which typically occur over the period of several hours. Equation 2.2 shows that VOC signals are dependent on the source output and must be normalized to primary ion counts in order to accurately quantify VOCs. Due to the much higher abundance of primary ions, they are trapped separately using much shorter trapping times (1-10 ms) than product ions. Product ions are typically trapped for 0.1-10 s depending on ambient VOC concentrations.

After trapping, a delay occurs where ions can optionally be held for collision-induced dissociation (Figure 2.4). CID is described in more detail below. After the delay period, ions are ejected through an orifice in the rear end cap. Ejection occurs when the RF amplitude on the ring electrode is ramped and an axial modulation is applied to the end caps to increase the energy of the ions in the trap (Figure 2.4). Lower mass ions have larger amplitudes of oscillation and are ejected at lower RF

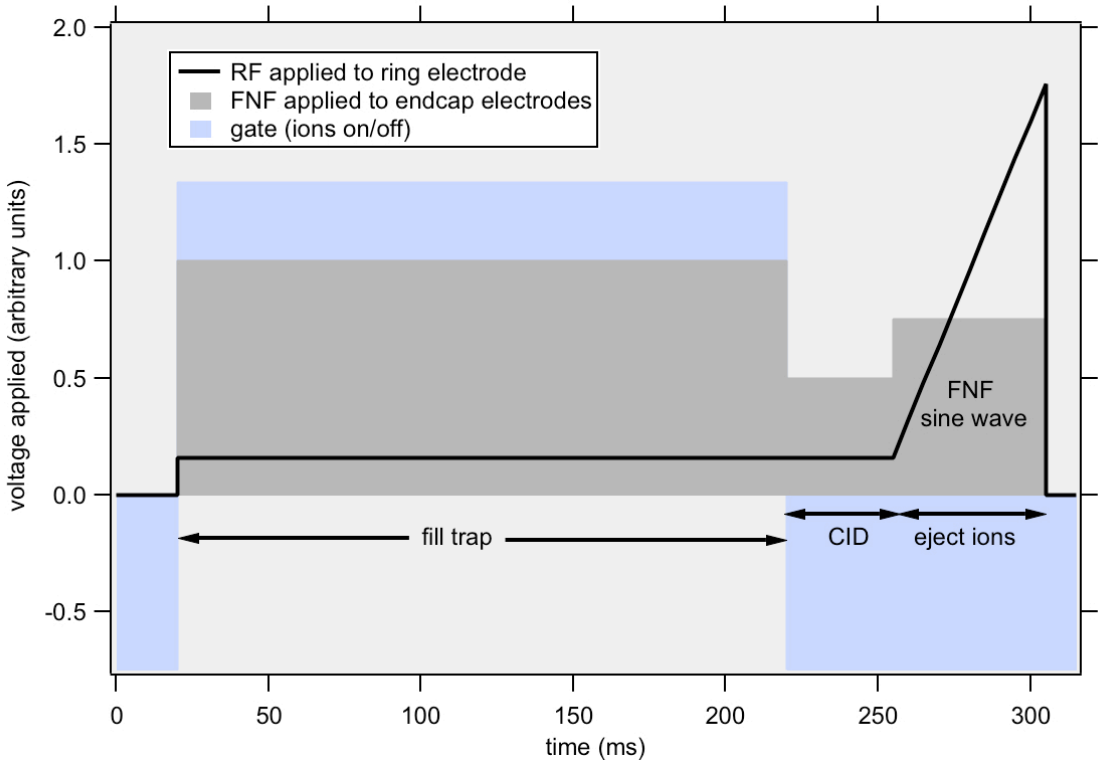

Figure 2.4. Typical ion trap voltage control sequence for the PIT-MS instrument showing the time periods using for ion trapping, CID (optional), and ion ejection. Modified from Warneke et al. (2005a).

amplitudes. A secondary electron multiplier (SEM) is used to detect ions after they are ejected from the ion trap.

4.4 PIT-MS Modes of operation

The PIT-MS instrument has two functionally distinct, mutually exclusive modes. The normal (mass spectral) mode and the CID mode. The normal mode is used for the detection and quantification of both primary and product ions and is used for the majority of the time including during GC-PIT-MS measurements (described below). The CID mode is used to select ions of one specific mass, fragment them inside the ion trap and get more information on their chemical identity.

4.4.1 Mass Spectral Mode

In normal mode, ions are ejected axially after trapping is complete, generating a mass spectrum from m/z 30-220. Primary ion scans, instrument backgrounds, calibrations, and ambient measurements (including GC-PIT-MS measurements) are all made in normal mode. A typical sequence in this mode starts multiple scans of primary ions, typically for a period of 30 seconds. During the primary ion scans, air samples are diverted through the catalytic converter to remove VOCs. After the cycle of primary ions is complete, a series of background scans is made, again using ambient air scrubbed of VOCs by the catalytic converter.

Both primary ion scans and background scans are interpolated during data processing and used to calculate ambient mixing ratios. After background scans are

complete, a series of ambient measurements are made (catalyst off), typically for a period of ~45 minutes. During ambient measurements, an FNF field is applied to exclude trapping of primary ions at m/z 19 (H_3O^+), m37 ($H_3O^+.H_2O$), and other undesirable primary ions like O_2^+ (m32), which would otherwise fill the trap too quickly to allow the detection of VOC ions. This cycle is repeated during field measurements. Calibrations are performed 2-3 times per day. Typical sample data for primary ion, background, ambient and calibration scans are shown in Figure 2.5.

4.4.2 CID Mode

The PIT-MS instrument can also be operated in CID mode. PTR-MS CID mode has been used previously both in the laboratory (Lindinger et al., 1998;Prazeller et al., 2003) and in the field (Warneke et al., 2005a). In this mode, ejection of ions from the trap is delayed while a secondary FNF field is applied to exclude particular m/z ratios. CID mode is typically used to isolate trapped ions of a single mass to charge ratio. In this mode, ions not isolated by the FNF field are lost and are not detected.

The amplitude of the FNF used during the CID delay period determines the energy of the ions in the trap. Collisions of the ions with atoms of the helium buffer gas in the ion trap can cause fragmentation of the trapped ions. Multiple trap/scans cycles at successively larger FNF amplitudes are used to generate a CID spectrum, which has fragments characteristic of, but not necessarily unique to, the parent compound. Spectra generated in CID mode are presented and discussed in

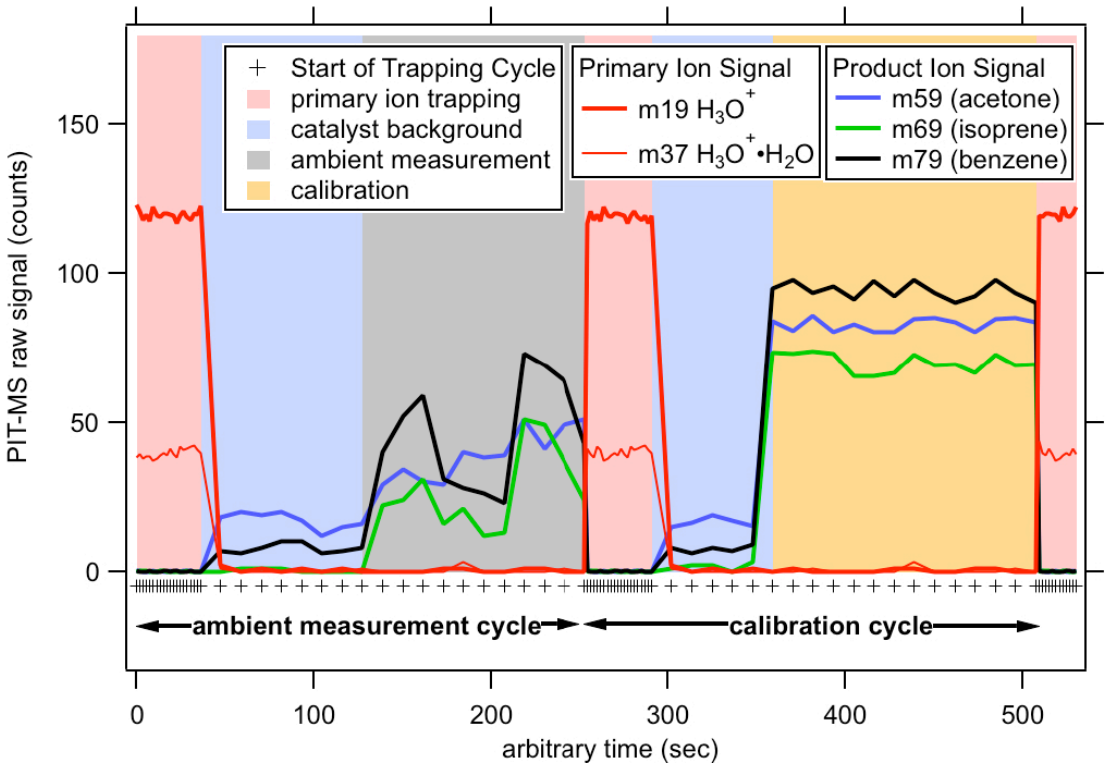

Figure 2.5. A typical PIT-MS instrument trapping cycle used for ambient measurements and calibrations.

Chapter 6. An example of a CID spectrum collected by the PIT-MS instrument during CID mode is shown in Figure 2.6.

4.5 GC-PIT-MS

Another method to distinguish isomers and identify unknown compounds detected by the PTR-method, involves the use of gas chromatography for separation of VOCs in a gas mixture prior to their introduction into the mass spectrometer. This method was used with the PIT-MS instrument (GC-PIT-MS) during several field campaigns and the results are presented in Chapters 3 and 5. In GC-PIT-MS, the PIT-MS instrument is coupled to a gas chromatograph fitted with a temperature programmed DB-624 column (Warneke et al, 2003). Air samples are collected in a liquid-nitrogen cooled cryogenic trap prior to injection onto the GC column. Column effluent is introduced into the PIT-MS instrument producing a GC-PIT-MS chromatogram for each of the about 180 product ion masses monitored by PIT-MS instrument. While measuring the column effluent, the PIT-MS is typically operated with a trapping time of 2 seconds. In GC-PIT-MS, VOC peak width is 4 seconds or less and therefore peaks are under-sampled during field operation and cannot be used for quantification. Figure 2.7 shows an example of the data typically collected in a GC-PIT-MS chromatogram. Results of GC-PIT-MS measurements in the field are discussed in Chapters 3 and 5.

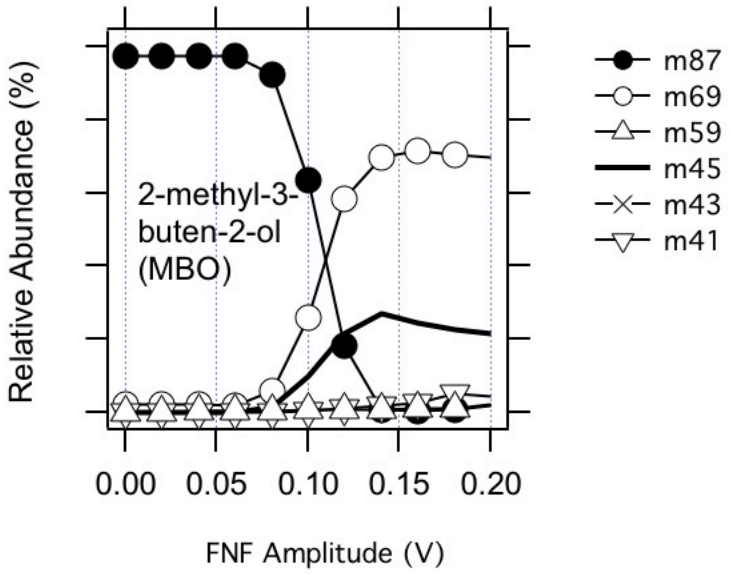

Figure 2.6. CID spectrum for 2-methyl-3-buten-2-ol made from a pure standard in the laboratory.

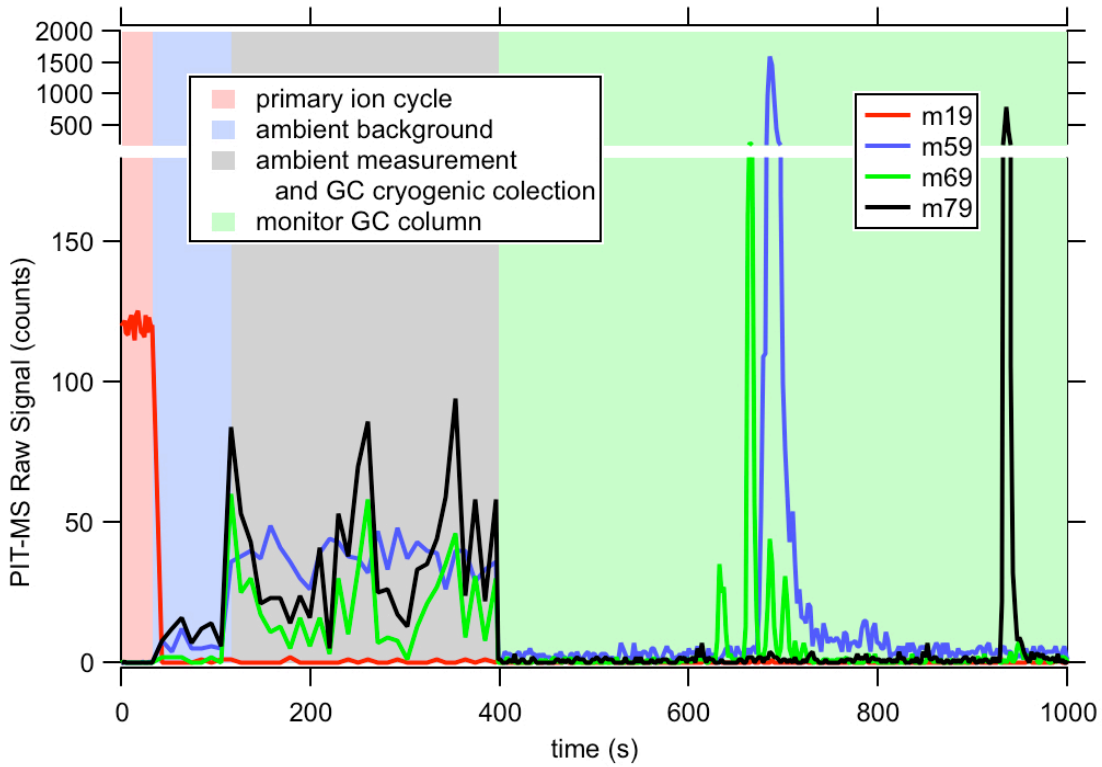

Figure 2.7. An example of a typical GC-PIT-MS chromatogram. The PIT-MS instrument can monitor ambient air while cryogenic collection occurs (grey shaded area), but must be taken off line to monitor the output of the GC column (green shaded area), resulting in the loss of about 30 minutes of ambient air sampling.

CHAPTER 3

VOC EMISSIONS IN MEXICO CITY

1. Introduction

The Mexico City Metropolitan Area (MCMA), a high-altitude sub-tropical megacity with a population of about 18 million people, is an urban center where a dense population and a local geography that restricts atmospheric transport, contribute to the city's significant air quality problems. Hydrocarbon measurements in 1993, 2002, and 2003 showed highly elevated levels of many anthropogenic VOCs within the city (Velasco et al., 2007;Blake and Rowland, 1995;Rogers et al., 2006). The MILAGRO campaign (Megacity Initiative: Local and Global Research Observations) in March 2006 was designed to address the impact of these emissions on air quality over a variety of scales from local to global, and builds on results from smaller multi-investigator campaigns such as IMADA-AVER and MCMA-2003 (Edgerton et al., 1999;Molina et al., 2007;Molina et al., 2010).

During MILAGRO a variety of different instruments and techniques were used to quantify VOCs from both fixed sites and mobile platforms (Heald et al., 2008;Apel et al., 2010). We made VOC measurements by two different ground-based instruments at the sub-urban T1 site (Fast et al., 2007): an in-situ gas chromatograph with flame ionization detection (GC-FID) was used to measure light hydrocarbons and a proton-transfer-reaction ion trap mass spectrometry (PIT-MS) instrument was used to measure acetonitrile, aromatics and oxygenated VOCs (de Gouw et al., 2009b). In this Chapter, these measurements are compared with

canister sample analyses and with proton-transfer-reaction mass spectrometry (PTR-MS) measurements made from the Aerodyne mobile laboratory and from the US Department of Energy G1 aircraft. Because the Aerodyne mobile laboratory and the G1 aircraft also sampled near other surface sites and because canister samples were collected at many surface sites and from the NASA DC-8 and NCAR C-130 aircraft, these comparisons can be used to evaluate the consistency of VOC data obtained throughout the campaign (Karl et al., 2009;Fortner et al., 2009;Apel et al., 2010;Kleinman et al., 2008). In addition, this study adds to our understanding of the specificity of PTR-MS measurements in a dense megacity with a complex VOC composition that challenges the analytical capabilities of this technique (de Gouw and Warneke, 2007).

Diurnal cycles of most VOCs at the T1 ground site were pronounced with a high peak in the morning when emissions accumulated in a shallow mixing layer (de Gouw et al., 2009b). A similar diurnal pattern was observed during the MCMA-2003 study and at the T0 ground site during the MILAGRO campaign (Fortner et al., 2009;Velasco et al., 2007). The effects of chemical removal and production of VOCs during the MILAGRO campaign were most pronounced in the afternoon and are discussed elsewhere in more detail (de Gouw et al., 2009b). The T1 ground site data are used in this Chapter to determine urban emission ratios versus the combustion tracer carbon monoxide (CO), and these are compared to those from previous studies in the U.S. (Ban-Weiss et al., 2008;Baker et al., 2008;Warneke et al., 2007).

2. Methods

2.1 VOC Measurements at T1

The T1 ground site (19°42'11"N, 98°58'55"W) was located 30 km to the northeast of Mexico City on the campus of the Universidad Tecnológica de Tecámac (UTTEC). VOC measurements at the site were made using (1) a custom-built proton-transfer ion trap mass spectrometer (PIT-MS instrument; Chapter 2), and (2) a gas chromatograph with flame ionization detection (GC-FID). These measurements will be compared here with the results of VOC measurements of canister samples collected at the site, and from two mobile platforms at or above T1. A PTR-MS instrument measured VOCs from the Aerodyne mobile laboratory while it was located at the site on March 20-21. Another PTR-MS instrument measured VOCs from the DOE G-1 aircraft during multiple over flights of T1. Figure 3.1 gives an overview of when the different VOC measurements at T1 were made. Sampling frequency, averaging periods and limits of detection are summarized in Table 3.1. A complete list of species quantified can be found in Table 3.2.

2.2 Instrumentation

2.2.1 NOAA GC-FID

Five-minute integrated samples of light hydrocarbons were collected cryogenically every 15 minutes and injected into a gas chromatograph equipped

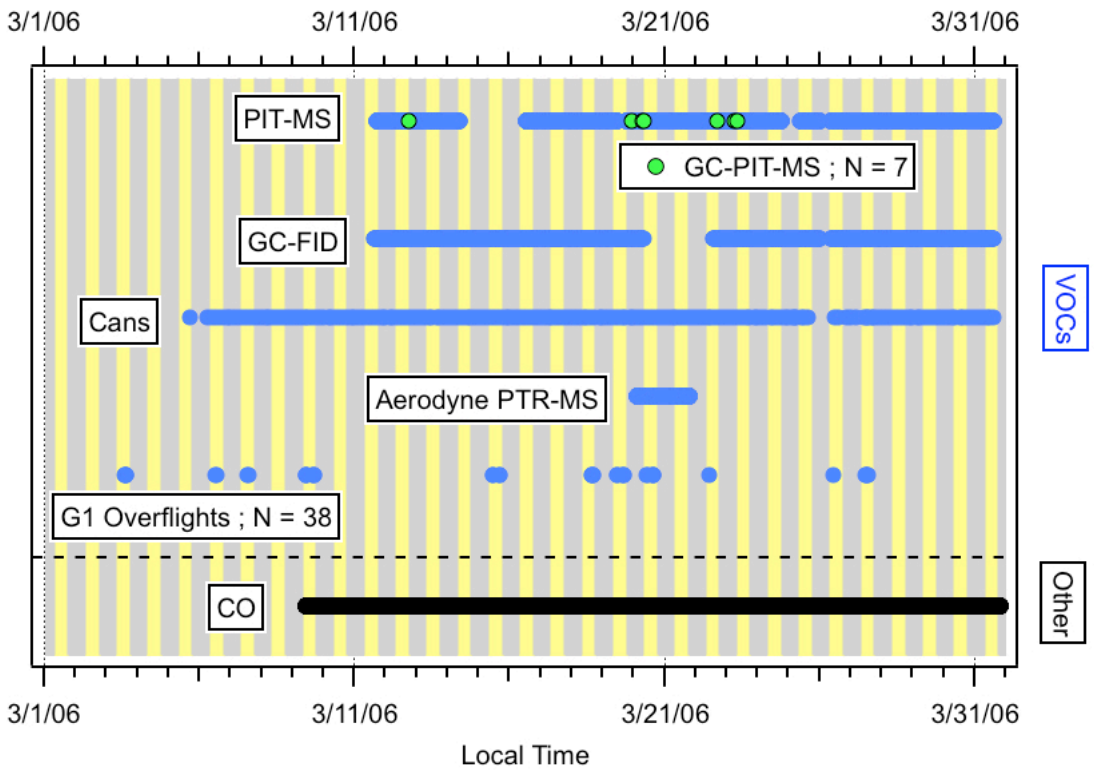

Figure 3.1. Sampling periods for the VOC measurement methods and CO at the T1 ground site in Mexico City during the MILAGRO campaign. Approximate daylight hours (7:00 AM – 19:00 PM local time) are shown in yellow.

Table 3.1. Limits of detection for individual VOCs quantified during the MILAGRO campaign by PIT-MS and PTR-MS.

Instrument:	NOAA PIT-MS		Aerodyne PTR-MS	DOE PTR-MS
period:	5 min		1 sec	1 sec
date:	3/11-3/27	(3/28-3/31)[a]		
Compound	Limit of Detection (pptv)			
toluene	150	(800)	110	100
ΣC8 aromatics	100	(800)	200	110
ΣC9 aromatics	100	(800)	160	110
ΣC10 aromatics	100	(800)		
ΣC11 aromatics	100	(800)		
naphthalene	100	(800)		
methanol	1500	(1500)	530	**
acetaldehyde	300	(1500)	400	350
acetone	150	(800)	230	250
acetic acid	300	(1200)		350
methyl ethyl ketone	300	(2000)		150
acetonitrile	100	(800)		85

[a]PIT-MS LODs reported for two periods March 11-27 & March 28-31. LOD changed due to hardware problems.

with a 50 m DB-5 alumina column divided in half to allow back flushing, which shortens analysis time. A flame ionization detector was used to quantify 18 VOCs in the C2-C6 range with a detection limit of ~5 pptv. Calibrations were made 1-2 times per day from a gas standard. A detailed description of this instrument is given elsewhere (Goldan et al., 2000). Samples were collected from an air intake approximately 6 m above ground level that was shared with the PIT-MS system described below. Both instruments sampled outside air pumped through ¼" PFA Teflon tubing at a rate of 3 SLM. The precision of the measurements is estimated to be 5% from the reproducibility of calibration measurements from one calibration mixture during the campaign. The accuracy is estimated to be 10% based on the variability between different calibration mixtures.

2.2.2 NOAA PIT-MS

The PIT-MS instrument uses an ion source and drift-tube reactor similar to that of a commercial PTR-MS instrument, but is equipped with an ion trap mass spectrometer instead of a quadrupole mass filter (Warneke et al., 2005a;Warneke et al., 2005b). The PIT-MS instrument was described in detail in Chapter 2 of this thesis. During MILAGRO, the PIT-MS provided simultaneous measurements of product ions with mass to charge ratios (*m/z*) from 33 to 225 amu at a frequency of 5 min^{-1}. Calibrations using a gas standard were performed automatically every 2 hours and manually using multiple dilution steps approximately once per week. Twelve different VOCs and OVOCs were quantified based on previous identification

in the literature (de Gouw and Warneke, 2007). Final PIT-MS data were reported as 5-minute averages for easy comparison with the GC-FID data and to improve signal-to-noise.

The measurement precision is calculated using ion-counting statistics as detailed elsewhere (Hayward et al., 2002;de Gouw et al., 2003;de Gouw and Warneke, 2007). Towards the end of the MILAGRO campaign, degradation of the PIT-MS secondary electron multiplier (SEM) detector resulted in increased noise and poorer limits of detection for this period (Table 3.1).

The accuracies for calibrated species quantified by PIT-MS are estimated at 20%. NOAA PIT-MS mixing ratios for C8 and C9 aromatics were calculated using p-xylene and 1,2,4-trimethyl benzene in a calibration standard. The quantification of acetic acid, formic acid, naphthlane, and the higher (> C7) aromatics is less accurate (50%) due to less adequate calibration standards for these compounds. Benzene was detected by PIT-MS during MILAGRO but suffered from interference from clusters of water with protonated acetic acid and was not reported in the final data for the campaign.

In order to distinguish isomers and identify unknown compounds detected by PIT-MS, a GC pre-separation method (GC-PIT-MS) was used on seven occasions predominantly at times when morning maxima in VOC mixing ratios occurred. In GC-PIT-MS mode, the PIT-MS instrument is coupled to a gas chromatograph fitted with a temperature programmed DB-624 column (Warneke et al, 2003). Air samples are collected in a liquid-nitrogen cooled cryogenic trap prior to injection onto the GC column. GC-PIT-MS produces a chromatogram for each of the about 180 product ion

masses monitored by PIT-MS. While measuring the column effluent, the PIT-MS instrument was operated with a time resolution of 2 seconds. Typical VOC peak width was 4 seconds or less and therefore peaks were under-sampled and can be used for identification but not for quantification.

2.2.3 UCI Canisters

Whole air samples were collected by the University of California, Irvine in 2 L electro-polished, pre-treated, evacuated stainless steel sampling canisters. Each canister was filled for 3 hours and was pressurized to about 100 kPa. After sample collection, the canisters were returned to the University of California, Irvine, where they were analyzed for CH_4, CO, hydrocarbons, halocarbons and alkyl nitrates. Detection limits for all species compared here were less than 3 pptv with precisions between 1% and 4%. For more detailed descriptions of the UCI measurements we refer to (Colman et al., 2001). Canister samples were also collected at the T0 ground site and onboard the NASA DC-8 and NCAR C-130 aircraft, and analyzed using the same methodology.

2.2.4 Aerodyne PTR-MS

A commercial PTR-MS (Ionicon Analytik, Austria) instrument was deployed on the Aerodyne mobile laboratory during the campaign (Rogers et al., 2006;Herndon et al., 2008). The mobile laboratory was parked at the T1 site for approximately 40 hours from 04:00 UTC on March 20, 2006 until 18:00 UTC on

March 21, 2006. Calibrations were made at regular intervals using a gas calibration standard and average calibration factors were applied to the data after the campaign. Two scan modes were used for the mobile laboratory PTR-MS. In the first mode, 24 scans of 9 masses were made each with a one second dwell time. This was followed by 12 cycles of the full mass range (20-160 amu) with a 0.1 second dwell time. The data obtained in both modes were averaged on a 1-min time basis for comparison to PIT-MS measurements during this period.

2.2.5 DOE PTR-MS

The Pacific Northwest National Laboratory deployed a commercial PTR-MS instrument on the DOE G1 aircraft. Eleven VOCs were measured with a frequency of 0.1 sec^{-1}. PTR-MS instrument dwell times on the aircraft ranged from 0.5-1.0 second per mass and calibrations were typically done at least twice per flight day. Thirty-eight over-flights of T1 occurred during MILAGRO.

2.2.6 Carbon Monoxide Measurements

Carbon monoxide measurements were made at the T1 ground site by a group from the Georgia Institute of Technology using a modified Thermo Electron 48C CO monitor (Parrish et al., 1994). CO measurements were reported on a 1-minute time base. The precision and accuracy of these data are estimated to be ±5 ppbv and ±5%, respectively.

CO was also quantified by gas chromatography from the UC Irvine canisters. These measurements agreed with the in-situ measurements averaged over the canister sampling periods to within 5% (r^2=0.90).

3. Data Quality Evaluation

The quality of VOC data obtained at T1 was evaluated using direct measurement comparisons between the two NOAA measurements and other measurements where possible. The selectivity of the PIT-MS data was evaluated using GC-PIT-MS analyses.

3.1 Measurement Comparisons

3.1.1 NOAA GC-FID vs. UCI Canisters

The on-line GC-FID measurements were compared to UCI canister measurements for 17 compounds. For the purpose of these comparisons, the on-line GC-FID data were averaged over the 3-hour sampling times of the UCI canisters. Examples are shown for propane, ethylene and acetylene (Figure 3.2a-c). The data in Fig. 3.2 were fit using 2-sided, orthogonal distance regressions (ODR). The resulting regression slopes (s), and values of the linear correlation coefficient (r^2) are summarized in Table 3.2 for all 17 overlapping VOC measurements. For all VOCs, the degree of correlation between the in-situ and canister measurements was high (r^2>0.87) and most measurements agreed within the 10% accuracy of the in

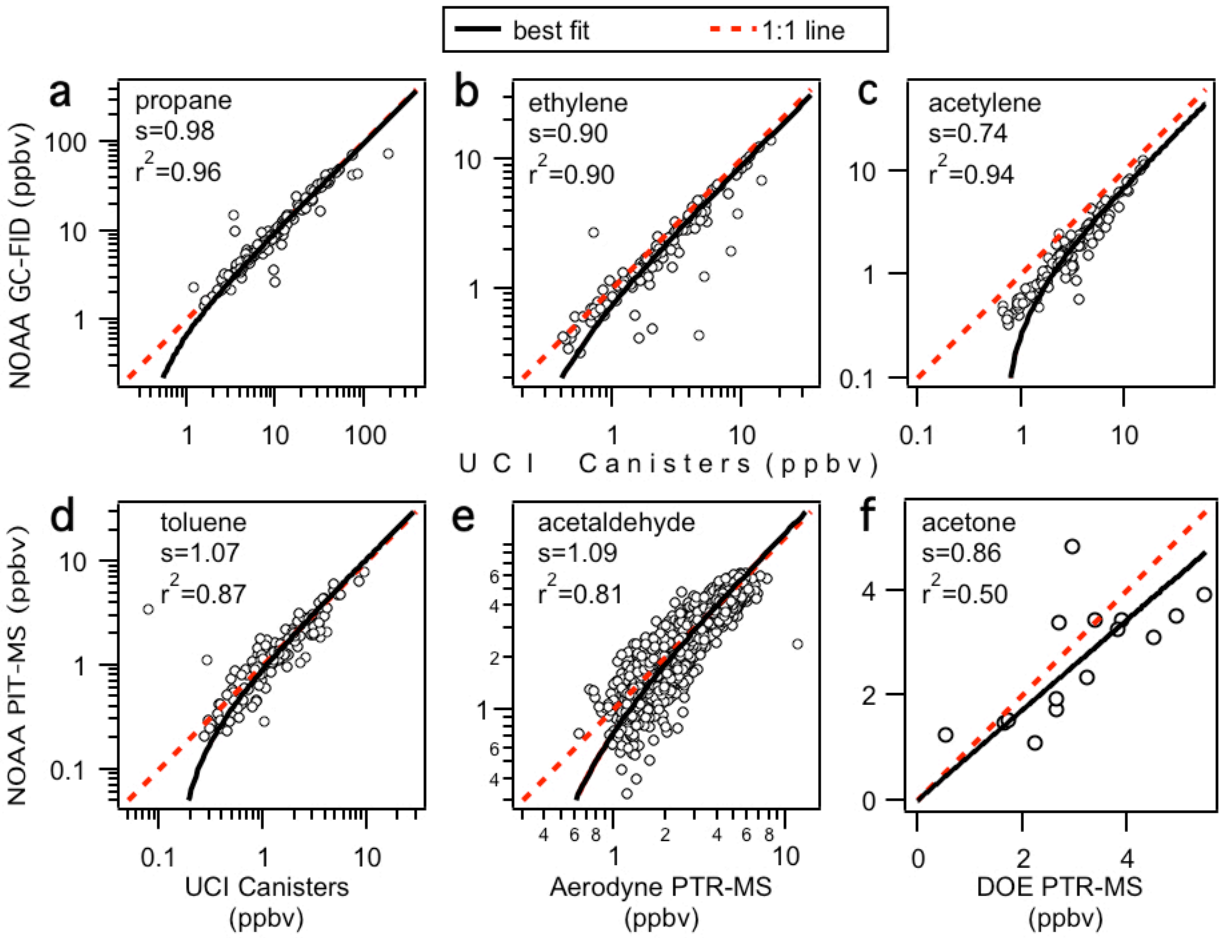

Figure 3.2. Selected results of the comparison of VOC measurements at the T1 site during MILAGRO. Panels a-c compare the measurements of the NOAA GC-FID and the UC Irvine canister measurements for the same compound. Panels d-f compare measurements made by the NOAA PIT-MS to those made from the UC Irvine Canisters and by the PTR-MS instruments on the Aerodyne Mobile Laboratory and the DOE G1 aircraft, respectively. Slopes from linear regressions (s) and correlation coefficients, r^2, for comparisons are tabulated in Table 3.2.

Table 3.2. Slopes resulting from ODR regression of scatter plots between VOCs measured by 2 or more techniques during MILAGRO. Also shown here are 1σ uncertainties in slopes, correlation (r^2) coefficients, and the number of points compared (N).

	best fit slope			r^2	N
	NOAA GC-FID : UCI Canisters				
propane	0.98	±	0.04	0.96	128
n-butane	1.02	±	0.03	0.97	128
i-butane	1.02	±	0.03	0.97	128
n-pentane	1.04	±	0.03	0.98	128
i-pentane	0.89	±	0.02	0.98	128
n-hexane	0.94	±	0.03	0.97	128
ethylene	0.90	±	0.03	0.97	129
propylene	1.00	±	0.03	0.97	128
1-butene + 2-methyl propene	0.99	±	0.04	0.96	128
cis-2-butene	0.95	±	0.04	0.95	128
trans-2-butene	0.79	±	0.03	0.96	128
1-pentene	1.18	±	0.16	0.87	71
cis-2-pentene	1.00	±	0.06	0.94	77
trans-2-pentene	1.03	±	0.04	0.96	98
2-methy 2-butene	0.78	±	0.07	0.90	60
3-methy 1-butene	0.93	±	0.12	0.87	82
acetylene	0.74	±	0.04	0.94	129
	NOAA PIT-MS : UCI Canisters				
toluene	1.07	±	1.74	0.87	112
Σ C8 aromatics	3.38	±	0.14	0.87	108
Σ C9 aromatics*	2.68	±	0.44	0.72	101
	NOAA PIT-MS : Aerodyne PTR-MS				
methanol	0.68	±	0.11	0.84	1605
acetaldehyde	1.10	±	0.21	0.81	1695
acetone	1.00	±	0.14	0.86	1695
toluene	1.61	±	0.18	0.89	1685
Σ C8 aromatics	1.39	±	0.18	0.87	1685
Σ C9 aromatics	1.38	±	0.22	0.84	1685
	NOAA PIT-MS : DOE G1 PTR-MS				
acetonitrile	0.93	±	0.17	0.06	15
acetaldehyde	0.97	±	0.13	0.18	15
acetone	0.86	±	0.07	0.50	15
acetic acid	0.50	±	0.08	0.10	15
methyl ethyl ketone	0.84	±	0.09	0.36	15
toluene	1.07	±	0.14	0.51	15
Σ C8 aromatics	0.88	±	0.17	0.04	15
Σ C9 aromatics	0.30	±	0.14	0.23	9

situ measurements. Notably, the canister measurements of acetylene (Figure 3.2c) were systematically higher than those made in-situ. The reasons for this difference are unknown; calibration standards were not compared for the purpose of this study. Our GC measurements of acetylene in the Arctic in 2008 were systematically higher than canister samples analyzed by the NOAA Global Monitoring Division (Gilman, et al., 2010). As reported in previous work (Apel et al., 1994), it appears that the accuracy of the measurement of acetylene is considerably outside the 10% calibration uncertainty estimated for other species. Further work is needed to resolve the considerable calibration discrepancies for this important species.

3.1.2 NOAA PIT-MS vs. UCI Canisters

Both the PIT-MS and the UCI canisters reported mixing ratios for aromatic compounds. An example of the comparisons is shown for toluene in Fig. 3.2d. The PIT-MS data were averaged onto the canister sampling times for the purpose of this plot. The two measurements of toluene correlated well and agreed quantitatively within 7%. The other PIT-MS measurements of aromatics correlated well but were systematically higher than the UCI canister measurements (Table 3.2). The reasons for these differences are unknown; calibration standards were not compared for the purpose of this study.

PTR-MS measurements of higher aromatics represent the sums of many different isomers, each with its own calibration uncertainty. As a result, inter-comparisons tend to show larger differences than for single compounds (de Gouw

and Warneke, 2007). For example, out of 5 published comparisons of C8 aromatic measurements, three studies compared within 20% and two showed differences of factors of 2 and 3. The GC-PIT-MS results presented later in this section show no significant interferences on masses associated with aromatic compounds that might explain these discrepancies. Previous work in the US also shows no evidence of interference on these masses (Warneke et al, 2003). We conclude that calibration uncertainties appear to be the most likely explanation for measurement disagreements.

3.1.3 NOAA PIT-MS vs. Aerodyne PTR-MS

The Aerodyne mobile laboratory collected data at the T1 site for two days during the campaign (Figure 3.1). Six VOCs were measured by both the NOAA PIT-MS instrument and the Aerodyne mobile laboratory PTR-MS instrument. Figure 3.2e shows the measurement comparison for acetaldehyde. Slopes and correlation coefficients for all 6 VOC comparisons are summarized in Table 3.2. Correlation coefficients (r^2) for all 6 compared compounds were greater than 0.80.

The calibration standards used by both instruments were compared in the field during MILAGRO. PIT-MS measurements of methanol were systematically 32% lower than those of the Aerodyne PTR-MS instrument. This difference is similar to the difference observed (35%) between the calibration standards used with each of the two instruments. The PIT-MS measurements of reported aromatics were systematically 40-60% higher than the Aerodyne PTR-MS measurements (Table 3.2)

but are within the combined measurement uncertainties. Unlike methanol, differences in calibration standards did not explain differences between measurements of aromatics.

3.1.4 NOAA PIT-MS vs. DOE PTR-MS

The DOE G1 aircraft flew over the T1 ground site 38 times during MILAGRO. All overpasses occurred in mid-afternoon when VOC mixing ratios for primary species were at or near daily minima. Aircraft overpass altitudes ranged between 800-2800 m above ground level with typical well-mixed daytime boundary layer depths of at least 2000 m. Measurements of boundary layer heights indicate that overpasses of T1 occurred within the boundary layer (Shaw et al., 2007;Fast et al., 2009).

Eight VOC measurements were compared for the 15 overpasses when both instruments were operating. Overpasses were defined as measurements made by the DOE-G1 instrument within a horizontal distance of 5 km from the ground site. DOE-G1 PTR-MS measurements for each VOC during a particular over flight were averaged and compared to PIT-MS ground measurements averaged within a window of ±10 minutes from the over flight period. An example of the comparison between surface and airborne measurements is shown in Fig. 3.2f for acetone. Due to the low number of data points, linear least-squares fits of the data were constrained to an intercept of zero for these comparisons. Slopes and r^2 values for fits are shown for all 8 VOCs in Table 3.2. The inter-comparison is challenging due

to: (1) low VOC mixing ratios in a narrow concentration range, (2) the large vertical separation, and (3) short duration of the over-flights. Therefore, correlation coefficients for individual VOCs were low ($r^2 < 0.55$), but most species except the C9-aromatics did not show large systematic differences between the two measurements. Calibration standards were not compared during this study.

3.2 GC-PIT-MS

The NOAA PIT-MS instrument was operated in GC-PIT-MS mode seven times during MILAGRO to identify VOCs and evaluate PIT-MS measurements at T1. The GC-interface was described in Chapter 2 and similar to that used in a previous study (Warneke et al., 2003); however, the present application using a PIT-MS instrument is unique in the sense that a chromatogram is obtained at each detection mass of the instrument. Most GC-PIT-MS analyses were performed early in the day coincident with peak VOC concentrations. Figures 3.3 and 3.4 show selected chromatograms from the use of this method for PIT-MS signal attribution. Individual masses of interest are discussed in the following section.

The chromatographic peaks observed at masses 33 (methanol), 45 (acetaldehyde), 59 (acetone), 93 (toluene), 107 (C8-aromatics), and 121 amu (C9-aromatics) were very similar to the results from previous GC-PTR-MS measurements in urban air (Warneke et al., 2003;de Gouw and Warneke, 2007) and provided no evidence of important interferences for any of these compounds.

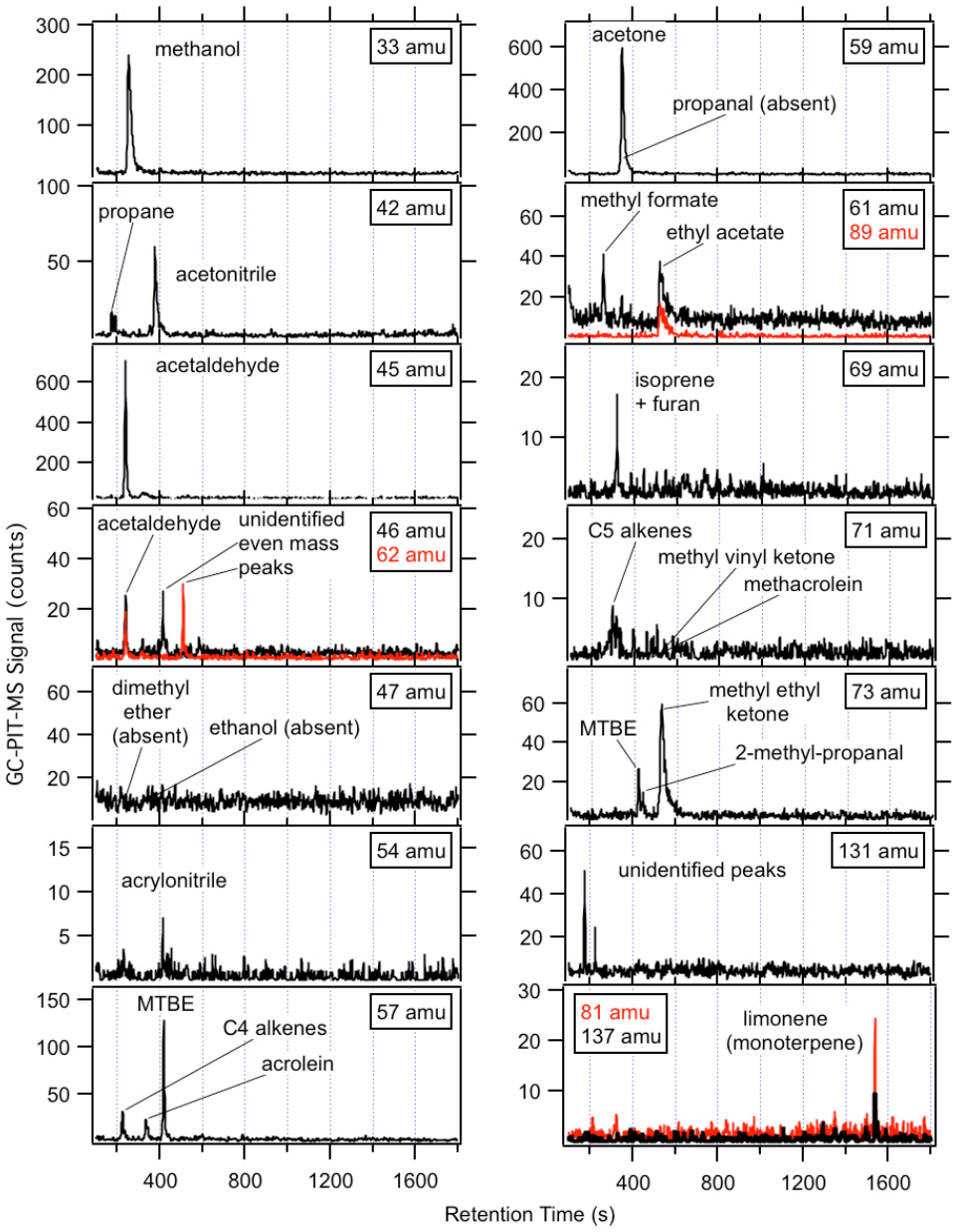

Figure 3.3. Selected GC-PIT-MS chromatograms obtained during the MILAGRO campaign. Signals reported are sums of six individual chromatograms. The retention time scale is slightly adjusted to be comparable with previously reported values for GC-PTR-MS using the same GC instrument and temperature program (Warneke et al., 2003).

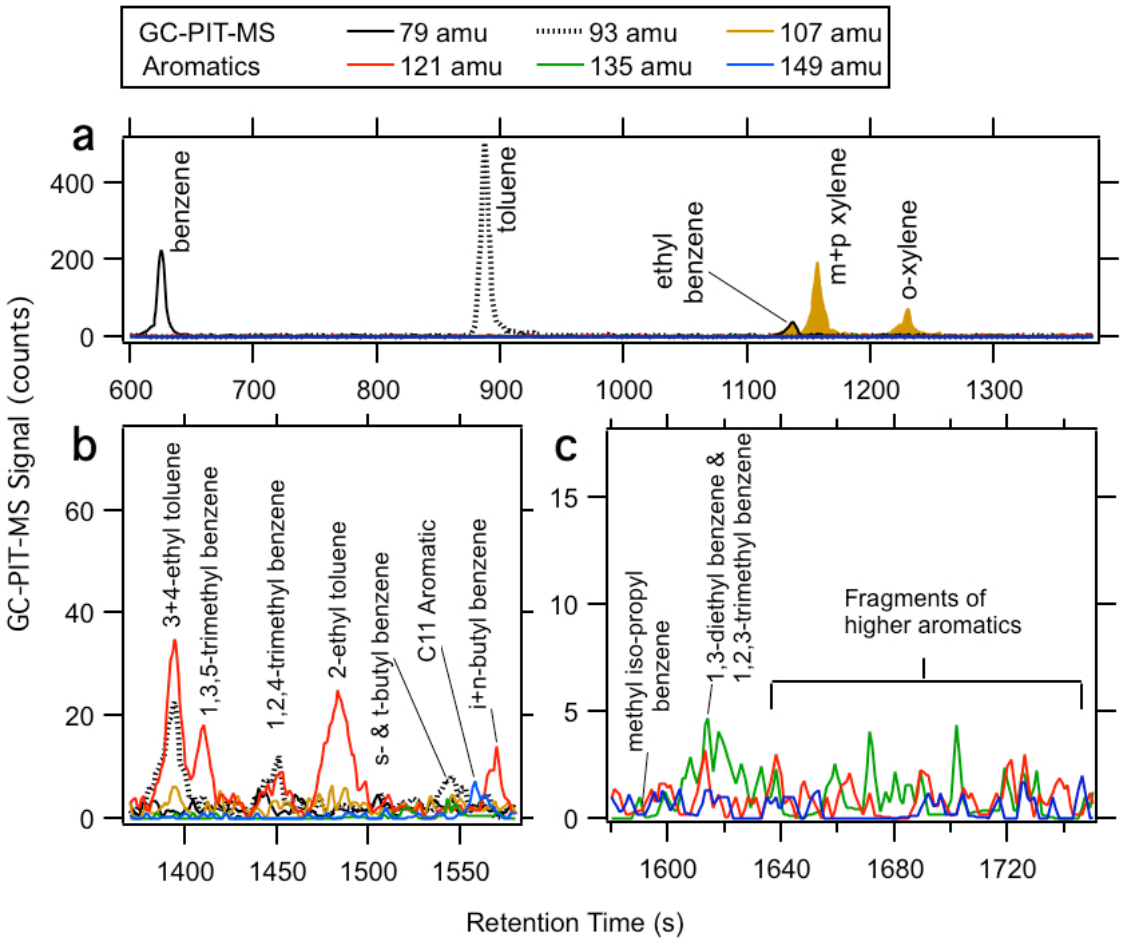

Figure 3.4. GC-PIT-MS chromatograms for aromatic measurements from 600-1400 seconds (a), 1300-1580 seconds (b) and 1580-1750 seconds (c). Identifications made after 1300 seconds retention time are more uncertain than those for the C6-C8 aromatics.

Acetonitrile is measured by PIT-MS at 42 amu. Interferences from the reaction of alkanes and alkenes with O_2^+ ions have previously been observed using GC-PTR-MS (de Gouw et al., 2003;de Gouw and Warneke, 2007). Interferences from propane were evident in GC-PIT-MS chromatograms from Mexico City where mixing ratios of propane reached as high as 250 ppbv. From the GC-PIT-MS measurements it is difficult to quantify the sensitivity of the signal at mass 42 amu to propane. However, scatter plots of the signal at 42 amu versus propane showed no correlation between the two measurements. We conclude that while propane contributed to the signal at 42 amu, most of the variability in the 42 amu signal was due to acetonitrile.

Even masses are typically associated with nitrogen-containing compounds in PTR-MS measurements. The chromatogram at 54 amu contained a small peak that is attributed here to acrylonitrile. However, a larger fraction of the signal at 54 amu in on-line measurements comes from $H_3O^+(H_2O)_2$ clusters at 55 amu; water cluster ions show a tail towards lower masses in PIT-MS. Two unidentified even-mass compounds were detected at 46 and 62 amu by GC-PIT-MS but no conclusive identification was established. Low mixing ratios and isotopic interferences at adjacent masses from more abundant compounds (acetaldehyde and acetic acid respectively) prevent even tentative quantification of these even mass compounds.

Formic acid has previously been reported as the dominant contributor to the PTR-MS signal at 47 amu (Veres et al., 2008). Organic acids do not elute from the GC column used in GC-PIT-MS and therefore cannot be positively identified by this technique. However, several other compounds (ethanol, dimethyl ether, and

formate esters) are detectable by GC-PIT-MS at 47 amu. These compounds did not appear in the chromatograms during MILAGRO and it is unlikely that they are major contributors to the signals on this mass.

The presence of the gasoline additive, methyl tert-butyl ether (MTBE) at 57 amu has been previously observed in field measurements by PTR-MS in the United States and Mexico City and confirmed in laboratory studies (Karl, 2003;Warneke et al., 2005b;Warneke et al., 2003;Rogers et al., 2006). During MILAGRO, GC-PIT-MS confirmed that the signal at 57 amu was dominated by a fragment of MTBE (62%) with minor contributions from the butenes (multiple peaks, 23%) and acrolein (15%), compounds that have been previously observed at this m/z in PTR-MS (Fortner and Knighton, 2008). MTBE also interfered (16%) with the measurement of methyl ethyl ketone (MEK) at 73 amu during the campaign. Previous work has shown that only about 0.2% of the signal from MTBE appears at its protonated parent ion (89 amu) and GC-PIT-MS showed no evidence of MTBE on this mass. Acetic acid has been quantified previously at 61 amu using PTR-MS (de Gouw et al., 2003). The chromatogram at 61 amu does not show acetic acid because it does not elute from the column. Two other species were observed in the chromatogram, tentatively identified as methyl formate and ethyl acetate. The latter compound is also observed at 89 amu and has been previously reported in Mexico City (Rogers et al., 2006;Fortner et al., 2009). Ion counts observed at T1 in GC-PIT-MS chromatograms are at least an order of magnitude smaller than those that would be expected from PIT-MS online measurements of 1-2 ppbv VOC at 61 amu. We

conclude that the online signal at 61 amu is dominated by acetic acid with only minor interference from methyl formate and ethyl acetate.

Isoprene mixing ratios measured from UCI canisters revealed average integrated mixing ratios of about 50 pptv ± 100 % but did not show daytime maxima normally associated with biogenic isoprene emissions. A small peak from isoprene was present in GC-FID chromatograms but this compound was not quantified by GC-FID because it was frequently below detection limit. GC-PIT-MS chromatograms did show peaks consistent with extremely small mounts of isoprene (69 amu), methyl vinyl ketone + methacrolein (71 amu) and one monoterpene (at 81 and 137 amu), possibly limonene. Isoprene, however, cannot be separated chromatographically (by GC-PIT-MS) from furan, and the chromatogram at 71 amu also showed contribution from several C5 alkenes. Additionally, measurements at 69 and 71 amu were highly correlated with primary species such as aromatics and alkenes, suggesting that non-biogenic sources dominate these mass signals in the MCMA. We conclude that PTR-MS measurements at masses 69 and 71 are not reliable indicators of biogenic emissions in the MCMA.

The chromatogram at 131 amu revealed the presence of two unknown compounds with relatively short retention times. On-line measurements show large intermittent spikes at this mass that often correlate with peaks (in order of decreasing signal magnitude) at 109, 145, 140, 122 amu and weak signals at numerous masses above 157 amu. The origin of this signal is unknown but could be due to a local source of halogenated hydrocarbons. Retention times suggest that these halogenated hydrocarbons, if present, have at least one fluorine substitution.

Fragmentation of protonated, high-mass halogenated hydrocarbons in PTR-MS is probable, but poorly characterized and this finding remains speculative.

Signals from aromatic compounds in GC-PIT-MS chromatograms are shown in Figure 3.4. Peaks for small aromatics can be clearly identified for benzene (79amu), toluene (93 amu), xylene isomers (107 amu), and ethyl benzene. (107 amu). Compound identification consistent with C9 aromatics (121 amu) and some of the C10 isomers (135 amu) can be assigned by retention times with some confidence (Figure 3.4b). Some of the peaks in chromatograms at 135 amu and all of those at 149 amu are tentatively identified in Figure 3.4c. C11 aromatics probably dominate the signal at 149 amu although the identification of specific peaks remains tentative (Figure 3.4).

PIT-MS measurements at 129 amu are reported here as naphthalene: few other hydrocarbons have this molecular mass, and high concentrations of gas-phase naphthalene exceeding 0.3 ppbv (1.5 $\mu g\ m^{-3}$) have been previously been reported for Mexico City (Marr et al., 2006). Maximum mixing ratios of naphthalene measured by PIT-MS were as high as 0.8 ppbv, however this compound was not calibrated during the campaign. GC-PIT-MS has a low sensitivity to naphthalene and it is very likely that ambient levels of naphthalene were below the limit of detection for the method. No peaks were observed in the GC-PIT-MS chromatogram at mass 129.

4. Other Results and Discussion

4.1 Diurnal VOC Patterns

VOC mixing ratios at T1 had a pronounced diurnal pattern during MILAGRO that is summarized graphically for a few representative VOCs in Figure 3.5. Large, direct emissions and a shallow boundary layer resulted in a maximum concentration for most compounds just before local sunrise (07:00 local time). After sunrise, mixing ratios for primary emissions decreased rapidly due both to photochemical oxidation and dilution into an expanding daytime boundary layer (Fig. 3.5a-d). Compounds with shorter lifetimes reached their minimum values more quickly and their normalized profile minima were closer to zero.
Photochemical production of oxygenated species (OVOCs) leads to a very different diurnal profile. The balance of the production and the dilution in an expanding boundary layer causes mixing ratios for most OVOCs to decline more slowly after sunrise than those with exclusively primary sources (Fig. 3.5e-f). The atmospheric processing of primary emissions and production of secondary products is discussed in detail elsewhere (de Gouw et al., 2009b).

4.2 Urban Emission Ratios

4.2.1 Hydrocarbons

The early morning maximum in most VOCs is likely to be due to the accumulation of primary emissions in a shallow boundary layer in the absence of significant chemical removal. Therefore, these data are very useful for the determination of urban emission ratios. Most VOCs with primary sources only

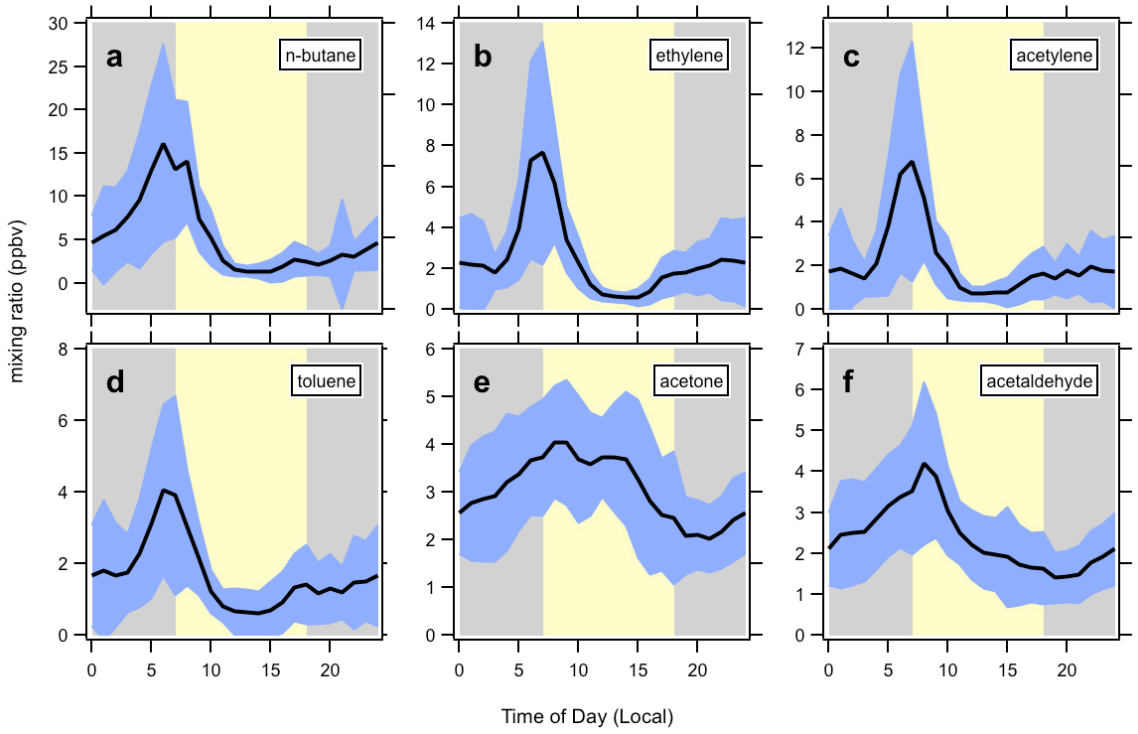

Figure 3.5. Diurnally averaged mixing ratios for select VOCs mentioned in the text for the MILAGRO campaign. The solid line is the mean of all the values and the shaded blue region represents 1σ. The number of points (N) averaged for GC-FID species (panels a-c) is 1586. For PIT-MS instrument measurements (panels d-f), N=127202.

(hydrocarbons) showed a high degree of correlation with inert combustion tracers such as carbon monoxide (CO) (Figure 3.6). Propane, n-butane and i-butane correlated poorly with CO, as their emissions are likely dominated by leakage of liquid propane gas (LPG) rather than from mobile sources (Blake and Rowland, 1995). For hydrocarbon emission ratios derived from PIT-MS measurements (e.g. C7 and higher aromatics), only morning (4-7 AM LT) values were used. Figure 3.6f shows an example of the contrast between morning and afternoon measurements for PIT-MS measurements of the C8-aromatics.

Here we derive emission ratios from the slopes of two-sided (ODR) fits of the VOC data versus CO. Table 3.3 summarizes these emission ratios for all measured hydrocarbons. Emission ratios for important VOCs not measured by GC-FID or PIT-MS (e.g. ethane, C7 and higher alkanes, and benzene) were calculated from UCI canister measurements of these compounds and CO. In Table 3.3 we report both the 1-sigma uncertainty in the regression slope and the calibration uncertainty. The same data are shown graphically in Figure 3.7.

We note that the emission ratios presented here for ethane and propane differ substantially from those calculated by Apel et al. (2010), which were derived from l-sided linear regression fits. Because of the poor correlation of ethane and propane with CO, their ratios versus CO have a limited value and a very large uncertainty. We are including them here for the sake of completeness.

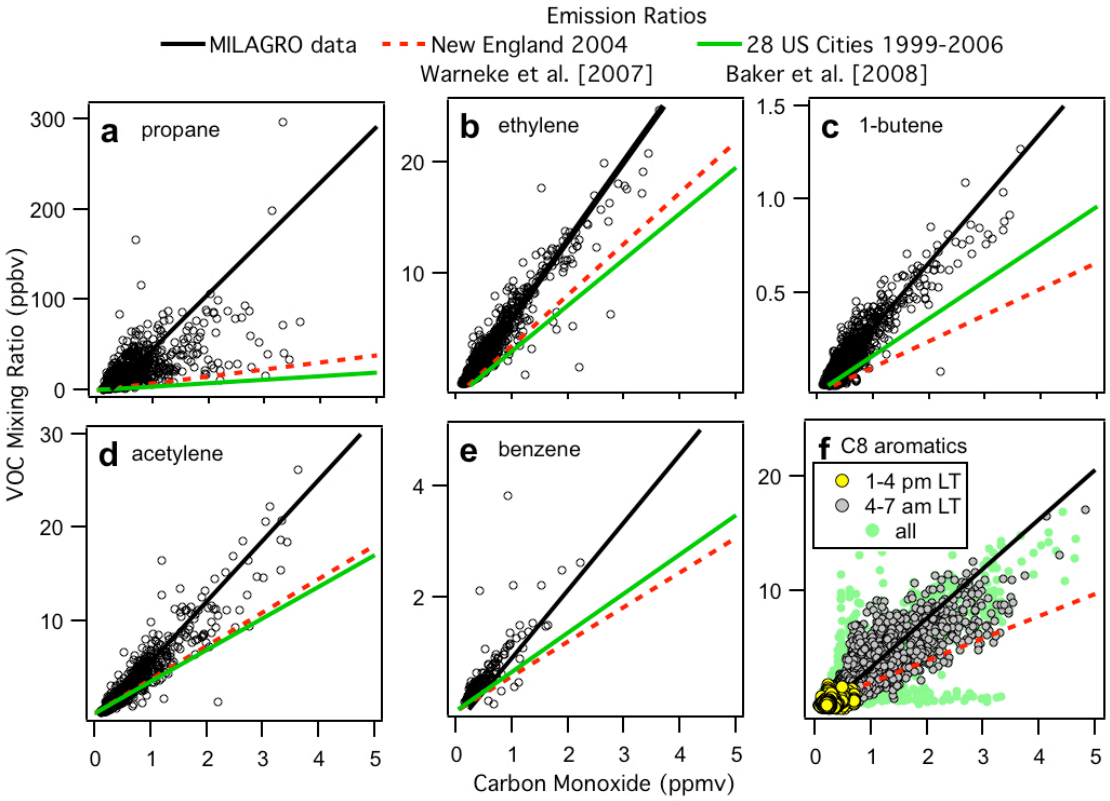

Figure 3.6. Selected plots used to calculate urban emission ratios (ERs) with respect to carbon monoxide (CO) for VOC measurements made by GC-FID (a-d), canister samples (e) and PIT-MS (f). Urban ERs calculated from measurements using ODR fits (black) and Positive Matrix Factorization results (purple) during MILAGRO. MCMA ERs are compared to literature values (red, green) obtained for cities in the United States. PIT-MS measurements are shown on a 1-minute time base (f) to highlight mixing ratio differences prior to local sunrise (grey) versus those observed during the mid-afternoon (yellow).

Table 3.3 Urban emission ratios for non-methane hydrocarbons quantified during MILAGRO versus carbon monoxide are compared to values for US cities from the literature. Correlation coefficients (r^2) and the number of points fit (N) are shown for measurement derived emission ratios. Reported errors for measurement-derived emission ratios are 1σ uncertainties in the slope of the ODR fit.

Compound	MILAGRO Emission Ratio Best Estimate 2006 (pptv [ppbv CO]$^{-1}$)			calibration uncertainty (%)	r^2	N	New England (Warneke et al. 2007) 2004 (pptv [ppbv CO]$^{-1}$)	28 US cities (Baker et al. 2008) 1999-2005
Alkanes								
ethane[a]	21.5	±	10.8	10 %	0.50	199	11.62	2.4
propane[b]	61.7	±	15.6	10 %	0.53	1242	7.73	3.8
n-butane[b]	21.7	±	5.0	10 %	0.57	1242	1.69	1.4
i-butane[b]	7.2	±	1.6	10 %	0.57	1242	1.01	0.9
n-pentane[b]	2.5	±	0.2	10 %	0.81	1241	1.55	1.2
i-pentane[b]	3.3	±	0.4	10 %	0.77	1242	3.99	2.9
n-hexane[b]	1.49	±	0.16	10 %	0.70	1240	1.07	0.6
cyclopentane[a]	0.153	±	0.008	10 %	0.88	166		
cyclohexane[a]	0.164	±	0.008	10 %	0.77	181	0.29	
methyl cyclopentane[a]	0.47	±	0.02	10 %	0.87	194	0.57	
2,2-dimethyl butane[a]	0.36	±	0.02	10 %	0.89	159	0.12	
2,3-dimethyl butane[a]	1.67	±	0.13	10 %	0.72	160	0.27	
2-methyl pentane[a]	1.33	±	0.07	10 %	0.89	165	1.11	
3-methyl pentane[a]	0.90	±	0.05	10 %	0.91	166	1.28	
n-heptane[a]	0.36	±	0.06	10 %	0.69	199	0.40	0.2
2,4-dimethyl pentane[a]	0.126	±	0.006	10 %	0.87	187	0.17	
n-octane[a]	0.122	±	0.006	10 %	0.33	152	0.20	0.1
n-nonane[a]	0.065	±	0.003	10 %	0.32	158		
n-decane[a]	0.042	±	0.002	10 %	0.26	182	1.E-04	
Alkenes								
ethylene[b]	7.0	±	0.4	10 %	0.90	1242	4.56	4.1
propylene[b]	3.0	±	0.2	10 %	0.86	1242	1.36	1.0
1-butene[b]	0.35	±	0.02	10 %	0.87	1236	0.14	0.2
2-methyl propene[b]	0.85	±	0.04	10 %	0.91	1236		
cis-2-butene[b]	0.18	±	0.02	10 %	0.82	1236	0.06	
trans-2-butene[b]	0.20	±	0.02	10 %	0.82	1235	0.05	
1-pentene[b]	0.152	±	0.011	10 %	0.88	1211		
cis-2-pentene[b]	0.100	±	0.009	10 %	0.86	1206	0.05	
trans-2-pentene[b]	0.190	±	0.017	10 %	0.85	1209		
2-methy 2-butene[b]	0.179	±	0.019	10 %	0.83	1202		
2-methyl 1-butene[b]	0.140	±	0.011	10 %	0.87	1213		
3-methy 1-butene[b]	0.044	±	0.006	10 %	0.80	1195		
1,3-butadiene[a]	0.278	±	0.014	10 %	0.84	147		
Alkynes								
acetylene[b]	6.5	±	0.3	10 %	0.90	1242	3.60	3.4
Aromatics								
benzene[a]	1.21	±	0.06	10 %	0.94	183	0.62	0.7
toluene [c]	4.2	±	0.4	20 %	0.69	2563	2.62	2.7
Σ C8 aromatics [c]	4.3	±	0.6	50 %	0.71	2563	1.93	
Σ C9 aromatics[c]	2.8	±	0.6	50 %	0.79	2563	1.07	
Σ C10 aromatics[c]	0.76	±	0.15	50 %	0.71	2563		
Σ C11 aromatics[c]	0.16	±	0.03	50 %	0.41	2563		
naphthalene[c]	0.12	±	0.01	50 %	0.24	2592		

[a] UCI-Canisters, data from entire campaign
[b] NOAA GC-FID, data from entire campaign
[c] NOAA PIT-MS, data from 4-7 am, local time

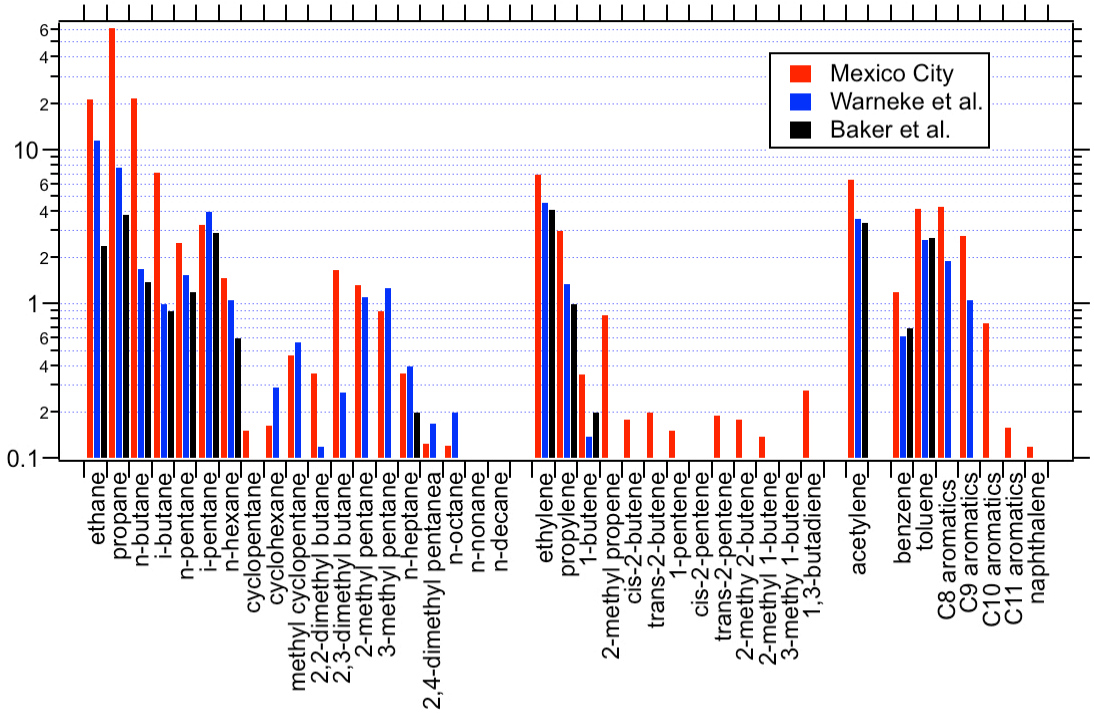

Figure 3.7. Graphical comparison of emission ratios to CO calculated for MILAGRO non-oxygenated hydrocarbon measurements with similar measurements from U.S. cities. The data are presented in Table 3.2

4.2.2 Oxygenated VOCs

Many OVOCs have both direct emission sources and are formed photochemically. In an urban environment, sources of OVOCs from combustion are likely minor compared with those from industrial, evaporative and particularly photochemical sources. As a result, poor correlation with CO is expected and observed for most OVOCs (Figure 3.8). Figure 3.8 also illustrates the large difference in mixing ratios for OVOCs in the morning and afternoon period. Fits made in the plots of morning OVOC mixing ratios versus CO tend to parallel the lower edge of the data (closest to the CO axis) suggesting a method for estimating OVOC measurements that might be useful in future studies.

Emission ratios versus CO were calculated from slopes of ODR fits for measurements made between 04:00 and 07:00 local time in order to minimize the effects of photochemical production. The results are shown by solid, black lines in Figure 3.8 and summarized in Table 3.4.

4.2.3 Comparison of Emission Ratios with those from U.S. cities

Emission ratios for hydrocarbons versus CO from measurements made in the United States (Warneke et al., 2007;Baker et al., 2004) are added to Figure 3.6 and to Table 3.3 for comparison purposes. For most alkenes and aromatics, Mexico City emission ratios to CO are approximately a factor of two larger than corresponding values from the United States. The difference is probably due to differences in automobile emission systems and fleet ages between the two countries. In ambient air,

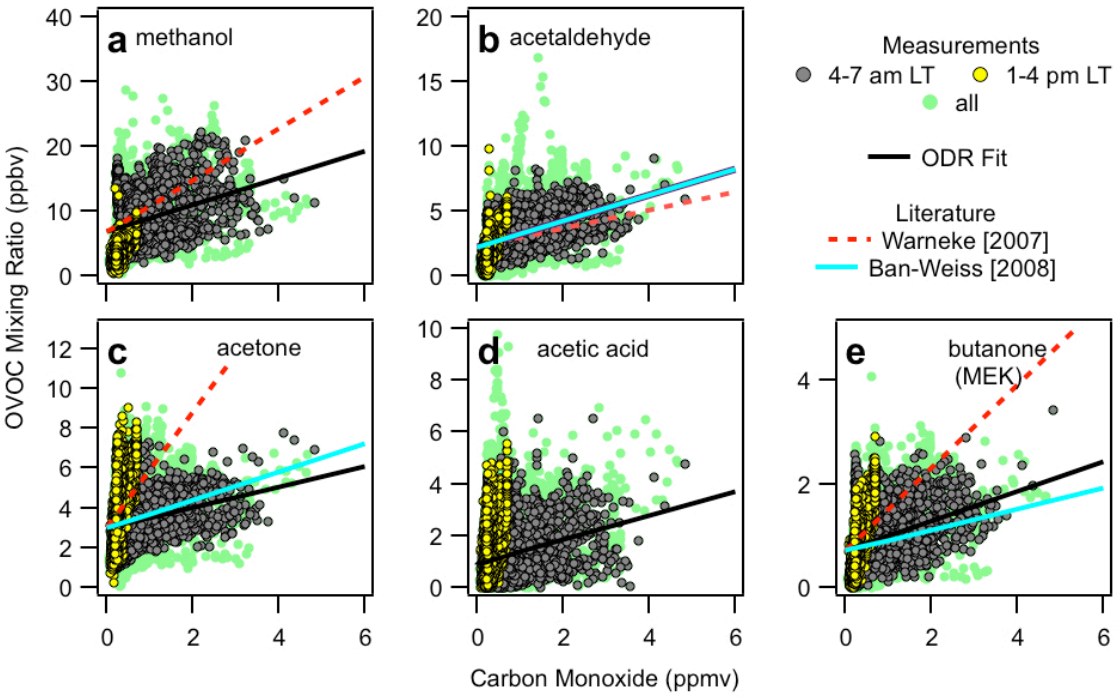

Figure 3.8. Plots used to calculate emission ratios with respect to carbon monoxide (CO) for 5 OVOCs quantified by PIT-MS. Emission ratios calculated from measurements using 2-sided regression fits (black) during MILAGRO are compared to literature values obtained during field studies in New England (red) and to a California tunnel study (blue). 1-Minute PIT-MS data show afternoon enhancements in OVOCs typically observed during the campaign.

CO to CO_2 ratios of about 45 ppbv $ppmv^{-1}$ were observed during the MILAGRO campaign (Vay et al., 2009); a value similar to the ratio observed in plumes originating in China and twice as large as the 10-20 ppbv $ppmv^{-1}$ observed in nations like Japan and the United States (Takegawa et al., 2004;de Gouw et al., 2004). It is worth noting, therefore, that VOC emission ratios per kg fuel burned are probably closer to a factor of 6±2 larger in Mexico City than those for US cities.

Emission ratios for OVOCs from 2004 measurements in New England and those from a 1999 California tunnel study are shown in Figure 3.8 and Table 3.4 (Warneke et al., 2007;Ban-Weiss et al., 2008). OVOC emission ratios for Mexico City more closely resemble values obtained in the tunnel study than those calculated from measurements in the Northeastern U.S. Differences between OVOC emission ratios from the MCMA and the Northeastern U.S. could be due to sampling methodology, i.e. the Northeastern U.S. data were largely collected outside city boundaries and although an attempt was made to account for the effects of secondary production using a photochemical lifetime method, the resulting emission ratios may still overestimate the direct emissions. Biogenic emissions may also account for some of the differences observed between Mexico City and New England, particularly for methanol, which has significant biogenic sources (Millet et al., 2008;Jacob, 2005).

Table 3.4. Urban emission ratio estimates versus CO for OVOCs and acetonitrile calculated by linear regression. For comparison, literature values from PTR-MS measurements made in New England and from a U.S. tunnel study are also shown. Methods used to calculate these values are discussed in detail in the text. Also shown are correlation coefficients (r^2) and the number of points fit (N). Reported errors for measurement-derived emission ratios are 1σ uncertainties in the slope of the ODR fit.

	MILAGRO				New England (Warneke et al. 2007)	Caldecot Tunnel (Ban-Weiss et al. 2008)			
	Emission Ratio Best estimate 2006[a]	calibration uncertainty	r^2	N	2004	1999	2001	2006	Diesel
	(pptv [ppbv CO]$^{-1}$)	(%)			(p p t v [p p b v CO]$^{-1}$)				
Oxygenates									
methanol	2.1 ± 0.5	20 %	0.11	2563	4.0				
acetaldehyde	1.0 ± 0.3	20 %	0.23	2563	0.7	1.0	0.5	0.7	12.0
formic acid[c]	0.22 ± 0.11	50 %	0.12	2592					
acetone	0.51 ± 0.13	20 %	0.06	2563	2.9	0.7	0.4		
acetic acid	0.5 ± 0.2	50 %	0.09	2563					
MEK	0.29 ± 0.07	20 %	0.13	2563	0.8	0.1	0.1	0.2	1.4
Other									
acetonitrile	0.27 ± 0.07	20%	0.24	2563					

[a]Ratios calculated from PIT-MS data collected between 4-7 am LT

4.3 Fraction of PIT-MS signal identified

The fraction of the PIT-MS signal that could be attributed to specific compounds is shown in Fig. 3.9 as a function of the time of day. The unidentified signal averaged 18% of the total for the entire campaign, a result which is consistent with previous estimates of unidentified signal from field measurements with PIT-MS (Warneke et al., 2005b). During the campaign, the majority of PIT-MS signal can be attributed to compounds clearly identified using GC-PIT-MS (Figure 3.9).

5. Conclusions

Two ground-based NOAA instruments were deployed during the MILAGRO campaign that provided quantitative analysis of 30 VOCs. Comparison of measurements from these two instruments with canister samples and two mobile PTR-MS instruments was performed and the measurements agreed within uncertainty estimates for most compounds.

PIT-MS provided on-line quantification of 12 VOCs and was used to monitor an additional 150+ product ion masses. The full mass scan of the PIT-MS instrument proved useful in identifying signal that might have been missed by a quadrupole PTR-MS and the use of the GC pre-separation method provided valuable identification and validation of PIT-MS measurements during the study. Many species quantified by the PIT-MS showed little evidence of interference from other compounds. About 85% of the total PIT-MS signal arose from identified compounds. Signals at 69 and 71 amu, commonly associated with biogenic emissions at other

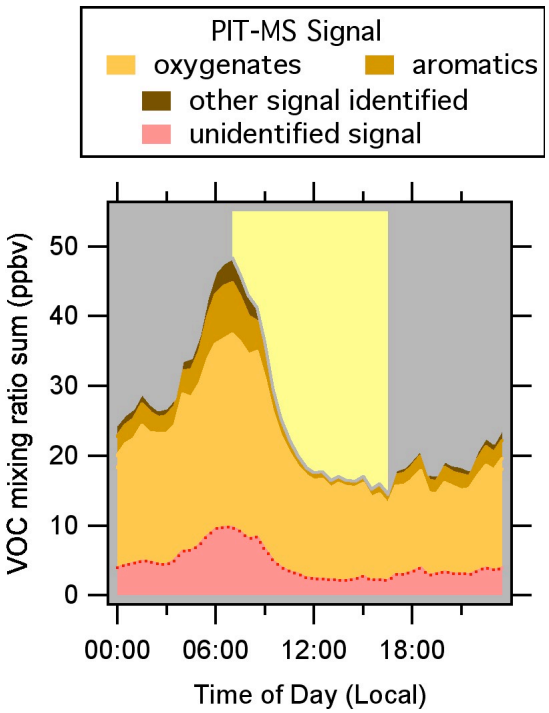

Figure 3.9. Average fraction of total PIT-MS signal attributed to oxygenates, aromatics and other identified signal during the MILAGRO campaign. Unidentified signal averages about 18% of the total.

locations, appear to come from different compounds and were dominated by traffic emissions in the MCMA. Product ion masses 69, 71, 75, 85, and 87 amu accounted for a large fraction of the unidentified signal from PIT-MS.

In this Chapter, we report values for VOC and OVOC emission ratios with respect to CO from Mexico City, and compare them with previously reported values from US cities. Urban VOC emissions in the MCMA are dominated by traffic emissions and LPG usage and emission ratios to CO for most hydrocarbons are generally about a factor of two larger than in the United States. VOC emission ratios to CO_2 appear to be about a factor of 6 (± 2) larger than US values. Urban OVOC emission ratios in Mexico City are consistent with vehicular sources of these compounds.

CHAPTER 4

FACTOR ANALYSIS AND SOURCE APPORTIONMENT OF VOC MEASUREMENTS FROM MEXICO CITY DURING THE 2006 MILAGRO FIELD CAMPAIGN

1. Introduction

VOC measurements made during the MILAGRO 2006 campaign in Mexico City were presented in Chapter 3. In this Chapter we will present the results of source-receptor factor analysis performed on the same data using the Positive Matrix Factorization (PMF) model. The goal of the analysis is to extract information from the data about VOC sources that contribute significantly to the VOCs observed at the suburban T1 ground site.

Positive Matrix Factorization (PMF) is a factorization model widely used for environmental source apportionment (Paatero and Tapper, 1994;Ulbrich et al., 2009). PMF is applied here to the VOC data collected at T1 during the campaign. PMF and other similar factorization methods (e.g. Principal Component Analysis) have been applied previously for VOC measurements at urban ground sites where VOCs have distinct sources or diurnal profiles (Song et al., 2007;Legreid et al., 2007;Millet et al., 2006;Harley et al., 1992;Buzcu and Fraser, 2006).

Here, we use the results from the PMF analysis to 1) identify major VOC sources in Mexico City, and use these results to 2) estimate emission ratios for comparison with the VOC emission ratios derived by linear regression versus CO

which were presented in Chapter 3. The analysis also provides information about the limitations of the PMF method as applied to VOC measurements.

2. Methods

2.1 The PMF Algorithm

The PMF algorithm solves the bilinear, receptor-only, un-mixing model, with positively-constrained factor values, and has been widely used for factor analysis and source-apportionment of both particulate matter and VOC measurements (Slowik et al., 2010;Ulbrich et al., 2009;Lanz et al., 2008;Reff et al., 2007;Engel-Cox and Weber, 2007;Brown et al., 2007;Zhao et al., 2004). Some concepts that are relevant to the understanding of this work are briefly described here. For additional details of the method, the reader is referred to the above references.

For PMF analysis, data are assembled into a 2 dimensional $m \times n$ matrix X such that each of the i rows contains the measured VOC mixing ratios at sampling time t_i and each of the j columns contains the time series of a sampled VOC_j. A corresponding matrix is assembled specifying the measurement precision ("uncertainty") for each point in the data matrix (σ_{ij}). The bilinear un-mixing model represents the measured VOC concentrations as the sum of the contributions of p factors, each of which is comprised of a chemical profile (f) and a factor time series (g), such that for each point in the data matrix (x_{ij}):

$$x_{ij} = \sum_{p} g_{ip} f_{pj} + e_{ij} \qquad \text{(equation 4.1)}$$

where e_{ij} is the fit residual for each matrix (Ulbrich et al., 2009;Paatero and Tapper,

1994;Paatero, 1997).

The PMF algorithm finds solutions of the model by minimizing a "quality of fit" parameter Q defined as:

$$Q = \sum_{i=1}^{m} \sum_{j=1}^{n} \left(e_{ij} / \sigma_{ij} \right)^2 . \qquad \text{(equation 4.2)}$$

The minimum expected value of Q /(Q_{exp}) is obtained when all data elements have been fit within their uncertainty (i.e., $e_{ij}/\sigma_{ij} \sim 1$), thus Q_{exp} should be approximately $m \times n$ for large datasets. Q values can be normalized to Q_{exp}, such that the expected best fit would have $Q/Q_{exp} \sim 1$. The larger the number of factors, the better the statistical description of the data set. In practice, the number of factors that best represent the dataset is ultimately chosen by the user, commonly based on both (1) quantities such as Q/Q_{exp} that characterize the quality of the reconstruction, and (2) the physical plausibility of the factors. PMF solutions for a given number of factors are not mathematically unique, i.e. linear transformations ("rotations") of the factor time series and source profiles may result in an acceptable fit to the data with similar but slightly larger values of Q (Paatero and Hopke, 2009). The PMF algorithm minimizes the Q value. A subset of approximate linear transformations can be explored in PMF using the FPEAK parameter. The FPEAK=0 solution is has the minimum possible Q value. Each FPEAK increment represents a discrete solution by the PMF algorithm with a particular Q value, which must be evaluated by the end user. In this study, we use the PMF2 algorithm in robust mode with default convergence and outlier criteria values. We evaluate the analysis using the recently-developed PMF Evaluation Tool (PET) (Ulbrich et al., 2009).

2.2 Data preparation

The VOC data discussed in Chapter 3 were used for the PMF analysis presented here. However, canister measurements from the University of California, Irvine (UCI canisters) and the Georgia Tech CO measurements were not used for the analysis; only VOC data from the NOAA GC-FID and PIT-MS instruments were used in the PMF analysis. PIT-MS measurements were averaged over GC-FID sampling periods (Figure 3.1, Table 3.1) for the period from March 11-27, 2006. Periods when either instrument was off line were excluded from the PMF analysis. The data matrix for the analysis presented here consisted of 851 simultaneous measurements (rows) from the GC-FID and PIT-MS instruments, arranged so that 18 columns contain the time series of 18 species from the GC-FID, 12 columns contain the time series of 12 VOCs quantified by PIT-MS, and the final 35 columns contain the time series of 35 PIT-MS ion signals not quantified (65 columns total). The 35 PIT-MS ion signals chosen were not identified as specific molecules, but all did show a significant signal during the campaign, and we use PMF here to obtain information on the possible source of the corresponding VOCs.

For the GC-FID data we used 5 pptv or 5%, whichever number was larger, to calculate errors for PMF analysis. Errors for the PIT-MS data were calculated using ion counting statistics (de Gouw and Warneke, 2007). The error for 11 PIT-MS masses with signal to noise ratios (SNR) less than 2 was increased by a factor of 4, as is typical for the PMF method (Ulbrich et al., 2009;Paatero and Hopke, 2003). None of the measurements considered in the analysis had a SNR < 1. Error was increased for only one quantified PIT-MS mass (m/z 129, naphthalene). Results of

PMF analysis and an estimate of the uncertainties involved in this analysis are discussed in Section 4.

3 The PMF Solutions

PMF solutions with 1 to 7 factors were examined using the method described in section 2.3. A three-factor solution was chosen based on the plausibility of the results, with factors identified as traffic, LPG leakage, and secondary + long-lived species, as described in more detail below. This solution has $Q/Q_{exp} = 4.07$ at FPEAK 0, which suggests that the errors may be somewhat underestimated or that there is substantial variability in the dataset that cannot be modeled well with a few fixed chemical profiles. Q/Q_{exp} increases by less than 10% over the range in FPEAK from -5 to +5. Over the narrower FPEAK range from -3 to +3, Q/Q_{exp} increases by 2% compared to the FPEAK 0 solution. Measurements from each instrument contributed 44 ± 0.1 % (GC-FID) and 56 ± 0.1 % (PIT-MS) to the parameter (Q) over the range from FPEAK -3 to +3. About 20% of the value of Q could be attributed to unidentified PIT-MS signal.

Source profiles for the 3-factor solution are shown in Figure 4.1. The first factor, referred to as "traffic", is comprised of hydrocarbons including highly reactive species and was easily recognized as the VOCs observed in the early morning when primary emissions accumulated in a shallow boundary layer and in the absence of significant chemical removal. The profile of the second factor, named

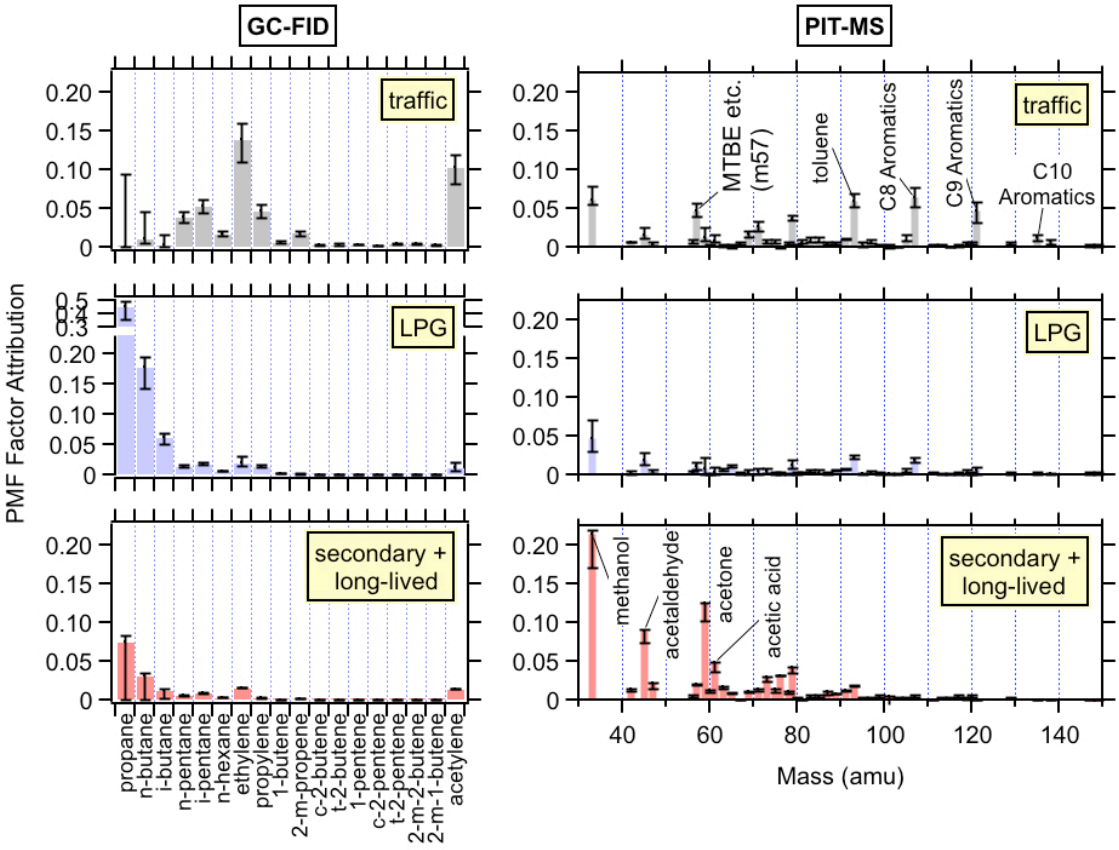

Figure 4.1. PMF profiles for compounds measured by the NOAA GC-FID (left column) and NOAA PIT-MS (right column) instruments for the three factors labeled traffic, LPG, and secondary + long-lived species. Error bars represent the variation in PMF factors from the FPEAK=0 solution (solid bars) over the FPEAK range from -3.0 to +3.0 as described in the text.

"LPG," contains propane and other small alkanes and is likely associated with LPG leakage. The third factor is named "secondary + long-lived species" and is comprised of more inert hydrocarbons and oxygenated species, and resembles the VOCs observed in more processed air masses observed during the day. In PMF solutions with 4 or more factors, additional factors resembled combinations of the three factors and did not provide additional insight into the data. Despite the presence of gas-phase chemical tracers for biogenic emissions (e.g. isoprene), biomass burning (e.g. acetonitrile), and known industrial emissions within the MCMA (Fortner et al., 2009), no factors were identified in the PMF analysis that were direct representations of these emission sources. A more detailed individual description of the three factors can be found below.

3.1 Robustness of the PMF Solutions

To study how robust the presented PMF solutions are, Figure 4.2 shows the variability in apportionment of a few important VOCs over the range of FPEAKS -3 to +3. Changes in the apportionment of individual compounds with FPEAK have no clear preference based on physical interpretations. For example, the apportionment of n-butane to the three factors changes sharply at FPEAKS above +1.5, where n-butane is attributed almost completely to the LPG factor, consistent with its expected source from LPG leakage as discussed above; however, the apportionments at FPEAKs less than -0.5, with significant contributions of n-butane to the traffic and secondary + long-lived species are also plausible and consistent

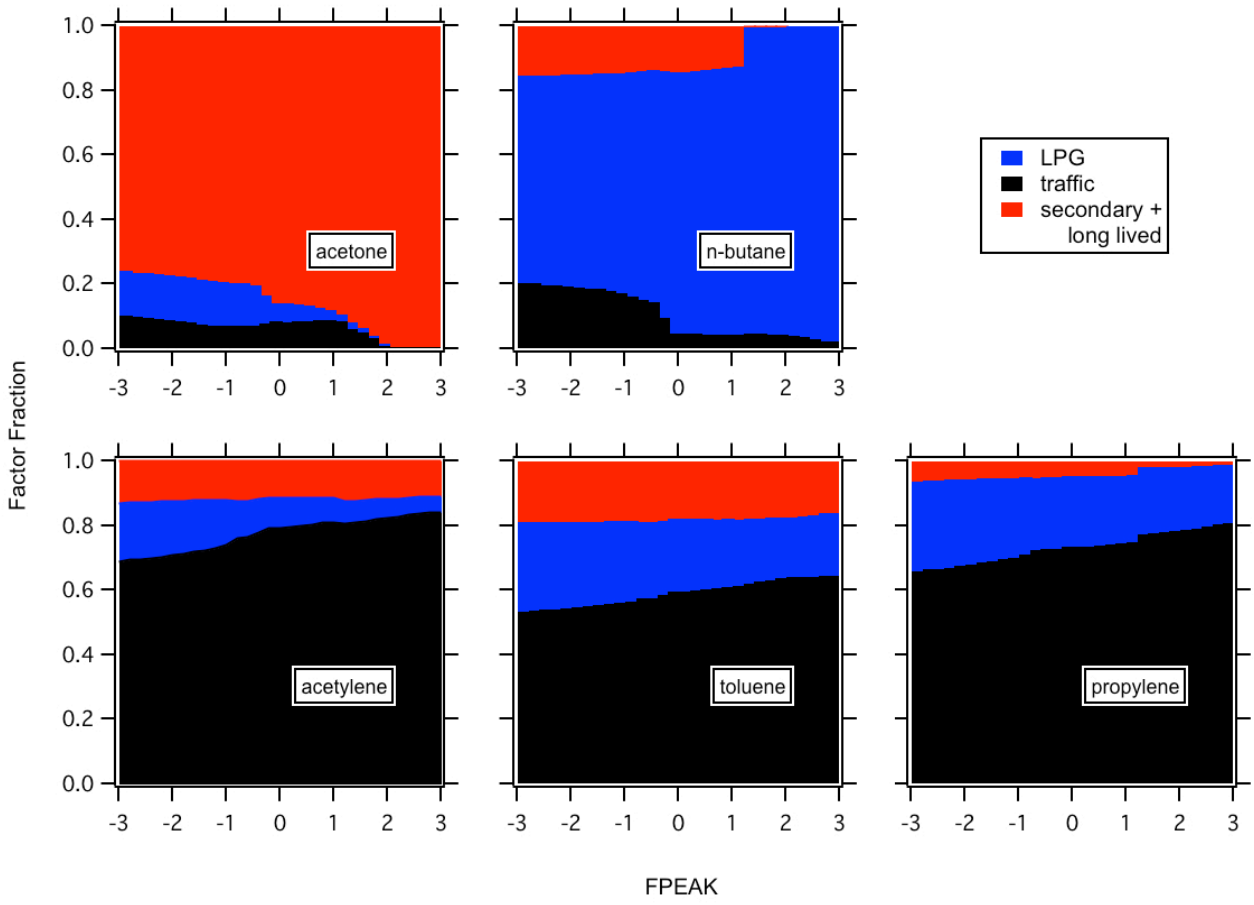

Figure 4.2 Variability in factor apportionment as a function of the PMF rotational parameter FPEAK for acetone, n-butane and three hydrocarbons dominated by traffic emissions (acetylene, toluene and propylene). The change in the PMF quality of fit parameter is less than 2% for the FPEAK values shown. The variability in factor fraction over the range of FPEAK from -3 to 3 is used here as an uncertainty of the PMF solution.

with the lifetime of n-butane and its emissions in vehicle exhaust. Acetone shows an opposite behavior with respect to FPEAK, where solutions with FPEAK > +2.0 apportion acetone exclusively to the secondary + long-lived species factor, which does not reflect its known sources from traffic. Thus, no single FPEAK value produces a solution that is uniquely the best. Therefore, the solutions presented herein are for FPEAK 0 while the range of solutions with FPEAK of ± 3 are used as an estimate of the uncertainty in the factor profiles and time series. We speculate that some of the variability in apportionment with FPEAK in this analysis is explained by the lack of strong contrast in the time trends of different species during the night when all direct emissions accumulate in the shallow boundary layer and chemical processing of the air mass is at its daily minimum. Other methods used to estimate uncertainties in the analyses, e.g. bootstrapping and seed variation (Ulbrich et al., 2009), were investigated but gave smaller variation in factor profiles. The three-factor solution was investigated as a function of the weighting errors assumed for the GC-FID and PIT-MS data. None of the observed variation changed the conclusions drawn here in any significant way. A more comprehensive analysis of the effects on PMF analysis of relative weighting of the data from different instruments can be found elsewhere (Slowik et al., 2010).

3.2 Diurnal Variability in the PMF Solution

The averaged diurnal variation in the factor time series is shown in Figure 4.3. Briefly, the traffic factor consists of aromatics, alkenes, alkanes and acetylene,

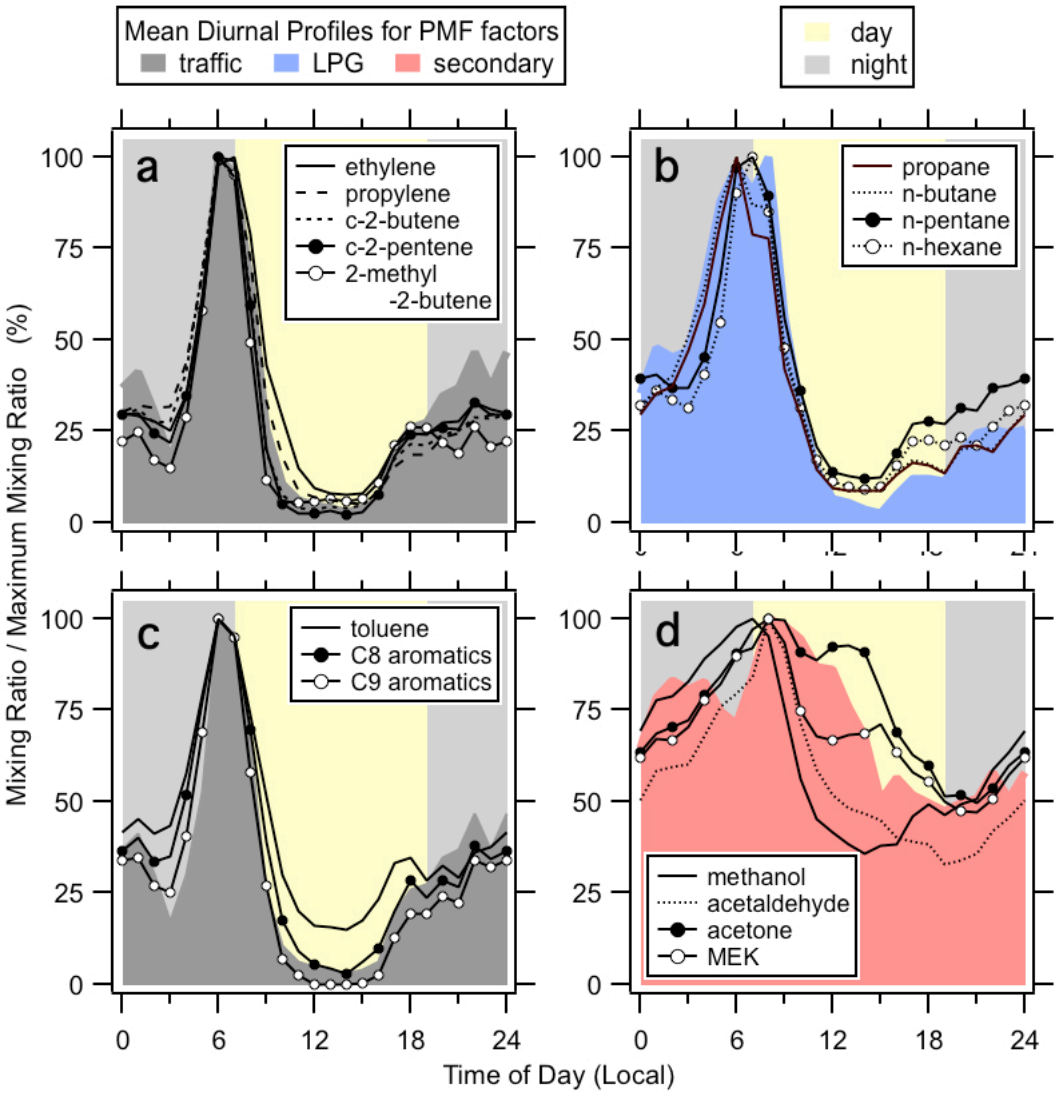

Figure 4.3. Measured VOC profiles as a function of local time (UTC - 6 hours) normalized to the maximum of the mean mixing ratio for individual compounds within chemical families: alkenes (a), alkanes (b), aromatics (c) and OVOCs (d). Normalized mean profiles for PMF factors (FPEAK=0) are shown as shaded areas for each chemical family.

and is at its maximum in the early morning. The LPG factor consists predominantly of propane, n-butane and i-butane and also has a maximum in the morning. The secondary + long-lived species factor is at its maximum about 2 hours later than the traffic factor and falls off much more slowly after sunrise. The averaged diurnal variations in factor time series were overlaid with the VOC data in Figure 4.3. The more reactive the compound, the faster it decreased with time after sunrise. The traffic factor closely follows the average diurnal variations in the more reactive alkenes and aromatics. The LPG factor is very similar to the measured diurnal variations in propane and other alkanes. The secondary + long-lived species factor does not directly match the diurnal variation of any single oxygenated species, but approximates the ensemble average diurnal variation of the oxygenated species shown.

3.3 PMF Time Series Reconstructions

The PMF reconstructions of the time series of selected VOCs are shown for acetylene, n-butane and acetone at FPEAK 0 in Figure 4.4. The variability in acetylene measurement is well described by the PMF time-series reconstruction (r^2=0.89) and the majority of this compound is attributed to traffic sources. The variability in n-butane is also reasonably well described by the PMF time-series reconstruction (r^2=0.76). In this case, most of the signal is attributed to LPG leakage. The measurement of acetone and its PMF time-series reconstruction (Fig. 4.4c) correlate well (r^2=0.93) and most of the signal is attributed to

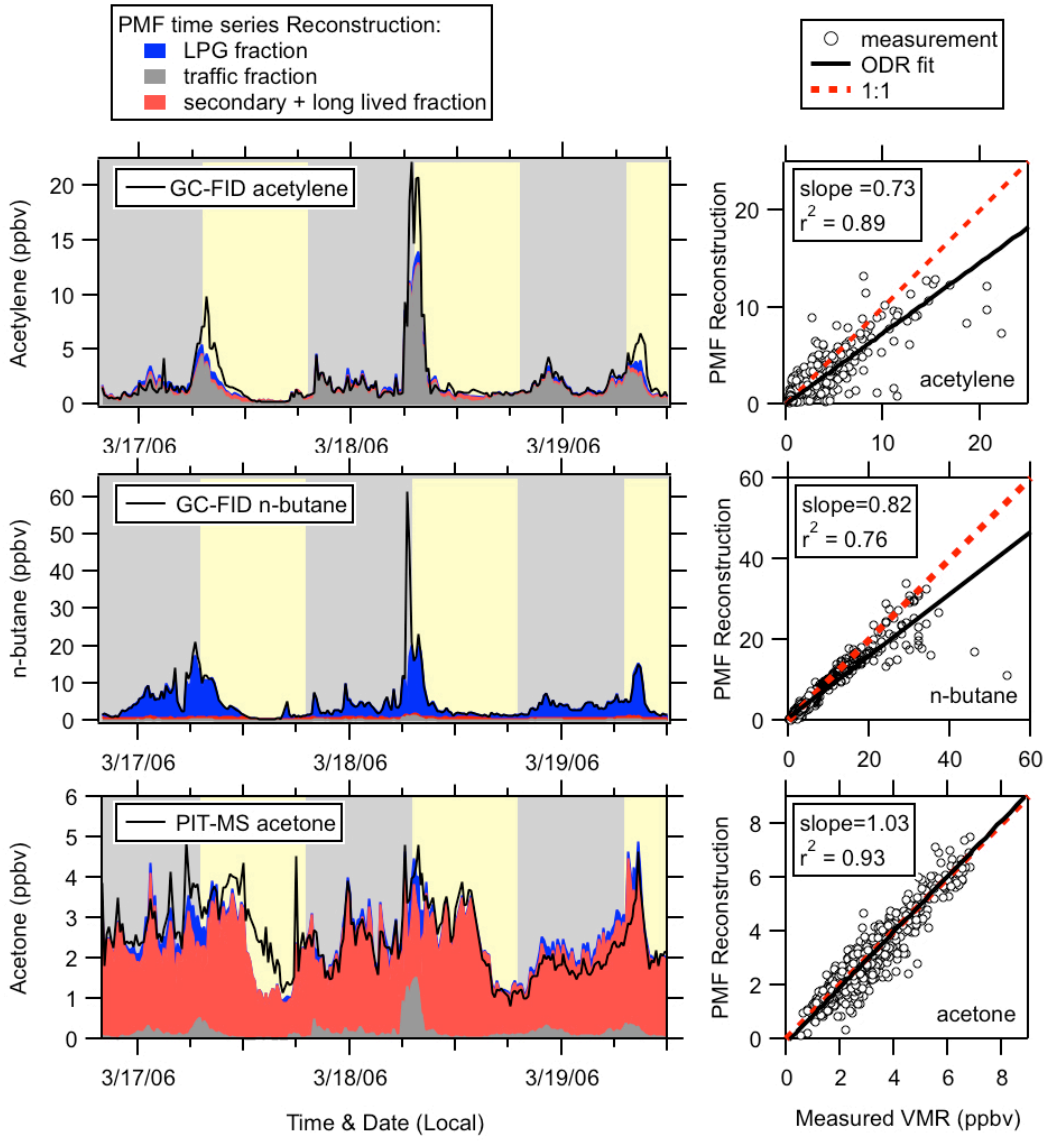

Figure 4.4. Selected comparisons between measurements and PMF reconstructions for one period during the MILAGRO campaign. The left column shows time series for representative compounds with dominant apportionment to the traffic factor (acetylene), the LPG factor (n-butane) and the secondary + long-lived factor (acetone). Measurements are shown as solid black traces for comparison. On the right are scatter plots of PMF reconstructions versus measurements showing single-sided fits (black) and 1:1 lines (red) for the same compounds.

the secondary + long-lived species factor with a smaller contribution from the traffic factor. Large residuals between measured and reconstructed concentrations were frequently correlated with simultaneous spikes in several VOCs without corresponding changes in CO mixing ratios. Examples of such spikes can be seen in Figure 4.4 for acetylene and n-butane, and they suggest the presence of local emissions, which are difficult to capture with PMF if the plume composition is sufficiently different from the dominant sources of variation.

Time series reconstructions for other species were compared to the measurements (results not shown here). Linear correlation coefficients were high for C7-C10 aromatics, alkenes and acetylene ($r^2 > 0.85$) and slightly lower for methanol, acetone, acetaldehyde and MEK ($0.82 < r^2 < 0.90$). PMF reconstructions for alkanes and the C11-aromatics correlated reasonably well with measurements ($0.60 < r^2 < 0.88$). Much lower correlations were found for acetonitrile ($r^2=0.42$), acetic acid ($r^2=0.48$), and naphthalene ($r^2=0.55$). Correlations for these species did not improve significantly even when PMF solutions with more than three factors were considered. Poor fits for time series reconstructions of these compounds suggest that they have important sources that are not correlated with the three factors identified here. For acetonitrile, the explanation may be the presence of biomass burning sources (de Gouw et al., 2009b) that were not identified as a separate factor in the PMF analysis. For other species (e.g. naphthalene and the C11 aromatics), signal to noise may explain part of this observation. For acetic acid, where signal to noise was high, the reason for the poor fit is not known.

4. PMF Factors During the MILAGRO Campaign

4.1 PMF Traffic Factor

The profile of the traffic factor is shown in Figure 4.1 (top panels). The profile is dominated by alkenes and aromatics. C5 and higher alkanes are also present. The only OVOC with significant partitioning to the traffic factor was methanol. Methanol mixing ratios were substantial during MILAGRO and have likely contributions from tailpipe and other vehicular sources previously observed by vehicle emission studies in the MCMA (Rogers et al., 2006) or by industrial sources. The PIT-MS product-ion signal at 57 amu was predominantly apportioned to the traffic factor, which is consistent with the major contribution of the gasoline additive MTBE to m57 (~80%), as determined by GC-PIT-MS (Chapter 3). Other product ion signals with significant presence in the traffic factor are at 69, 71, 83 and 85 amu. The signals at 69 and 71 amu are typically used to quantify isoprene and its photoproducts MVK and methacrolein by PTR-MS. This analysis suggests that the importance of other species with traffic-related sources (such as the presence of C5-alkenes at 71 amu shown in Chapter 3) at these masses in Mexico City can be is also suggested by the results of PMF analysis. The absence of a PMF factor representing biogenic emissions for compounds measured at m/z 69 and 71 by PIT-MS is consistent with the observations discussed previously (Chapter 3) for theses masses (e.g. low mixing ratios during the day, good correlation with CO and the GC-PIT-MS results shown in Chapter 3).

4.2 PMF LPG Factor

The LPG factor profile is dominated by the three light alkanes (propane, n-butane and i-butane) associated with the use of liquefied petroleum gas in the MCMA (Figure 4.1, middle panel) (Vega et al., 2000;Blake and Rowland, 1995;Velasco et al., 2007). The reconstruction of n-butane in the 3-factor PMF solution is compared with its measurement in Figure 4.4 (middle panel). The three major LPG alkanes also contribute to the traffic factor, possibly because LPG is used as a vehicle fuel (Diaz et al., 2000), and also to the secondary + long-lived species factor, due to their lower reactivity with the hydroxyl radical (k_{OH}) as discussed below. However, the contribution of propane to these factors is strongly dependent on FPEAK (Fig. 4.2) and therefore not quantified well by this analysis.

Other compounds apportioned to this factor include other light alkanes (pentane and hexane), some traffic-related VOCs, methanol and also a few unidentified PIT-MS signals (m/z > 100) but the amount of signal associated with the LPG factor for these other VOCs strongly depends on FPEAK. The diurnally averaged profile for the LPG factor has a similar shape to that of the traffic factor, but has a larger magnitude and wider morning maximum (Figure 4.5) probably due to the longer photochemical lifetime of major LPG species.

4.3 PMF Secondary + Long-Lived Species Factor

The profile for the secondary + long-lived species factor consists of mostly oxygenated compounds: methanol, acetone, acetaldehyde, acetic acid, methyl ethyl

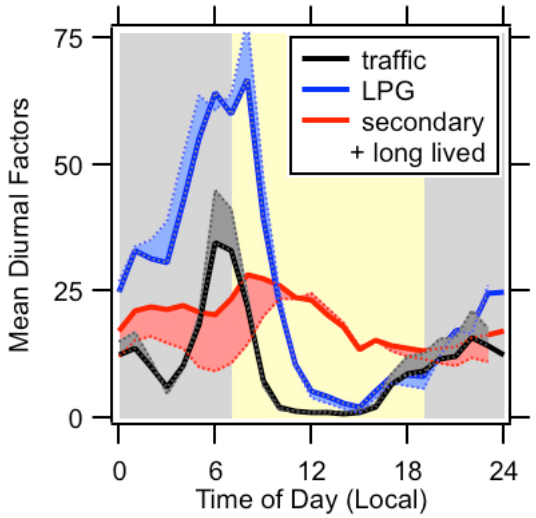

Figure 4.5. Mean diurnally averaged profiles for the 3-factor PMF solution obtained from MILAGRO VOC measurements. Solid lines represent the mean diurnal profile for each factor at FPEAK 0 while the shaded regions bordered with dashes show the variation from the FPEAK = 0 solution over the FPEAK range from -3.0 to +3.0. FPEAK range from -3.0 to +3.0.

ketone (MEK), and formic acid. For all quantified OVOCs except acetic acid, at least 66% of the measured concentration was explained by this factor. Good agreement was found between PMF reconstructions and measurements of methanol, acetone, acetaldehyde, and MEK-(slopes > 0.90 and r^2 > 0.80). Although acetic acid, formic acid and acetonitrile received majority apportionment to the secondary + long-lived species factor, measurements of these compounds correlated poorly (r^2 < 0.50) with PMF reconstructions. Variations in the mixing ratios of these 3 compounds were not well described by the PMF analysis. These results could suggest additional sources for these compounds. However, instrument precision also limits the degree of correlation for these species.

The relative contribution to the secondary + long-lived species factor increased with FPEAK for all quantified OVOCs and acetonitrile. Because OVOCs have known vehicular emission sources (Rogers et al., 2006), the near absence of OVOCs from the traffic factor at FPEAKS > 2.0 provides a physical constraint on the results of PMF analysis. An example of such a change in the apportionment of an OVOC is shown for acetone in Figure 4.2.

A comparison of measurements and PMF reconstructions for acetone are shown in Figure 4.4 (bottom left panel). The diurnal average for the PMF secondary + long-lived factor looks similar to the measured diurnal profiles of OVOCs (Figure 4.1.d), although diurnally averaged measurements of OVOCs show considerably more variation as a group than the hydrocarbons do.

PIT-MS product-ion signals at masses 75, 87, 89, and 101 amu were mainly attributed to the secondary + long-lived factor. This suggests the presence of OVOCs

at these masses. Specifically, it is possible that propanoic and butanoic acids contributed to the signal at masses 75 and 89.

5. Application of PMF results to VOC measurements

5.1 Estimation of VOC emission ratios using PMF results

Linear regression (ODR) of individual PMF factors plotted versus CO showed that the traffic factor correlated well with CO (r^2=0.86) in the predawn period but showed poor correlation ($r^2 < 0.50$) after noon. The LPG and secondary + long-lived species factors showed poor correlation with CO in the morning (4-7 AM LT) but stronger correlations in the afternoon (1-4 PM, LT) (r^2 = 0.81, 0.77 respectively). To estimate urban emission ratios for VOCs and OVOCs in the MCMA from the PMF results, the sum of the contributions of the traffic and LPG factors were plotted against CO ($r^2 < 0.42$) measurements for the 30 compounds quantified and reported during the campaign plus formic acid (m/z 47). The slopes of the resulting plots are presented in Table 4.1 for both VOCs and OVOCs.

The relative uncertainties (1σ) in the slopes of the linear regression used to calculate PMF-derived emission ratios were small (1- 3%) for all compounds. Uncertainty in PMF-derived emission ratios was also assessed using changes in apportionment as a function of the PMF FPEAK parameter. The maximum relative difference in apportionment from FPEAK 0 over the range from FPEAK -3 to 3 for the sum of the traffic and LPG source profiles was larger (4%-100%) than the regression uncertainty for all compounds. The sums of the relative uncertainties for

Table 4.1 Comparison of emission ratios versus CO for VOCs measured by GC-FID and PIT-MS during the MILAGRO campaign versus those calculated from PMF analysis of the same data.

Compound	Measurement (pptv [ppbv CO]$^{-1}$)	PMF (pptv [ppbv CO]$^{-1}$)
Alkanes		
propane	61.7 ± 15.6	43.5 ± 4.1
n-butane	21.7 ± 5	17.3 ± 1.5
i-butane	7.2 ± 1.6	6 ± 0.5
n-pentane	2.5 ± 0.2	2.6 ± 0.3
i-pentane	3.3 ± 0.4	3.4 ± 0.4
n-hexane	1.49 ± 0.16	1 ± 0.1
Alkenes		
ethylene	7 ± 0.4	7.1 ± 0.9
propylene	3 ± 0.2	2.8 ± 0.4
1-butene	0.35 ± 0.02	0.32 ± 0.04
2-methyl propene	0.85 ± 0.04	0.76 ± 0.11
cis-2-butene	0.18 ± 0.02	0.16 ± 0.02
trans-2-butene	0.2 ± 0.02	0.16 ± 0.02
1-pentene	0.152 ± 0.011	0.15 ± 0.02
cis-2-pentene	0.1 ± 0.009	0.09 ± 0.02
trans-2-pentene	0.19 ± 0.017	0.17 ± 0.03
2-methy 2-butene	0.179 ± 0.019	0.15 ± 0.02
2-methyl 1-butene	0.14 ± 0.011	0.14 ± 0.02
Alkynes		
acetylene	6.5 ± 0.3	5 ± 0.7
Aromatics		
toluene	4.2 ± 0.4	4 ± 0.4
Σ C8 aromatics	4.3 ± 0.6	3.8 ± 0.5
Σ C9 aromatics	2.8 ± 0.6	2.3 ± 0.4
Σ C10 aromatics	0.76 ± 0.15	0.6 ± 0.14
Σ C11 aromatics	0.16 ± 0.03	0.12 ± 0.01
naphthalene	0.12 ± 0.01	0.11 ± 0.01
Oxygenates		
methanol	2.1 ± 0.5	6.1 ± 2.1
acetaldehyde	1 ± 0.3	2 ± 0.9
formic acid	0.22 ± 0.11	0.4 ± 0.3
acetone	0.51 ± 0.13	1 ± 1
acetic acid	0.5 ± 0.2	0.5 ± 0.5
MEK	0.29 ± 0.07	0.5 ± 0.3
Other		
acetonitrile	0.27 ± 0.07	0.4 ± 0.1

each compound were used to calculate the absolute uncertainties in PMF-derived emission ratios shown in Tables 4.3 and 4.4.

Emission ratios calculated from PMF results are compared to values calculated directly from VOC measurements (and previously described in Chapter 3) in Figure 4.6 and 4.7. Individual points represent VOC species and are colored according to the PMF factor that explained the majority of the variation of that species. Emission ratios estimated for compounds mainly associated with traffic and LPG emissions were systematically lower by 20% than those derived directly from measurements, while the values of PMF-derived emission ratios for secondary + long-lived compounds were larger by an average of 80%. As described in Chapter 3, emission ratios for OVOCs were calculated only from the measured data from 04:00 to 07:00 local time, when the direct emissions should dominate the variability of these species. Emission ratios for OVOCs estimated from the traffic + LPG factors from the PMF analysis attempt to include only the directly emitted fraction of the OVOCs. Thus, both methods used here for calculating OVOC emission ratios attempt to correct measurements for secondary production. Uncertainty in the emission ratios calculated from PMF results is dominated by the uncertainties in the PMF results, particularly strongly for OVOCs.

5.2 Limitations of the PMF analysis as applied to VOC measurements

Some limitations of the application of PMF to VOC mixing ratios became apparent over the course of this work. First, the bilinear un-mixing model makes

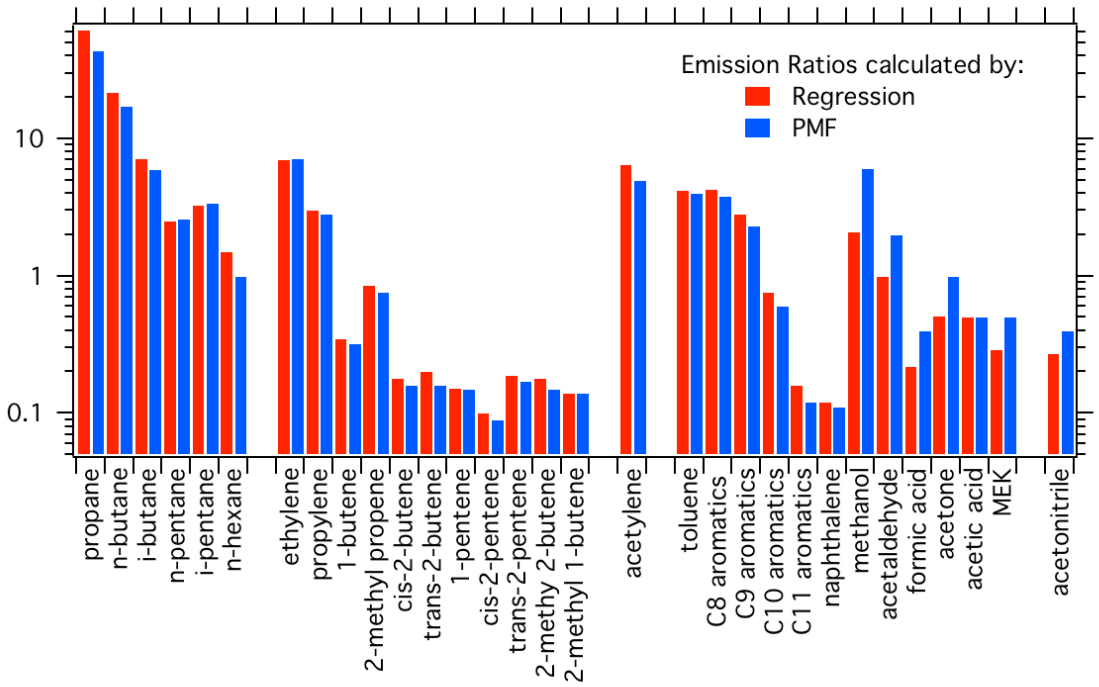

Figure 4.6 Graphical comparison of emission ratios to CO calculated by regression (red) and from PMF analysis results (blue).

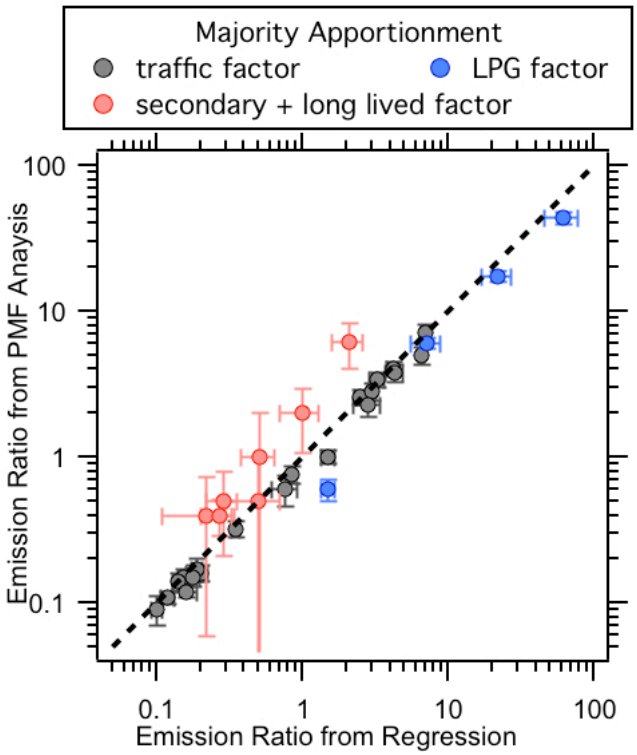

Figure 4.7. Comparison of PMF emission ratio estimates to those calculated from linear regression of measurements. Each point represents one compound while colors represent the dominant PMF apportionment for the respective measurement.

the assumption that the species identified together in one factor occur in constant relative proportions over the entire measurement period. However, individual VOCs and OVOCs have photochemical lifetimes (k_{OH}) that span several orders of magnitude, and so VOCs emitted from a single source are removed in the atmosphere at very different rates and thus the ratios of their concentrations will change continuously. This helps explain the way individual VOCs are apportioned between the factors. For example, the traffic factor closely matches the diurnal variability of the shortest-lived compounds that have low mixing ratios, while primary hydrocarbons with long lifetimes are partially explained by the secondary + long-lived species factor in proportion to their photochemical lifetimes (Figure 4.8), because they are still present in highly processed air. As another example, strict interpretation of the PMF factors (Fig. 4.1) as sources would suggest that a small portion of toluene and methanol can be attributed to LPG leakage and that benzene and propane are partially attributed to secondary formation, even when this contradicts our knowledge of the sources of these compounds. Thus, the PMF factors identified for this dataset reflect the convolution of VOC sources, timing of emissions, and VOC lifetimes, and interpretation of the factor profiles strictly in terms of different sources is inappropriate.

Second, for this dataset, the fraction of the variation for some important LPG and OVOC species (e.g., n-butane and acetone) explained by each factor was strongly dependent on the FPEAK parameter (Fig. 4.2). Known characteristics of sources and lifetimes for these VOCs did not help to significantly narrow the range of FPEAKs of

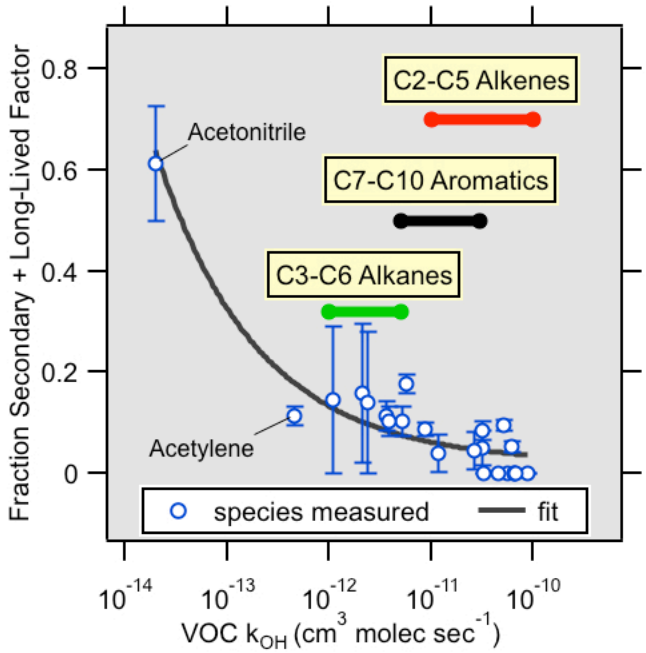

Figure 4.8. PMF apportionment of measured compounds to the secondary + long-lived factor plotted versus the rate coefficient for the reaction with OH radicals (k_{OH}) (Atkinson and Arey, 2003). Longer lifetimes (lower k_{OH}) are associated with higher secondary + long-lived source apportionment. Colored bars represent the range of lifetimes by compound class for alkanes (green), aromatics (black) and alkenes (red). Error bars represent variability in apportionment due to PMF FPEAK parameter from -3 to 3.

plausible or physically reasonable solutions. For some species, therefore, it is difficult to quantify the fraction emitted by particular sources with much certainty.

6. Conclusions

Positive Matrix Factorization analysis performed on the combined data from the two NOAA instruments allowed the identification of 3 dominant factors attributed to traffic, LPG usage and secondary production plus long-lived species, respectively. These factors described much of the variability in VOC mixing ratios, especially for compounds with vehicular and liquid propane gas sources. OVOCs and compounds with long photochemical lifetimes were identified as a single factor in the analysis. PMF solutions with more than 3 factors resulted in splitting of major factors rather than the identification of minor emission sources. The PMF analysis did not identify distinct factors consistent with industrial, biomass burning or biogenic VOC emissions. Factor profiles (grouping of VOC species) are influenced by both sources and photochemical lifetimes of individual VOCs.

PMF results were also used in a novel way to estimate emission ratios for VOCs and OVOCs. Estimates agreed within uncertainties with the corresponding emission ratios derived directly from measurements for most hydrocarbons typically associated with vehicle usage. PMF-derived emission ratios were about 20% lower and 80% higher for light alkanes and OVOCs respectively.

In this Chapter, we have evaluated the PMF method as it applies to VOCs. We conclude that PMF describes major sources of VOCs well, but strongly caution against the over-interpretation of PMF factors as strictly corresponding to actual

sources of VOCs. In this analysis, we show that PMF factors are sensitive to the photochemical lifetimes of individual compounds, which can lead to blending of factor source profiles. As a result, PMF solutions may not be unique with respect to rotation and can lack a clear physical interpretation.

CHAPTER 5

SHIP-BASED MEASUREMENTS OF HIGHLY REACTIVE VOCS DURING THE 2006 TEXAQS CAMPAIGN AND COMPARISON WITH AN INDUSTRIAL EMISSION INVENTORY

1. Introduction

Houston, Texas is the fourth largest city in the United States and routinely has some of the highest observed ozone mixing ratios in the country. The area is highly industrialized and has one of the highest concentrations of petrochemical industrial facilities in the U.S. (Parrish et al., 2009;Ryerson et al., 2003). In the Houston area, co-located emissions of NO_x and VOCs from industry, power plants and vehicles lead to very efficient production of ozone. The 2000 Texas Air Quality Study (TexAQS 2000) identified large industrial emissions of the highly reactive VOCs (HRVOCs) propylene and ethylene as important contributors to ozone formation in the area (Kleinman et al., 2005;Jobson et al., 2004;Ryerson et al., 2003;Wert et al., 2003;Kuster et al., 2004). Ryerson (2003) estimated that the emissions of these compounds were underreported by an order of magnitude or more in emission inventories. In contrast, NO_x emissions are much more accurately reported and were found to agree well with emission inventories (Ryerson et al., 2003).

An automated sampling network established in the Houston area since the 2000 study routinely shows highly elevated levels of propylene and ethylene. Positive Matrix Factorization (PMF) analysis of the data from this network in 2001

and 2003 identified industrial factors with high correlations to propylene and ethylene measurements (Kim et al., 2005;Xie and Berkowitz, 2006;Buzcu and Fraser, 2006).

In 2006, a second major field campaign was conducted in the Houston area (TexAQS 2006). Characterizing the emissions of propylene and ethylene (de Gouw et al., 2009a;Parrish et al., 2009;Mellqvist et al., 2010;Washenfelder et al., 2010) was one of the major objectives of the campaign due to the high ozone-production potential of the two compounds. VOC measurements from both the 2004 and 2006 campaigns were used to calculate OH reactivity in the Houston area (Gilman et al., 2009;Jobson et al., 2004), which can be used as a proxy for ozone formation potential. Gilman (2009) observed an OH reactivity of up to 200 s^{-1} in industrial plumes during the 2006 campaign based on VOC measurements onboard the research vessel Ronald H. Brown. In contrast, marine air from the Gulf of Mexico had a maximum OH reactivity of 1.4 s^{-1} and an average of 1.0 s^{-1} (Gilman et al., 2009).

Industrial emissions of many pollutants are regulated by the U.S. EPA and must be reported (Frost, 2009). In the Houston area, industrial emissions are reported to and compiled by the Texas Commission on Environmental Quality (TCEQ). The critical evaluation of the reported emissions of not just ethylene and propylene, but a range of VOCs, was an important objective of TexAQS 2006 and for that purpose the research vessel Ronald H. Brown sampled in close proximity to numerous industrial sources, including during several transects of the Houston Ship Channel. Two instruments were used to measure VOCs. An in-situ GC-MS collected

5-min samples every half hour and analyzed these for >80 VOCs [Gilman et al., 2009]. A subset of these VOCs was measured with a 10 second time resolution by PIT-MS. For the purpose of emissions evaluation, the high time resolution of the PIT-MS was an advantage over GC-MS in characterizing industrial plumes in close proximity to the sources. In this Chapter, PIT-MS measurements from the 2006 TexAQS field campaign will be used to characterize such plumes in the Houston Ship Channel and from nearby areas where large VOC plumes were observed by both GC-MS and PIT-MS instruments. Here, we compare the measurements of some HRVOCs in large industrial plumes to emissions reported from nearby industrial facilities in the emission inventory. Using PIT-MS measurements, we can assess the temporal and compositional variability of major industrial emissions in the area, at least for the subset of HRVOCs that can be measured by the technique. We also evaluate previous observations that emissions of HRVOCs are underreported by 1-2 orders of magnitude by estimating the fluxes directly from the measurements and by comparing mixing ratios for VOCs and NOx to observations expected based on compiled inventory values.

2. Methods

2.1 Measurements

The measurements used in this analysis were made during the second Texas Air Quality Study (TexAQS 2006) onboard the NOAA research ship Ronald H. Brown between July 27 and September 11, 2006. Figure 5.1 shows a map of the study area

and the ship track near Houston, Texas. All gas phase measurements were made from inlets located on an 8 m tall tower on the bow of the ship, approximately 20 m above the water. VOC measurements by GC-FID/MS and PIT-MS instruments were made from a common inlet from a 15 m long Teflon line with a sample flow of 7 liters per minute. More detailed descriptions of the measurements used in this work can be found elsewhere (Gilman et al., 2009;Lerner et al., 2009;Tucker et al., 2010) and only a brief overview will be presented here. Wind velocity, ship velocity and location were obtained from official cruise data from the R/V Ronald H. Brown at a frequency of 1 min^{-1}.

2.1.1 NOAA GC Measurements

A field-portable two-channel gas chromatograph instrument was used to quantify VOCs during the campaign [Gilman et al., 2009]. Every half hour, two separate 5-minute *in situ* air samples were cryogenically collected. The first sample was injected into an 18 m PLOT column and analyzed for light hydrocarbons (C2-C5 alkanes, C2-C5 alkenes, and acetylene) by flame ionization detection (GC-FID). This channel was configured and operated in a manner similar to that described for the GC-FID used during the MILAGRO campaign (Chapter 3). The second sample was injected on a DB-624 capilary column and detected by an Aglilent 5973 electron impact quadrupole mass spectrometer (GC-MS instrument). The GC-MS method was used to quantify 100+ VOCs including the C5–C9 alkenes, C6–C9 aromatics, C1–C5 alcohols, C2–C7 aldehydes and ketones, acetonitrile, and several monoterpenes

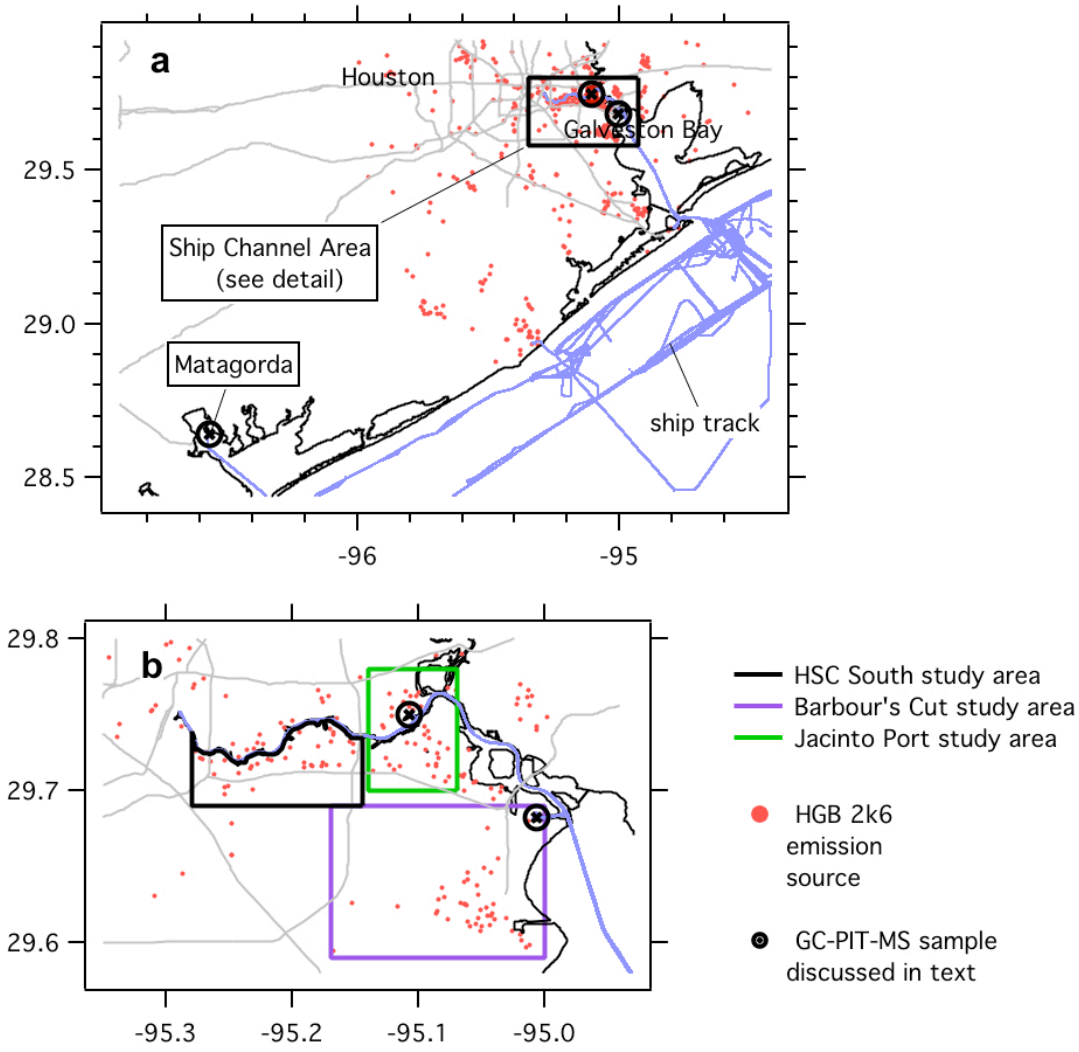

Figure 5.1. Map of the (a) areas visited by the R/V Ronald Brown during the TexAQS 2006 field campaign and (b) study areas in the Houston Ship Channel area.

among others (Goldan et al., 2004;Gilman et al., 2009).

Detection limits ranged from about 1-10 pptv for most quantified VOCs by GC-FID/MS. Field calibrations for many compounds were made and referenced to laboratory calibrations made before and after the campaign. Calibration accuracy is estimated to be 15% for VOCs and 25% for OVOCs (Gilman et al., 2009).

2.1.2 PIT-MS

During TexAQS, the PIT-MS instrument (Chapter 2) provided simultaneous measurements of product ions with mass to charge ratios (*m/z*) from 33 to 200 amu at a frequency of 5 min^{-1}. VOCs and OVOCs were quantified based on previous product ion signal identification in the literature (de Gouw and Warneke, 2007). Configuration of the PIT-MS instrument was similar to that used during the MILAGRO study described in Chapter 3. In addition to quantified VOCs, PIT-MS detected numerous VOCs in industrial plumes in the Houston area. Table 5.1 summarizes the relevant mass to charge ratios where signal was observed. A more detailed description of the PIT-MS instrument is presented in Chapter 2.

Calibrations using a gas standard were performed automatically every 2 hours and manually using multiple dilution steps approximately once per week. Calibration uncertainty is estimated at 20% for methanol, acetaldehyde, acetone, MEK, acetonitrile, and for benzene and toluene. Comparison with GC-FID/MS measurements showed that previously reported (Chapter 3) interferences in the PIT-MS benzene measurement from the acetic acid•water cluster could be corrected

Table 5.1. Compounds measured by PIT-MS compared to compounds listed in the HGB2K6 emission inventory. Names used in this work for individual mass to charge ratios represent our best understanding of the dominant compounds at that m/z.

PIT-MS Measurements		Inventory Comparison		
PIT-MS signal (m/z)	compounds observed (dominant)*	entries summed	detectable compounds summed	not reported or not included in inventory
	oxygenates			
m33	methanol	1	methanol	
m45	acetaldehdye	1	acetaldehyde	
m59	acetone, propanal, propylene oxide	2	acetone, propanal	propylene oxide
m73	methyl ethyl ketone (MEK), methyl propanal, tetrohydrofuran	2	MEK, butryaldehyde	butylene oxide, tetrahydrofuran
m87	unidentified oxygenate	2	methyl propyl ketone, valeraldhyde	
m101	unidentified oxygenate	2	methyl butyl ketones (MNBK, MIBK)	ethyl acrylate
	nitriles			
m42	acetonitrile	1	acetonitrile	
m54	acrylonitrile	1	acrylonitrile	
	aromatics			
m79	benzene	1	benzene	
m93	toluene	1	toluene	
m105	styrene	1	styrene	
m107	m,p,o-xylene, ethyl benzene	4	xylenes+ethyl benzene	
m121	6 aromatic isomers	6	6 aromatic isomers	acetophenone
m135	aromatic isomers		*not compared*	C10 aromatics
m149	aromatic isomers		*not compared*	C11 aromatics
	other			
m43	vinyl acetate, propylene, acetone, others		*not compared*	
m57	C4 alkenes, MTBE, acrolein	7	butene isomers, n-butanol, MTBE, acrolein	
m69	isoprene/furan, cyclopentenes, pentadienes, others	2	isoprene, cyclopentene	pentadienes, furan
m71	C5 alkenes, methyl vinyl ketone (MVK), methacrolein (MACR)	7	pentenes, methyl butenes, crotonaldehyde	MVK, MACR
m85	C6 alkenes, other unidentified	1	hexene isomers	
m137	monoterpenes	2	α-pinene, β–pinene	limonene

*Mostly likely dominant compounds during the TexAQS 2006 campaign based on measurements presented here and from GC-FID/MS measurements from the same cruise (Gilman et al., 2009).

during the TexAQS campaign by subtracting approximately 20% of the acetic acid (m61) signal considerably improving the correlation between the measurements made by the two instruments. The reason that this correction did not work during the MILAGRO campaign is not known. Calibration uncertainty for the C8-and C9-aromatics is estimated to be 50%.

Using average calibration factors, we report here mixing ratios for signals interpreted as industrial oxygenates at m87 and m101, and for C11 aromatics, acrylonitrile, and industrial emissions observed at m43, m57, m69, m71, m85, and m137. In many cases, these masses showed signal from multiple isobaric compounds and have large (>50%) uncertainties. Identification of compounds contributing to signal at different m/z during TexAQS 2006 is based on GC-FID, GC-MS and GC-PIT-MS and also on industrial VOCs reported in the emission inventory.

2.1.3 GC-PIT-MS

In order to distinguish isomers and identify unknown compounds detected by PIT-MS, a GC pre-separation (GC-PIT-MS) was used on about 40 occasions onboard the R/V Ronald Brown. In GC-PIT-MS mode, the PIT-MS instrument is coupled to a gas chromatograph outfitted with a temperature programmed DB-624 column as described in more detail elsewhere (Warneke et al, 2003). GC-PIT-MS has been used on several different occasions for this purpose (Bon et al., 2011, Warneke et al., 2011) and is also described in Chapter 3. Air samples are collected in a liquid-nitrogen cooled cryogenic trap prior to injection onto the GC column.

During TexAQS 2006, unlike during the MILAGRO campaign (Chapter 3), the PIT-MS instrument was configured such that it continued to monitor ambient air during the 5-minute cryo-collection of the air sample, thus allowing the comparison of the on-line PIT-MS measurement with the off-line GC-PIT-MS measurement. GC-PIT-MS produces a chromatogram for each of the about 180 product ion masses monitored by PIT-MS. While measuring the column effluent, the PIT-MS was operated with a time resolution of 2 seconds. The typical VOC peak width was 4 seconds or less and therefore peaks were under-sampled and cannot be used for precise quantification. Because the column is the same as that used for the NOAA GC-MS, identification of unknown VOCs can often be made based on the elution order of the peaks.

2.1.4 Measurement of NO_X

NO_x measurements are the sum of nitric oxide (NO) and nitrogen dioxide (NO_2) measurements. NO was quantified on the research cruise using a chemi-luminescence method described elsewhere (Lerner et al., 2009). To measure NO_2, it was converted to NO by photolysis using a mercury lamp (185 nm) and then detected by chemi-luminescence. Both measurements were calibrated using a NO gas standard obtained from Scott-Marrin, Riverside, CA. Zeros were performed each hour during the campaign. For plumes where NO_x > ~1 ppbv, the measurement accuracy is estimated as ± 7% (Lerner et al., 2009).

2.1.5 Mixing Layer Heights

Mixing layer heights used here for flux estimates were determined using the NOAA high-resolution Doppler lidar (HRDL) located on the stern of the Ronald H. Brown during the research cruise. HRDL uses wind, wind shear and velocity variance to determine the boundary layer depth and therefore the maximum height to which industrial VOC plumes will mix. A detailed description of the use of HRDL on the Ronald H. Brown during TexAQS 2006 can be found elsewhere (Tucker et al., 2010).

2.2 Houston-Galveston-Brazoria 2006 Point Source Emission Inventory

Throughout this work, we refer to the Revised Houston-Galveston-Brazoria 2006 Point Source Emission Inventory (referred to hereafter as HGB2K6), version 1, compiled by Greg Frost at NOAA in Boulder, CO. The inventory and a detailed description of how it was compiled is available online (Frost, 2009) and only a brief description will be presented here.

The HGB2K6 inventory is a bottom-up point source industrial emission inventory containing 506 industrial accounts based on emissions data reported to the Texas Commission on Environmental Quality (TCEQ). The accounts include refineries, chemical manufactures, power plants, shipping terminals, chemical storage facilities, waste processing sites, medical facilities, universities and government agencies, among others, which are required to report emissions of both gas and particle phase pollutants. HGB2K6 contains entries for major gas phase (e.g.

NO_x, CO, CO_2, SO_2) and particle phase emissions including speciated entries for hundreds of VOCs. Annual average emissions were updated to include hourly emissions provided by 86 accounts for the period from 15 August to 15 September, 2006 (Frost, 2009;Washenfelder et al., 2010). However, few facilities reported significant variability in emissions over the course of the 2006 TexAQS 2006 campaign.

For the purposes of comparison with PIT-MS measurements, the HGB2K6 inventory was supplemented with the emissions reported to TCEQ of five compounds not included in the online version. These five compounds and the major mass to charge ratios where they are observed by PIT-MS are methyl tert-butyl ether (MTBE) (m57), acrolein (m57), acetonitrile (m42), crotonaldehyde (m71), and vinyl acetate (m43). Individual VOCs in the inventory detected by PIT-MS at the same m/z were summed to provide a subset inventory of VOCs detectable by PIT-MS. We summarize the VOCs in the inventory and how they were summed for comparison with PIT-MS measurements (m/z) in Table 5.1. We will refer to individual inventory accounts by their point number in the HGB2K6 inventory, numbered consecutively from zero.

For comparison with PIT-MS measurements, individual HGB2K6 sources were grouped into batches based on the location of an observed VOC plume and wind direction at the time of the plume. Figure 5.1 shows the inventory source batches used for Barbour's Cut (43 accounts), Jacinto (39 accounts) and the Houston Ship Channel (35 accounts). Plume compositions by %VOC from PIT-MS mixing ratios (in ppbv) are compared with %VOC reported by the sum of reported

emissions (molec sec^{-1}) of VOCs visible to PIT-MS for one or more account. We will note in the text and figures where accounts have been summed for comparison to plume compositions measured by PIT-MS.

3. Results and Discussion

3.1 Measurement Comparisons between GC-MS and PIT-MS

Measurements made by the GC-FID/MS and the PIT-MS instruments made onboard the ship were compared in order to evaluate data quality. The complex and unusual composition of VOCs in the Houston area poses a significant analytical challenge for PIT-MS instrument in particular, which primarily uses the product ion mass for compound identification. For the purpose of the comparison, PIT-MS data were averaged over the sampling periods of the GC-MS instrument. Scatter plots of PIT-MS versus GC-MS data are shown in Figure 5.2. A brief discussion of the findings follows next.

Oxygenates. PIT-MS measurements of oxygenates (Figure 5.2) during TexAQS did not agree with GC-MS measurements as well as in past studies using the PIT-MS instrument (de Gouw and Warneke, 2007;Warneke et al., 2005b). For methanol (m33) and acetone + propanal (m59), PIT-MS measurements were systematically lower than those of the GC-MS (slope 0.6 and 0.7 respectively). The m59 measurements were highly correlated with the GC-MS measurements (r^2=0.97), while methanol did not correlate as well (r^2=0.72). Acetaldehyde

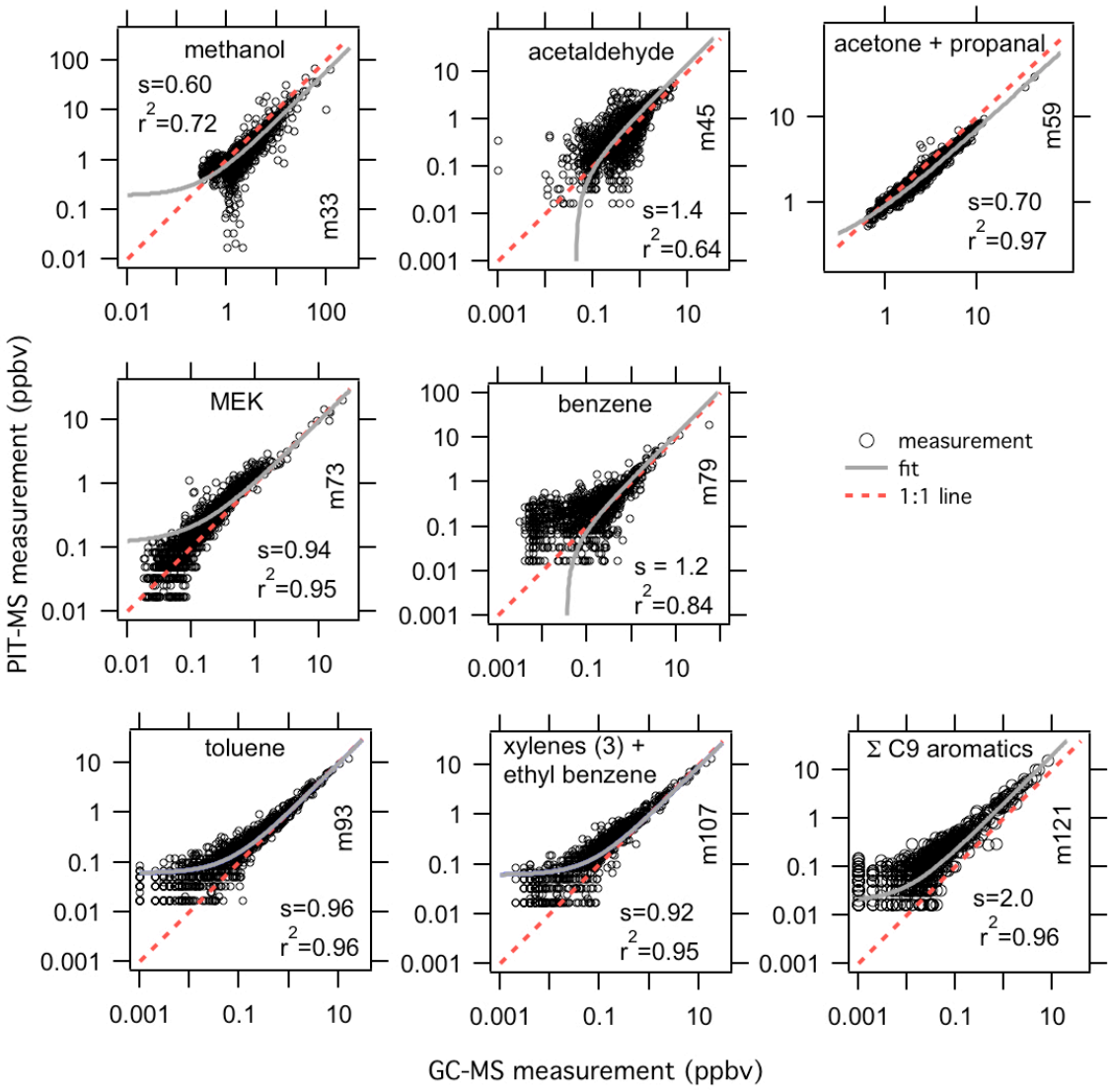

Figure 5.2. Comparison of select PIT-MS versus GC-MS measurements. Where GC-MS measurements of isobaric compounds have been summed, the number of compounds summed is reported in parentheses. Slopes from 2-sided fits and correlation coefficients are shown for each comparison.

measurements by PIT-MS (m45) were systematically larger for PIT-MS (slope 1.4) and correlations were similar to those for the methanol comparison (r^2=0.64). MEK (m73) did compare well between the two instruments (slope=0.94, r^2=0.95). Exact reasons for these disagreements are not known.

Aromatics. Benzene, toluene and m107 (xylene isomers + ethyl benzene) compared within expected uncertainties (20%) during the campaign. The C9 aromatics measured by PIT-MS were a factor of 2 higher than the sum of the isomers measured by GC-MS. This is within the range of measurements at this m/z previously reported and similar the difference between PIT-MS and the UCI Canisters observed during MILAGRO campaign (Chapter 3).

Industrial Compounds. In this work a number of PIT-MS measurements are compared with inventory entries for a variety of industrial compounds. Figure 5.3 shows the result of comparison of PIT-MS signals at m43, m54, m57, m69, and m71 with GC-MS measurements of industrial compounds that contribute to the corresponding PIT-MS signals.

Propylene is detected at m43 by PTR-MS (Karl, 2003;Kuster et al., 2004). However, during TexAQS 2006, other compounds contributed to PIT-MS signal at this mass including vinyl acetate (see section 3.2.2). The scatter plot versus the GC-MS analysis shows poor agreement between measurements of propylene and the PIT-MS m43. In this work, m43 has not been interpreted or reported as propylene.

Acrylonitrile was observed at m54 during the study. The results of the comparison of PIT-MS and GC-MS are shown in Figure 5.3. At high mixing ratios (i.e. in industrial plumes), the agreement between the two methods is close to 1:1. At

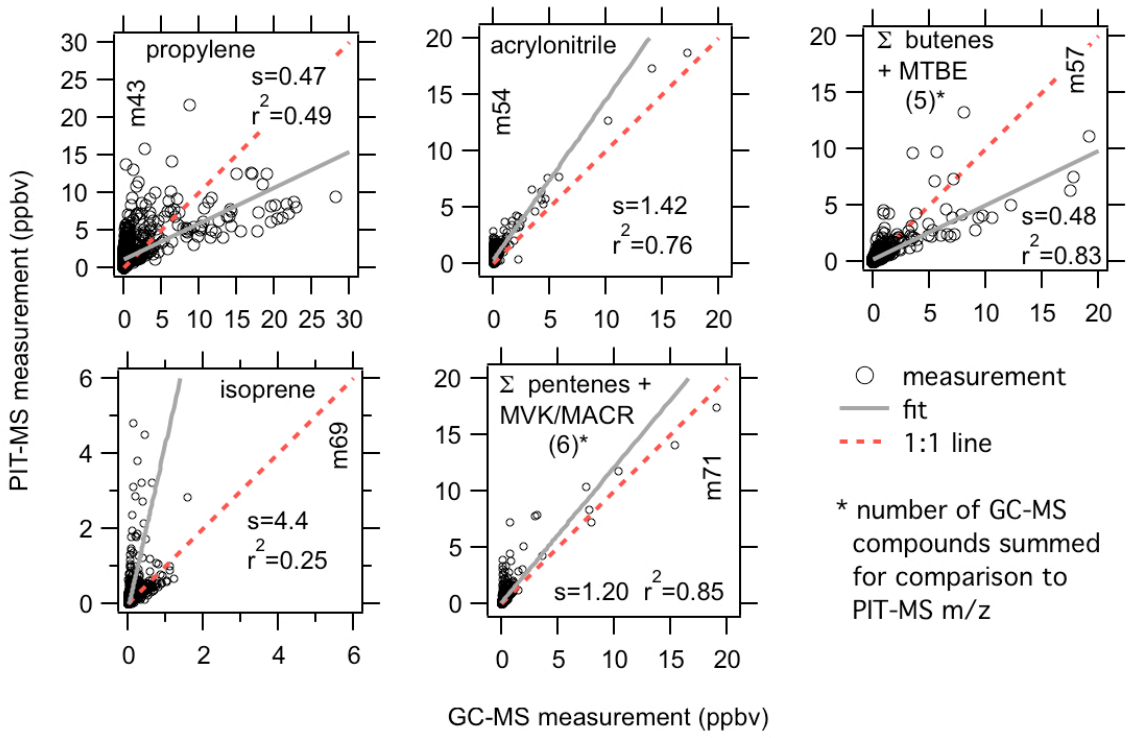

Figure 5.3. Comparison of selected GC-MS measurements with PIT-MS measurements at the corresponding product ion masses. Industrial plumes typically give rise to the highest mixing ratios in each plot. Where GC-MS measurements of PIT-MS isobaric compounds have been summed, the number of compounds summed is shown in parentheses. Slopes from 2-sided fits and correlation coefficients are shown for each comparison.

low mixing ratios, instrumental backgrounds are present in PIT-MS, and measurements at low mixing ratios should not be interpreted as acrylonitrile.

In the Houston area, signals at m57, m69 and m71 are dominated by industrial emissions, especially at high mixing ratios. For these species, PIT-MS measurements do not correlate well with GC-MS measurements. As we will show, however, the compositions of industrial VOC plumes are complex and variable and pose a substantial challenge to all analytical methods. Not all compounds measured in a plume are present in another plume at the same location at a different time. Differences in sensitivity of PTR-based instruments to different compounds at a particular mass to charge ratio are variable by about a factor ± 2 (de Gouw and Warneke, 2007). Such sensitivity differences can contribute to a lack of agreement between methods. However, some species measured by PIT-MS were not quantified (e.g. n-butanol) or even identified by GC-FID/MS (e.g., tetrohydrofuran, acrolein). As a result, comparisons between methods are inherently inexact, particularly at mass to charge ratios with multiple but common isobaric compounds. In Table 5.1, we define and summarize our use of PIT-MS m/z signals for comparison with industrial emissions in this Chapter. We note in the text additional compositional information where available.

3.2 GC-PIT-MS

GC-PIT-MS chromatograms illustrate the complexity and variability of mass assignment by PTR-based instruments in the Houston area. Separating compounds

by GC shows the extent to which the signal at one PIT-MS mass to charge ratio can be assigned to a particular compound or compounds. Mass assignments in industrial plumes can be very different than those typical in other environments.

GC-PIT-MS results for plumes from three different locations are shown in Figure 5.4. Many VOCs from industrial sources are observed in the chromatograms shown. Identifications of unknown compounds are based on PIT-MS m/z and elution order compared to the GC-MS, which is possible because both GC-MS and GC-PIT-MS use the same GC column. Locations where the three GC-PIT-MS chromatograms were collected are shown in Figure 5.1. These chromatograms are discussed in detail in the following three subsections.

3.2.1 GC-PIT-MS Matagorda

Figure 5.4a shows a GC-PIT-MS chromatogram collected near an industrial facility in Matagorda, TX on July 23 at just before 4 PM LT. Winds were about 4 m/s from the SE and the mixing height above the ship was about 650m. The R/V Ronald H. Brown visited the Matagorda area only one time by during the research cruise and industrial VOC emissions in this area are not included in the HGB2K6 emission inventory. Mixing ratios of benzene and isoprene measured by the PIT-MS instrument during the cryogenic collection of the air sample were high but variable with peaks at about 5 and 4 ppbv respectively. Notable compounds in this GC-PIT-MS chromatogram include isoprene, acetonitrile, acrolein, MVK, methacrolein, benzene, toluene and several of the C8 aromatic isomers. The GC-FID/MS sample at

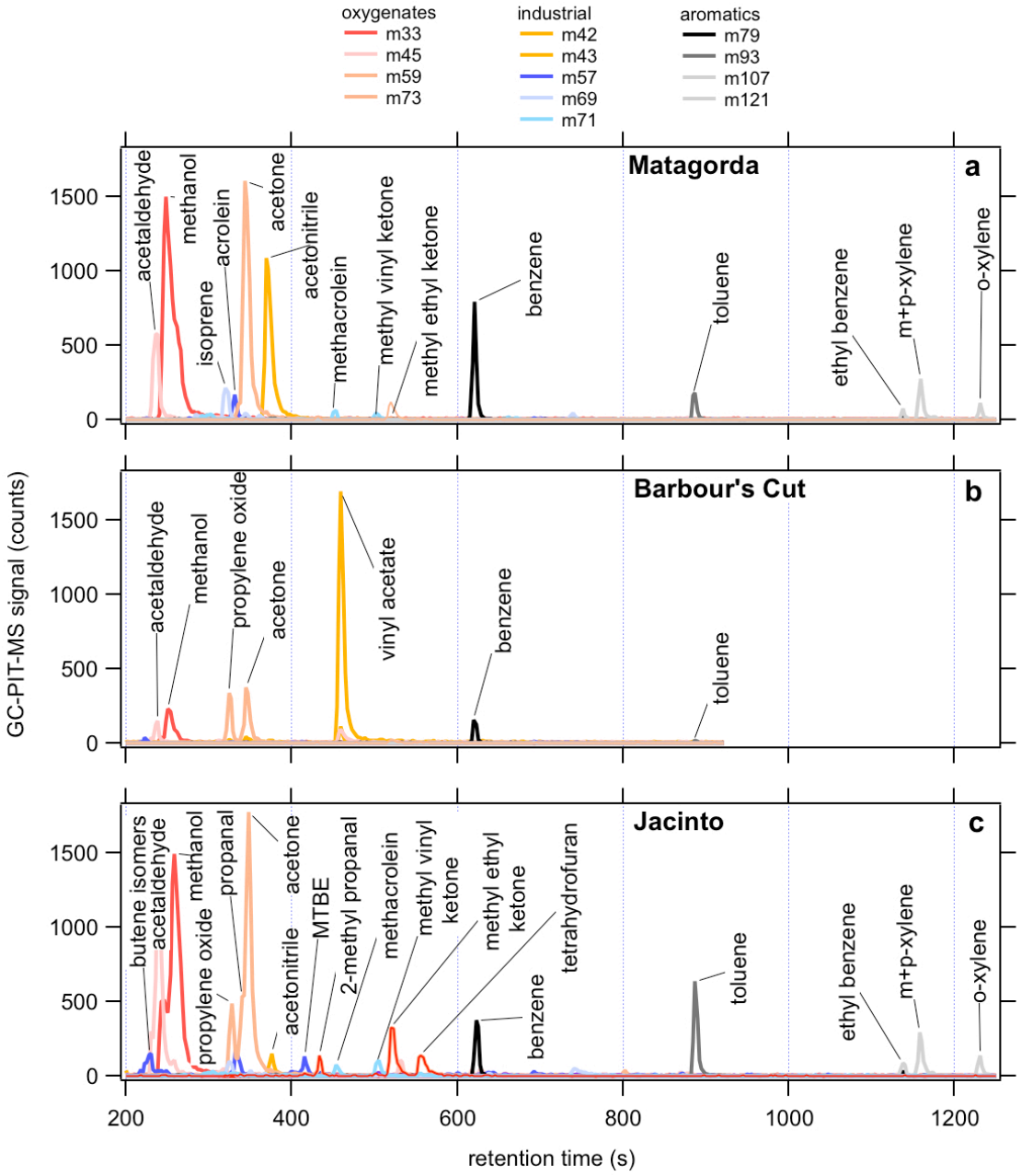

Figure 5.4. GC-PIT-MS chromatograms of industrial plumes from three different locations during the TexAQS 2006 campaign. The locations where samples were collected are shown in Figure 5.1. Peaks are identified by m/z and by retention time.

4 PM showed high mixing ratios of benzene (3.8 ppbv), isoprene (2.7 ppbv), 1-pentene (1 ppbv) and n-pentane (3.7 ppbv). The identity of most compounds observed in this plume are consistent with standard PTR-method mass assignments (de Gouw and Warneke, 2007). However, the presence of acrolein at m57 in the GC-PIT-MS is atypical for other environments (urban, biogenic, etc.) and suggests a direct industrial emission. The high mixing ratios and complex VOC composition are clearly indicative of an industrial plume.

3.2.2 GC-PIT-MS Barbour's Cut

A map of Barbour's Cut showing nearby VOC sources is shown in Figure 5.5. Other plumes observed at this site will be discussed in more detail in Section 4.1.1. The GC-PIT-MS sample shown in Figure 5.4b was collected in Barbour's Cut on August 14 at 9:40 PM LT. The wind during this event was 6 m/s from the south and the HRDL mixing height was 300m. Two peaks in the chromatogram clearly stand out. First, vinyl acetate was observed at m/z 43 and identified by GC-FID/MS using the electron impact ionization database in that instrument. Second, propylene oxide was identified by retention time in this plume at m59. The GC-FID/MS sample collected a few minutes later (10 PM LT) showed 76 ppb vinyl acetate and 9.3 ppb propylene oxide as well as smaller (< 5 ppb) enhancements in other VOCs including benzene, methanol, ethane and propane. Vinyl acetate plumes were observed on several occasions from Barbour's Cut, and this was the largest plume observed during the campaign. According to the HGB2K6, the largest source of this

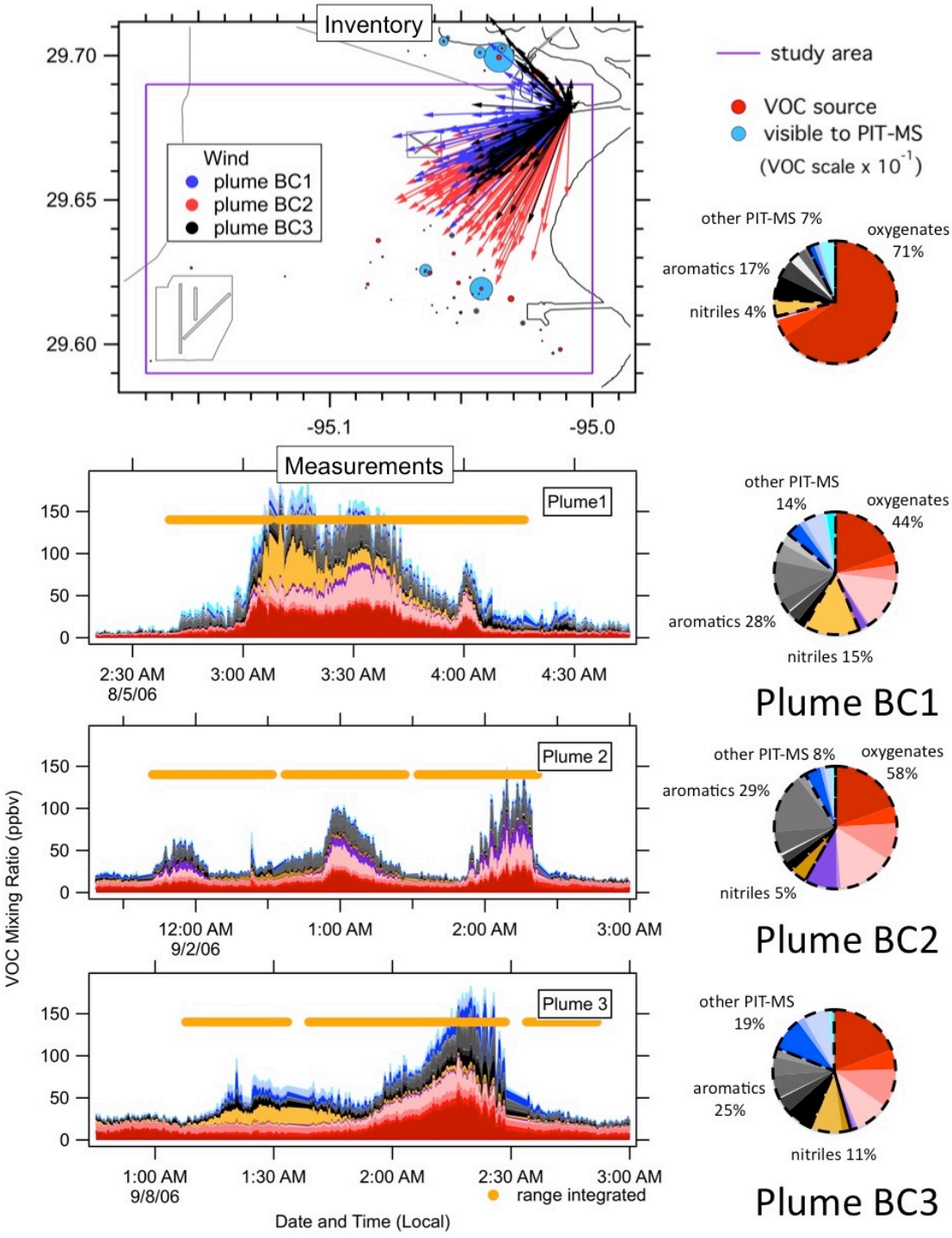
Inventory
29.70
29.65
29.60
-95.1
-95.0
Wind
plume BC1
plume BC2
plume BC3
study area
VOC source
visible to PIT-MS
(VOC scale x 10-1)
other PIT-MS 7%
oxygenates 71%
aromatics 17%
nitriles 4%
Measurements
Plume1
150
100
50
0
2:30 AM 8/5/06
3:00 AM
3:30 AM
4:00 AM
4:30 AM
other PIT-MS 14%
oxygenates 44%
aromatics 28%
nitriles 15%
Plume BC1
Plume 2
12:00 AM 9/2/06
1:00 AM
2:00 AM
3:00 AM
other PIT-MS 8%
oxygenates 58%
aromatics 29%
nitriles 5%
Plume BC2
Plume 3
1:00 AM 9/8/06
1:30 AM
2:00 AM
2:30 AM
3:00 AM
range integrated
other PIT-MS 19%
aromatics 25%
nitriles 11%
Plume BC3
VOC Mixing Ratio (ppbv)
Date and Time (Local)

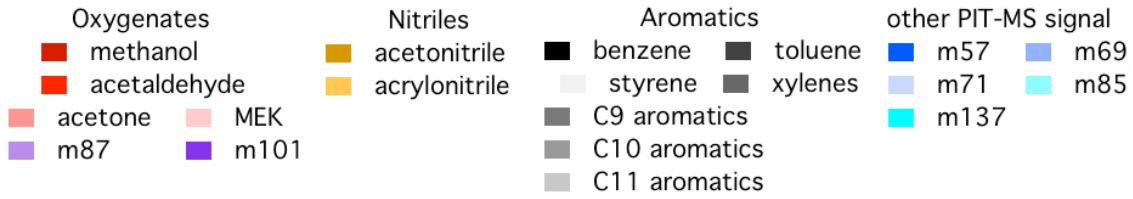

Figure 5.5. Comparison of the composition of the HGB2K6 emission inventory (top) to three plumes observed from Barbour's Cut. The winds were from the south-west during all three plumes. Inventory entries inside the purple box shown were summed for comparison with plumes. Plumes were integrated over the areas shown by the orange bars for each plume. VOC sources in the inventory are shown in red sized by emissions in molecules sec^{-1}. The subset of VOCs visible to PIT-MS are shown in blue with sizes scaled by a factor of 10 relative to the red markers.

compound in the area is 25 miles to the south in Texas City. There is a smaller source of vinyl acetate 3 miles to the northwest (visible in Figure 5.5) and smaller plumes of vinyl acetate were in observed from Barbour's Cut when the wind was from the north and west. The source of this large plume measured at Barbour's Cut is therefore not known. Vinyl acetate and propylene oxide clearly distinguish this plume as having an industrial origin.

3.2.3 GC-PIT-MS Jacinto Port

The Ronald H. Brown moored overnight at Jacinto Port on the northeast portion of the Houston Ship Channel (Figure 5.1). The sum of VOC mixing ratios measured by the PIT-MS instrument peaked at over 200 ppbv at this location (Figure 5.6). The GC-FID/MS instrument measured highly elevated mixing ratios (peaks > 1 ppm) of light (C3-C5) alkanes at Jacinto Port during this period.

The individual GC-PIT-MS chromatogram shown in Figure 5.4c was collected simultaneously with the 11 AM LT GC-FID/MS when winds were light winds (~1.5 m/s) from the SE with a HRDL mixing height of 440 m. At the time the chromatogram was taken, the sum of PIT-MS mixing ratios was about 100 ppb (Figure 5.6). Notable industrial emissions seen in this GC-PIT-MS chromatogram are aromatics, butene isomers (m57), tetrohydrofuran (m73), and propylene oxide (m59). Tetrohydrofuran and propylene oxide were identified by mass and retention time and are not typically observed on this mass in PTR-MS at other locations. Comparison of VOC measurements at Jacinto Port with the HGB2K6 industrial emission inventory will be discussed in Section 4.1.2.

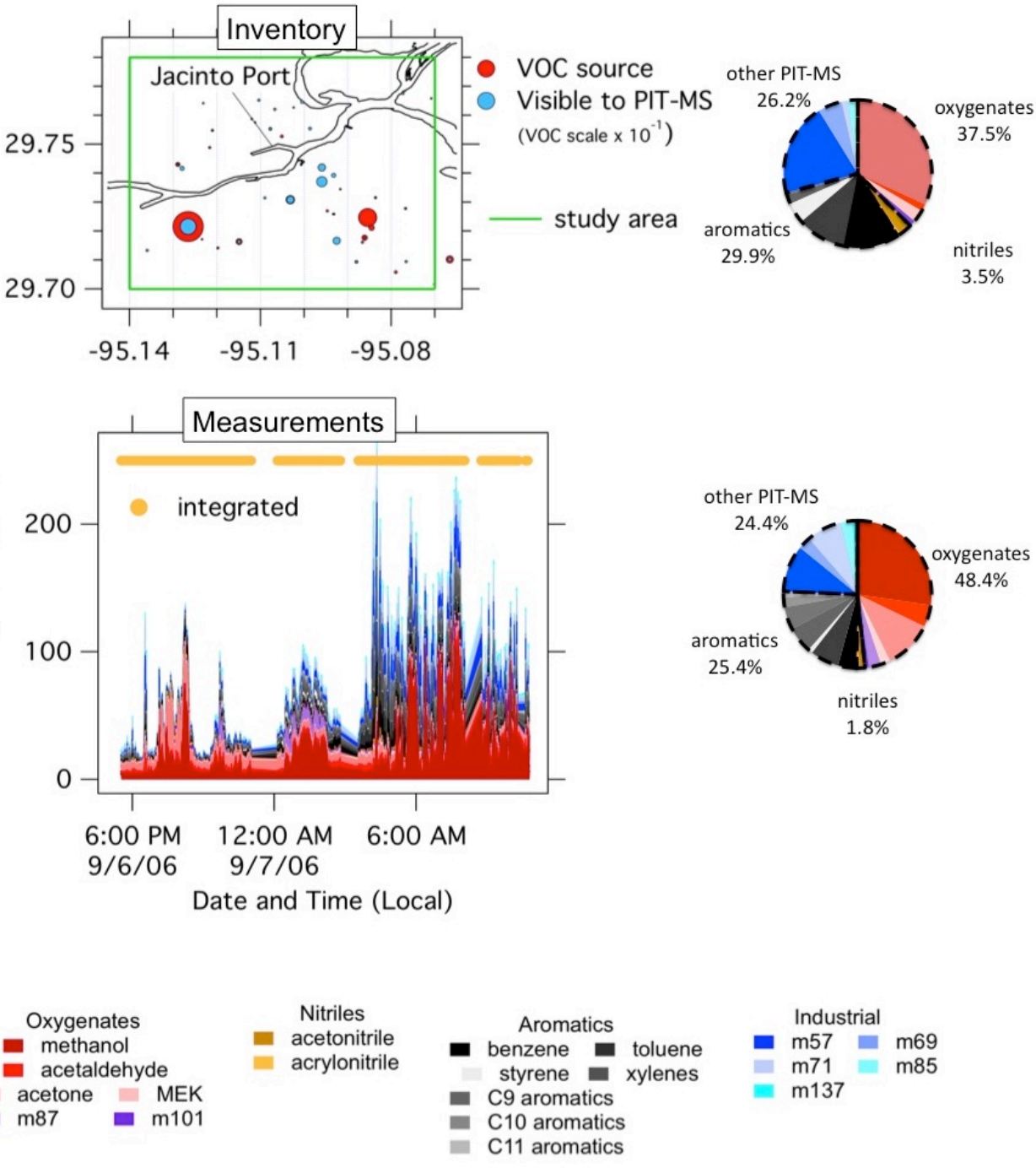
Inventory
Jacinto Port
29.75
29.70
-95.14
-95.11
-95.08
VOC source
Visible to PIT-MS
(VOC scale x 10^-1)
study area
other PIT-MS
26.2%
oxygenates
37.5%
aromatics
29.9%
nitriles
3.5%
Measurements
integrated
VOC mixing ratio (ppbv)
200
100
0
6:00 PM
9/6/06
12:00 AM
9/7/06
6:00 AM
Date and Time (Local)
other PIT-MS
24.4%
oxygenates
48.4%
aromatics
25.4%
nitriles
1.8%
Oxygenates
methanol
acetaldehyde
acetone
MEK
m87
m101
Nitriles
acetonitrile
acrylonitrile
Aromatics
benzene
toluene
styrene
xylenes
C9 aromatics
C10 aromatics
C11 aromatics
Industrial
m57
m69
m71
m85
m137

Figure 5.6. Comparison of the composition of the HGB2K6 emission inventory (top) measurements made over 13 hours in Jacinto Port. Inventory entries inside the green box shown were summed for comparison with measurements. Measurements were integrated over the areas shown by the orange bars for each plume. VOC sources in the inventory are shown in red sized by emissions in molecules sec^{-1}. The subset of VOC emissions visible to PIT-MS are shown in blue with sizes scaled by a factor of 10 relative to the red markers.

4. Methods for Comparison of Measurements and Inventory

In this section we will compare the VOC measurements made by the PIT-MS instrument to the HGB2K6 industrial emission inventory in three different ways. First, we will compare individual plumes as directly as possible to sources using the equivalencies shown in Table 5.1. Second, we will integrate measurements from two transects of the Houston Ship Channel for VOCs and NO_x and compare the results to the VOC:NO_x ratio from the inventory. Finally, we will calculate the absolute VOC flux for a single large VOC plume from the ship channel and compare it directly to the flux reported in the inventory for the plume source.

4.1 Individual Plumes

In this section we compare the compositions (%VOC by volume mixing ratio) of major (> 100 pbbv) plumes observed during TexAQS 2006 by PIT-MS in three different locations (Figure 5.1) with reported VOC composition data from the HGB2K6 inventory using the equivalencies shown in Table 5.1. As a metric for plume and inventory complexity, we define the parameter MC_{67} (measurement complexity) as the number of "compounds" (PIT-MS m/z signals) needed to account for 66.7% of the VOC by mixing ratio in a given plume. We will compare this directly to the parameter IV_{67} (inventory complexity), defined here as the number of "compounds" needed to account for 66.7% of the VOC emissions listed in the HGB2K6 inventory (%VOC by molecules sec^{-1}) using the equivalencies shown in Table 5.1. We note here that because there are multiple isobaric VOCs that can

contribute to PIT-MS signal at a given m/z, this metric represents a comparable but conservative estimate of the number of compounds in both cases.

4.1.1 Barbour's Cut

The R/V Ronald H. Brown spent many days and nights in Barbour's Cut to the south and east of the Houston Ship Channel (Figures 5.1 and 5.5). Three large (> 100 ppb) VOC plumes were observed when the winds were from the southwest on three different dates (between 1 AM and 4 AM LT). Wind velocities are shown in Figure 5.5 color-coded by plume. More than 540 individual PIT-MS measurement cycles were made in each plume totaling over 5 hours of continuous measurements. The HRDL instrument measured mixed layer heights between 50m and 200m during all three plumes at this location.

Inventory. The emissions from 43 individual sources were summed for comparison with PIT-MS measurements. The most likely source of the emissions is a cluster of industrial facilities located about 5 miles to the southwest of the ship's location. The pie charts in Figure 5.5 show speciated VOCs reported in the inventory (top) and from measurements of each of the three plumes. From the top pie chart, we obtain a value of IC_{67}=2. Thus, according to the inventory, two thirds of detectable PIT-MS instrument signal should come from just 2 compounds, methanol (65.6%) and benzene (6.4%). Other industrial emissions noted in the inventory and detectable by PIT-MS include toluene, acrylonitrile and hexene isomers (at m93, m54, and m85 respectively).

Plume BC1. Two thirds of VOCs detected by the PIT-MS instrument during this plume were accounted for by methanol, acrylonitrile, MEK, the C9 aromatics, m71 and the C10 aromatics (MC_{67}=6). The NOAA GC FID/MS was not operating during this plume.

Plume BC2. PIT-MS measurements were dominated in this plume by methanol, the C9 aromatics, MEK, acetone, and m101 (MC_{67}=5). GC-MS/FID measurements also showed 30 ppb of ethylene and 30 ppb of light alkanes (propane + n-butane + i-butane) during this plume, which are not detectable by PIT-MS.

Plume BC3. Methanol also dominated PIT-MS measurements of this plume followed by acetone, MEK, m57, acrylonitrile, benzene and m71 (MC_{67}=7). During the plume GC-FID/MS measurements showed considerable enhancements in propylene (17 ppb) and alkanes (n+i-pentane = 230 ppb, n+i-butane=130 ppb) that were not detectable by the PIT-MS instrument.

Conclusions for Barbour's Cut. The inventory lists methanol as the major emission from the area southwest of Barbour's Cut and this was observed by PIT-MS to be the case in all three individual plumes. However, proportions of both methanol and benzene are larger in the inventory than measurements by a factor of 3. At the same time, inventory proportions for toluene and MEK are larger than measurements by factors of 2 and 80, respectively. Considerable amounts (2-8%) of the C10 and C11 aromatics were observed by PIT-MS in plumes and not accounted for at all in the emission inventory. Speciated emission reporting is required only for benzene (C6) through the C9 aromatics (Frost, 2009).

The measured VOC composition of all three plumes was significantly more complex than that described by the inventory. And, while inventory values are static, plumes showed variability both within and between plumes. For example, the HRVOC acrylonitrile accounts about 5% of inventory emissions while plume averages were 14%, 0.3% and 9%. Although alkanes and alkenes are not detectable by PIT-MS, proportionate mixing ratios reported by GC-FID/MS differed considerably between plumes 2 and 3.

4.1.2 Jacinto Port

The plume shown in Figure 5.6 was observed overnight at the same location as the GC-PIT-MS chromatogram described above (Figure 5.6, map). Winds were light (1-2 m/s) and the daytime mixed layer of 500-1000 m dropped to about 100 m overnight before rising again after dawn. The measurement period for this plume was over 4700 individual PIT-MS cycles or 13 hours.

Inventory. The map in Figure 5.6 shows 39 individual inventory entries that were summed for comparison with measurements. The boxed area contains only a few large inventory sources of VOCs. Inventory emissions were dominated by emissions detectable by the PIT-MS instrument as methanol, m57, benzene and toluene (IC_{67}=4). For theses sources, the inventory suggests the PIT-MS signal at m57 should be 55% MTBE, 33% butenes, and 11% n-butanol.

Measurements. Integrated PIT-MS measurements at Jacinto Port are summarized in Figure 5.6 where MC_{67}=6. The six most abundant compounds

detectable by PIT-MS were methanol, acetone, m57, m71, toluene and the C8 aromatics. Large mixing ratios (> 1 ppm) of light alkanes (C3-C5) were also observed in the plume by GC-FID/MS (Section 3.2.3). The GC-PIT-MS chromatogram taken at Jacinto Port (Section 3.3) shows the presence of propylene oxide (m59), tetrahydrofuran (m73) and signals from several C4 alkene isomers + MTBE at m57.

Speciated GC-FID/MS measurements during the Jacinto Port sampling period show only two individual samples with large (≥ 5 ppbv) enhancements of MTBE with one large peak of 9.3 ppbv MTBE. Mixing ratios of the C4 butenes during the same GC-FID/MS sample exceded 25 ppbv. In addition, there were multiple large enhancements in the C4 butenes at Jacinto Port, the largest of which exceeded 60 ppbv. The ratio of C4 butene isomers to MTBE for all GC-FID/MS measurements made in the Houston and Galveston Bay area exceeded 6 (Gilman et al., 2009). We conclude that the majority of PIT-MS signal at m57 should be attributed to the C4 butene isomers rather than MTBE.

Although the proportion of methanol measured by PIT-MS in the Jacinto Port plume was relatively constant, proportional mixing ratios for other compounds measured by PIT-MS changed considerably during the measurement period (Figure 5.6). Proportions of compounds measured by GC-FID/MS (e.g., MTBE and alkenes) at this location were also variable as discussed above.

Conclusions for Jacinto Port. Measurements and the inventory agree that the dominant emission is methanol and that it makes up about 30% of the total VOCs detectable by the PIT-MS instrument. Measured proportions of other compounds do not agree as well. According to the inventory, benzene and m57

should respectively contribute factors of 3 and 2 more to PIT-MS signal. The inventory and measurements differ by a factor of 2 in the opposite direction for PIT-MS signal at m71 and for the C9 aromatics. Signal from the C10 and C11 aromatics, which are not represented in the inventory at all.

As we saw in Barbour's Cut, the observed VOC composition of emissions at Jacinto Port is significantly more complex than the inventory suggests ($6=MC_{67} > IC_{67}=4$). GC-FID/MS measurements show that there are at least 4 isomers of the C4 aromatics and MTBE contributing to the PIT-MS signal at m57 and the inventory suggests considerable emissions of n-butanol also contribute to PIT-MS signal. The GC-PIT-MS chromatogram shows considerable contamination of PIT-MS signals compounds at m59 (normally acetone) and m73 (normally MEK) by other industrial compounds. Proportions of VOCs in the plume also changed over time.

4.1.3 Houston Ship Channel

Analysis of measurements made during two of the eight transects of the Houston Ship Channel (HSC) by the Ronald H. Brown are presented here. These transects were selected because the wind was consistently from the south in both cases minimizing the possibility of contamination from other emissions sources in the area.

Transect 3 (Figure 5.7) occurred at night while transect 4 (Figure 5.8) occurred the following morning. Similar VOC plumes were observed at similar

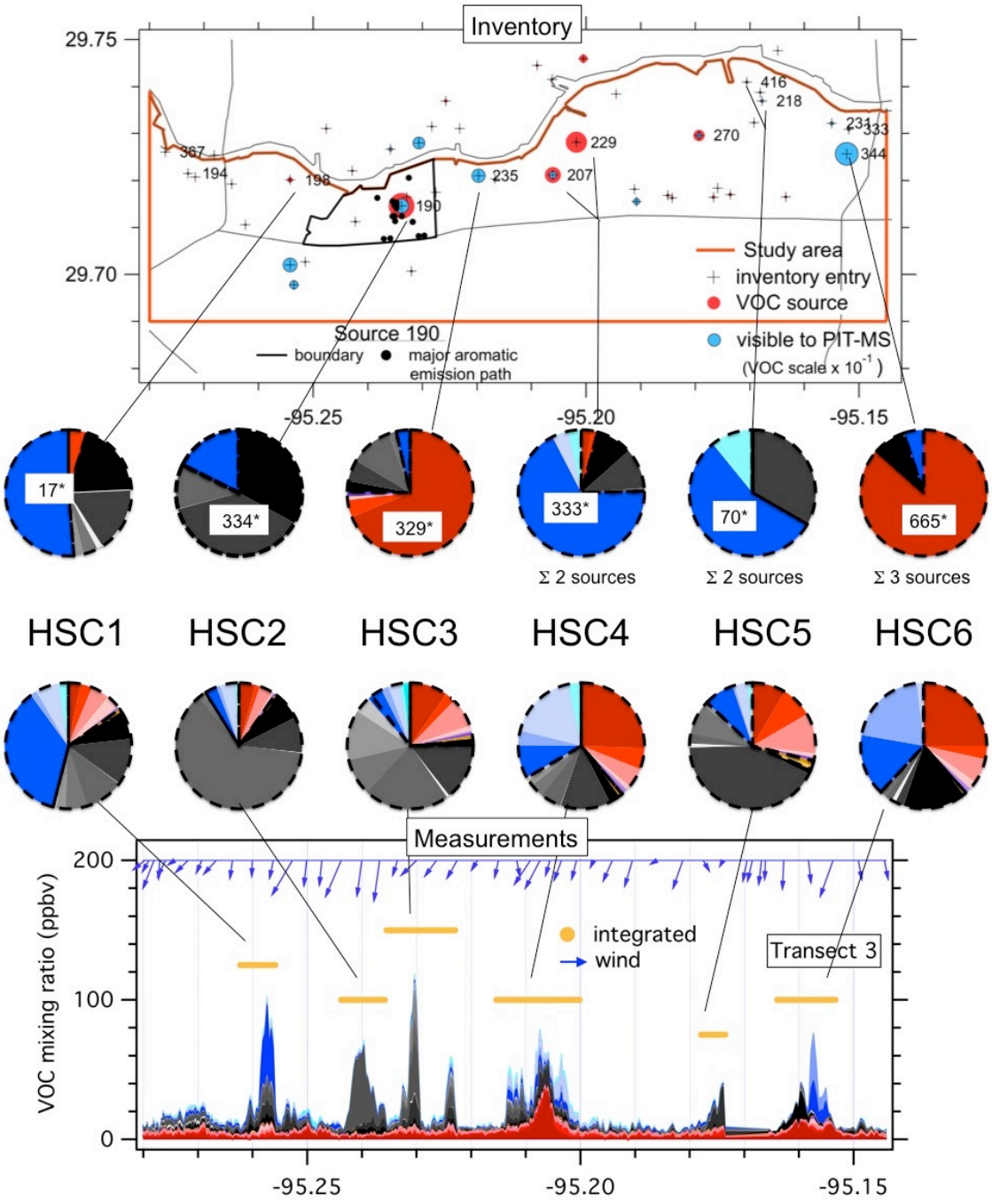
Inventory
29.75
29.70
-95.25
-95.20
-95.15
367
194
198
190
235
207
229
270
416
218
231
333
344
Study area
inventory entry
VOC source
visible to PIT-MS
(VOC scale x 10-1)
Source 190
boundary
major aromatic emission path
17*
334*
329*
333*
70*
665*
Σ 2 sources
Σ 2 sources
Σ 3 sources
HSC1
HSC2
HSC3
HSC4
HSC5
HSC6
Measurements
VOC mixing ratio (ppbv)
200
100
0
integrated
wind
Transect 3
-95.25
-95.20
-95.15

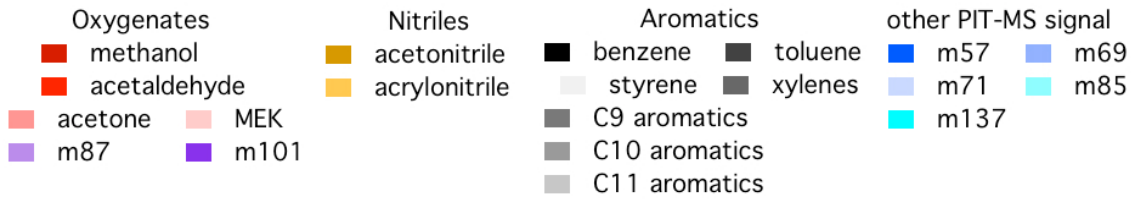

Figure 5.7. Comparison of the composition of the HGB2K6 emission inventory (top) measurements made during the night transect (transect 3) of the Houston Ship Channel. Measurements were integrated over the areas shown by the orange bars for each of 6 major industrial plumes for comparison with inventory values. Measurements are compared to inventory entries for nearby industrial sources of VOCs visible to PIT-MS (top row of pie graphs). The composition of the plume VOCs visible to PIT-MS from the nearest likely industrial source(s) are shown in red sized by emissions in molecules sec^{-1}. The subset of VOC emissions visible to PIT-MS are shown in blue with sizes scaled by a factor of 10 relative to the red markers. Sizes of blue markers are reported in white boxes in units of 10^{20} molecules sec^{-1}.

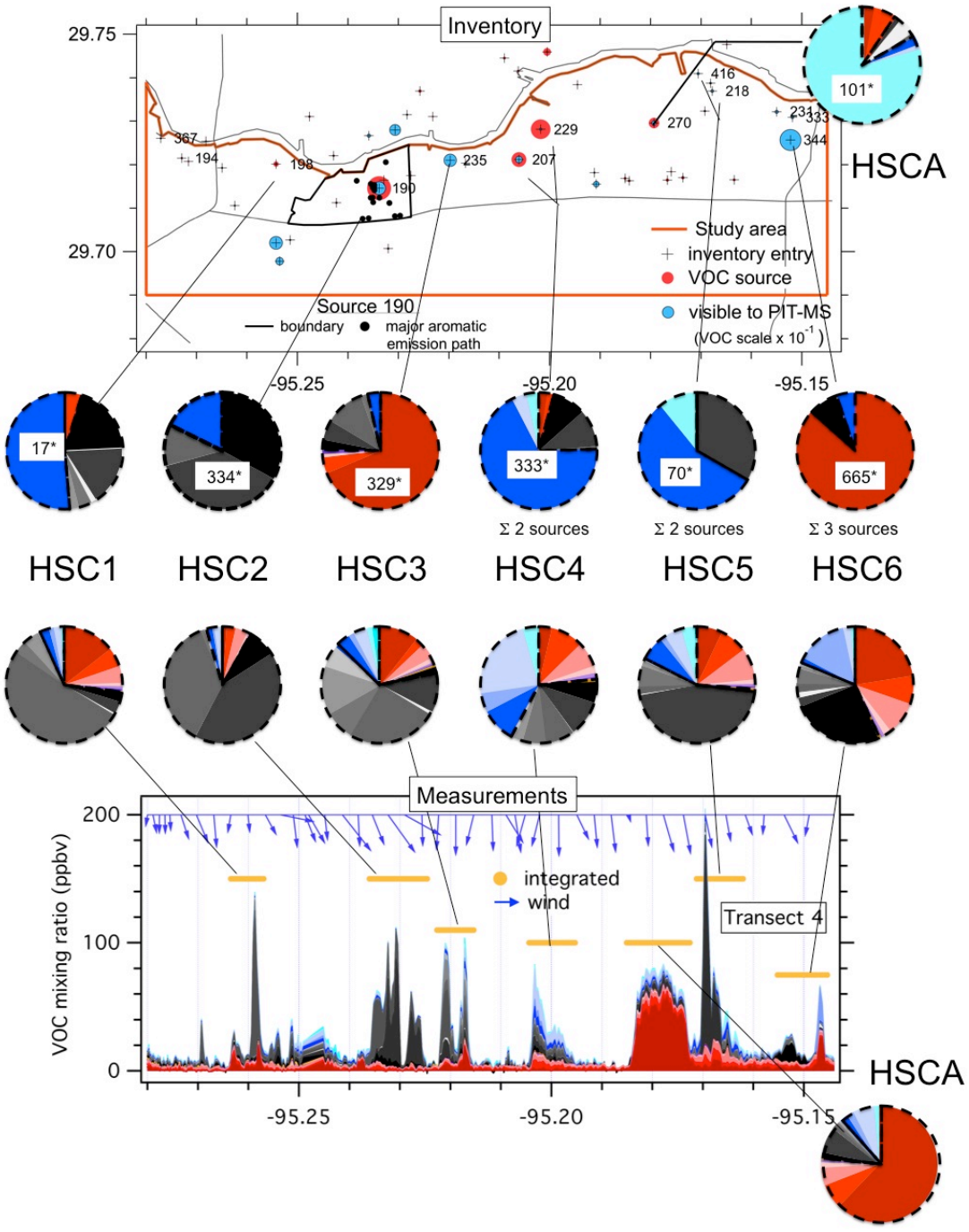
Inventory
29.75
29.70
-95.25
-95.20
-95.15
101*
HSCA
416
218
231
333
344
270
229
207
235
198
194
367
190
Study area
inventory entry
VOC source
visible to PIT-MS
(VOC scale x 10^-1)
Source 190
boundary
major aromatic emission path
17*
334*
329*
333*
70*
665*
Σ 2 sources
Σ 2 sources
Σ 3 sources
HSC1
HSC2
HSC3
HSC4
HSC5
HSC6
Measurements
VOC mixing ratio (ppbv)
200
100
0
integrated
wind
Transect 4
HSCA
-95.25
-95.20
-95.15

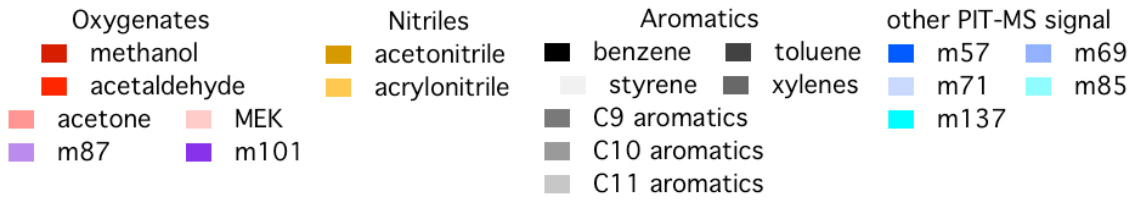

Figure 5.8. Comparison of the composition of the HGB2K6 emission inventory (top) measurements made during the morning transect (transect 4) of the Houston Ship Channel. Measurements were integrated over the areas shown by the orange bars for each of 7 major industrial plumes for comparison with inventory values. Measurements are compared to inventory entries for nearby industrial sources of VOCs visible to PIT-MS (top row of pie graphs). The composition of the plume VOCs visible to PIT-MS from the nearest likely industrial source(s) are shown sources in the inventory are shown in red sized by emissions in molecules sec^{-1}. The subset of VOC emissions visible to PIT-MS are shown in blue with sizes scaled by a factor of 10 relative to the red markers. Sizes of blue markers are reported in white boxes in units of 10^{20} molecules sec^{-1}.

locations during both transects. In several cases, the observed plumes exceeded 100 ppb VOC detectable to PIT-MS. Both transects consisted of more than 350 individual measurements by PIT-MS. The GC-MS only acquired about 3 samples over the same transect.

VOC measurements were integrated for six large plumes observed by PIT-MS near the same location in both transects (Figures 5.7 and 5.8). These plumes are numbered consecutively HSC1-HSC6 from west to east in the figures. A seventh large plume was visible at longitude -95.18 in transect 4 (Figure 5.8) but not in transect 3 (Figure 5.7). This plume was composed mostly of methanol and will be referred to separately as plume HSCA.

Thirty-five individual inventory sources from south of the Houston Ship Channel were considered in this analysis (between -95.28 and -95.145 lat, north of 29.69 lon) as shown in Figures 5.1, 5.7 and 5.8. Eleven individual inventory entries were chosen for comparison with measurements based on proximity to observed plumes and the wind direction at the time of sampling. For plumes HSC4-6, two or more sources were in close proximity to each other and inventory entries were summed. To give the reader an idea of the emissions reported in the inventory, the magnitude of emissions are shown in white boxes in the pie charts (Figures 5.7 and 5.8). The number shown represents emissions detectable by the PIT-MS instrument in units of 10^{20} molecules sec^{-1}.

Source 198 vs. Plume HSC1. Inventory source 198 (IC_{67}=3) reported that the majority of its emissions detectable to PIT-MS should be m57 (>99% butenes), benzene and toluene. Methanol and 1-pentene (m71) were also listed (9% and 5%)

in the inventory for this source. The plumes measured by the PIT-MS instrument differed significantly in composition from transect 3 to 4. In the plume measured in transect 3 (MC_{67}=5), dominant signals came from m57, toluene, xylenes (m107), benzene and m71. In transect 4, the plume at the same location (MC_{67}=3) consisted of mostly xylenes (m107), methanol and acetaldehyde.

Source 190 vs. Plume HSC2. Inventory source 190 (IC_{67}=2) reported its major detectable emissions as toluene and benzene. In both measurements of the HSC2 plume(MC_{67}=2), xylenes (m107) and toluene were dominant. Benzene made up >8% of the VOCs measured by PIT-MS in both plumes. Data from this plume intercept will be used further down to estimate absolute xylene fluxes for comparison with the inventory (Section 4.3).

Source 235 vs. Plume HSC3. Inventory entries for source 235 (IC_{67}=1) were dominated by methanol with only 21% aromatics, mostly xylenes (11%) and toluene(5.5%). In both transects (MC_{67}=5), aromatic compounds (toluene, xylenes and the C9 and C10 aromatics) accounted for 65% of the PIT-MS instrument signal by mixing ratio, while methanol was ~10% in both cases.

Sources 207 and 229 vs. Plume HSC4. These sources were similar in VOCs emissions reported detectable by PIT-MS but plume HSC4 could not be clearly attributed to one or the other. The sum of inventory values (IC_{67}=1) for these two sites showed emissions dominated by m57, which in this case was mostly MTBE (80%) with small proportions (~10% each) of benzene and toluene. Measurements of the HSC4 plume showed a more complex mixture (MC_{67}=5 and 7). The major difference between the transects was that there was a considerably higher

proportion of methanol in transect 3. In both transects major compounds measured by PIT-MS included m71, toluene, m57, xylenes, acetaldehyde and acetone. Signal (4-5%) was observed at m69, although there were no reported emissions from these sources that could explain it. In fact, there are few sources of either isoprene and none of cyclopentene in the study area. Isoprene emissions are only reported by source 187, south and west of source 190 on the map (Figures 5.7 and 5.8) and by one source outside the study area about a mile east of source 344.

Sources 416 and 218 vs. Plume HSC5. Source 416 lists emissions detectable by the PIT-MS instrument about a factor of three greater than source 218. Only three compounds listed in the inventory should be detectable by PIT-MS. Of these compounds, m57 (only butene isomers are shown in the inventory) and toluene should be dominant (IC_{67}=2) with about 10% signal from the hexene isomers. In fact, source 416 reports no emissions detectable at m57 but reports 93% of the combined toluene emissions. Measurements show only considerably more diversity (MC_{67}=4, both plumes). The plumes are similar in composition in both transects with 42-45% toluene, and smaller amounts of acetone, acetaldehyde and methanol. About 7% of the PIT-MS measurement by mixing ratio comes from m57 in both plumes. The C9 aromatics and m71 are also measured, but not listed in the inventory. Between 3-5% of the signal in the plumes is seen at m85 and could be attributed to emissions of hexene isomers.

Sources 231, 333, and 344 vs. Plume HSC6. Source 344 emits 86% of the VOCs detectable by the PIT-MS instrument in this grouping and the majority of inventory emissions are methanol (IC_{67}=1). Measurements show a much greater

complexity in plume HSC6 (MC_{67}=4 in both transects). Major VOCs measured by the PIT-MS instrument in both transects included methanol, m69, acetone and benzene. Plume 3 also contained m57 (16%). The inventory does show small emissions of m57, which are a mixture of butene isomers (66%) and n-butanol (33%). None of these sources, located an average of 0.5 miles south of the channel, report emissions of m69 (isoprene or cyclopentene). A source (281) of m69 (isoprene) is reported outside the study area centered about 1.5 miles further east. However, the isoprene emitted by the more distant source 281 is only 2.4% as large as the methanol emissions reported by source 344. Based on the distance and wind direction, it seems unlikely that source 281 could have been the source of the m69 observed by the PIT-MS instrument.

Source 270 vs. Plume HSCA (transect 4 only). Source 270 (IC_{67}=1) reports large emissions of hexene isomers, which are detected by the PIT-MS instrument at m85. A large plume was observed in transect 4 north of this source and between plumes HSC4 and HSC5. The plume was large and broad, consisting of methanol and toluene (MC_{67}=2) and smaller amounts of many other compounds detectable by the PIT-MS instrument. The inventory emissions thus have a completely different composition than the plume measured by the PIT-MS instrument.

Conclusions for HSC plume comparisons. Measurements made by the PIT-MS instrument showed significantly greater complexity than VOC emissions listed in the HGB2K6 inventory. The complexity in measurements was greater than the complexity listed in the inventory (MC67 > IC67) in 6 of the 7 plumes examined.

Some (2 of 7) of the plumes differed considerably in VOC composition as measured by PIT-MS within a span of less than 24 hours.

4.1.4 Conclusions from Plume Analyses

VOC plumes observed during the TexAQS 2006 research cruise were complex, often with high concentrations (> 100 ppb measured by the PIT-MS instrument), and their compositions varied in time. Methanol is reported in the inventory as the largest emission detectable by PIT-MS and was most abundant industrial emission visible to PIT-MS by mixing ratio at all three of locations examined in this work. The measured ratio of methanol to benzene in plumes did approximate the ratio of the two compounds reported in inventory emissions at all three locations. The reason for this is not specifically known, although we speculate that because both compounds are solvents commonly used in industrial processes the emissions may reflect the quantities used, which are more accurately known than the actual amounts leaking to the atmosphere.

Plume complexity results are summarized in Figure 5.9. Average plume complexity measured by the PIT-MS instrument was more than a factor of 2 times greater than what the inventory suggested. This result is supported both by NOAA GC-FID/MS (Gilman et al., 2009) and by GC-PIT-MS measurements (Section 3.2) which identified dozens of industrial compounds during TexAQS 2006 research cruise. Because isobaric compounds are detected by the PIT-MS instrument at a single m/z, our measurements suggest that the factor of two observed here is a conservative estimate of the diversity of VOCs emitted versus reported in the

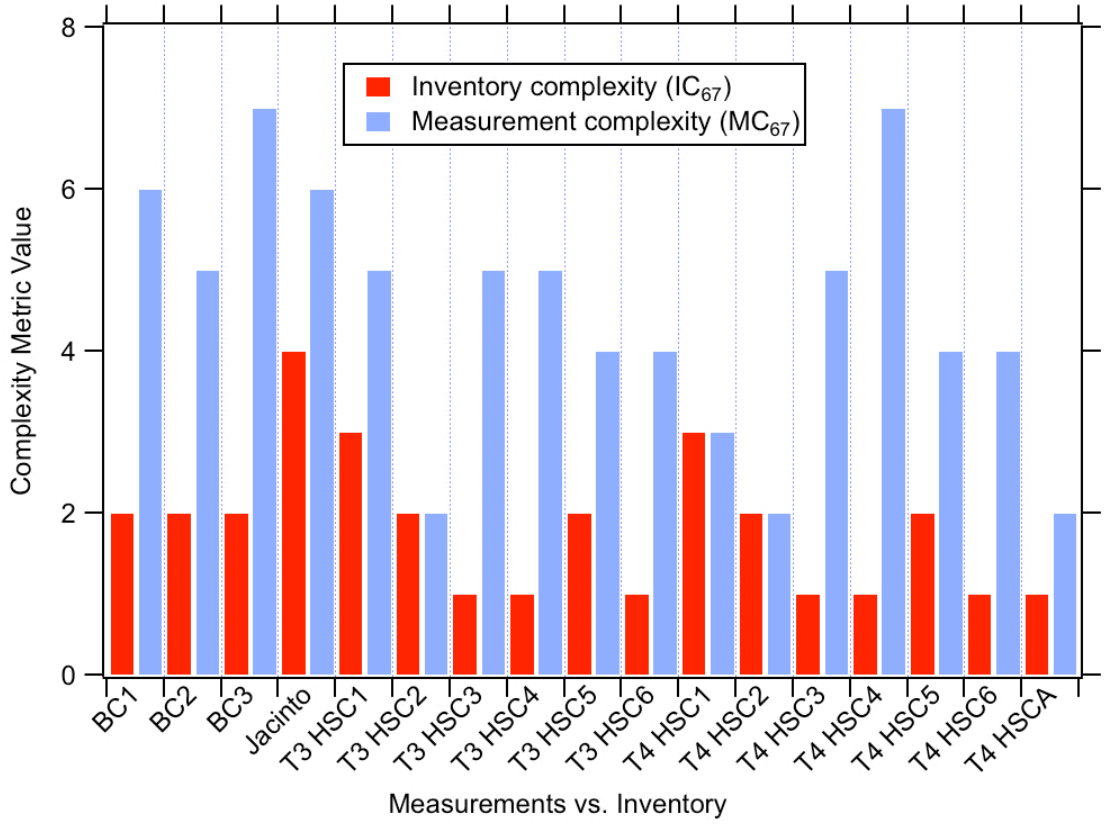

Figure 5.9. Summary of the Complexity Metric comparison for HGB2K6 inventory (IC_{67}) and measurements of individual VOC plumes made by PIT-MS (MC_{67}). Metrics are defined in the text based on 20 m/z detected by the PIT-MS instrument.

HGB2K6 inventory. We conclude that VOC composition of emission plumes is in many cases inconsistent with the speciated emissions in the inventory.

4.2 Transect Sums

The emission inventory for NO_x in the Houston area has been found to be accurate to within 30% (Ryerson et al., 2003). In this section, we evaluate the accuracy of absolute VOC fluxes in the inventory by comparing measured VOCs to NOx ratios to similar ratios from the inventory. Similar analyses have been used elsewhere to show that VOC fluxes are underestimated by 1-2 orders of magnitude in the inventory (Ryerson et al., 2003; Washenfelder et al., 2010).

Measurements of NO_x and 9 selected VOCs were integrated over two transects of the Houston Ship Channel (transects 3 and 4, also discussed above) totaling over 2 hours of continuous measurements. Emissions of NO_x and corresponding VOCs (based on the equivalencies defined in Table 5.1) were summed for the 35 inventory accounts south of ship channel shown in the boxed areas of Figures 5.7 and 5.8. Table 5.2 summarizes the VOC:NO_x ratios from each measurement transect and compares them to similar values obtained from the emission inventory.

Table 5.2 shows that transect average values for methanol:NO_x, benzene:NO_x and m57:NO_x were about a factor of 5 larger than the similar ratios from the inventory values. Measured values of toluene:NO_x and xylenes:NO_x, were 23 and 60 times larger than inventory equivalents. Ratios of m71:NO_x and the C9

Table 5.2. Comparison of measurements for two transects of the Houston Ship Channel with emission sources in the HGB2K6 emission inventory. Speciated measurements of individual VOC and NO_x measurements were integrated for each transect. The ratio of invidual VOCs to NO_x are compared with similar ratios for nearby emission sources of the same compounds. The wind was consistently from the south in both transects.

	ΣVOC:ΣNOx measured		ΣVOC: ΣNOx inventory	Ratio measurement: inventory	
	transect 3	transect 4			
VOC[a]	N=354	N=379	35 sources		
methanol	0.19	0.18	0.029	6.4 ±	0.02
m57	0.12	0.043	0.017	4.6 ±	2.1
m71	0.11	0.061	5.E-04	185 ±	51
benzene	0.041	0.033	0.007	5.6 ±	0.6
toluene	0.13	0.17	0.007	23 ±	3
ΣC8 aromatics	0.16	0.14	0.003	60 ±	5
ΣC9 aromatics	0.052	0.039	4.E-04	129 ±	19
ΣC10 aromatics	0.038	0.026	*not reported in inventory*		
ΣC11 aromatics	0.015	0.012			

[a]See Table 1 for list equavalencies used for comparisons of inventory to measurements

aromatics:NO_x ratios from PIT-MS measurements were more than 2 orders of magnitude larger than inventory values. This method could not extended to the C10 and C11 aromatics, which were measured by the PIT-MS instrument but are not reported in the inventory. However, transect average values for C10 aromatics:NO_x were similar to those measured for benzene:NO_x.

In Section 4.1, we defined measurement and inventory complexity metrics. In Figure 5.10, we graphically compare the average integrated measurement complexity metric (MC_{67}=3) for the 2 ship channel transects with the inventory complexity metric (IC_{67}=2) for the 8 industrial hydrocarbon compounds from Table 5.2. For this plot, we have chosen to exclude the OVOC methanol because it is has low ozone production potential and high area backgrounds compared to the 8 other industrial hydrocarbon compounds (Gilman et al., 2009).

From this analysis, we conclude that measurements again suggest considerably more VOC complexity than is reported in the HGB2K6 industrial emission inventory. From Table 5.2, we conclude that compared to NO_x, VOC emissions detectable by the PIT-MS instrument are underreported in the inventory by factors ranging from 5 (for methanol, benzene and m57) to over two orders of magnitude. These observations are consistent with underreported emissions in the inventory as reported previously (de Gouw et al., 2009a;Mellqvist et al., 2010;Parrish et al., 2009;Washenfelder et al., 2010;Ryerson et al., 2003).

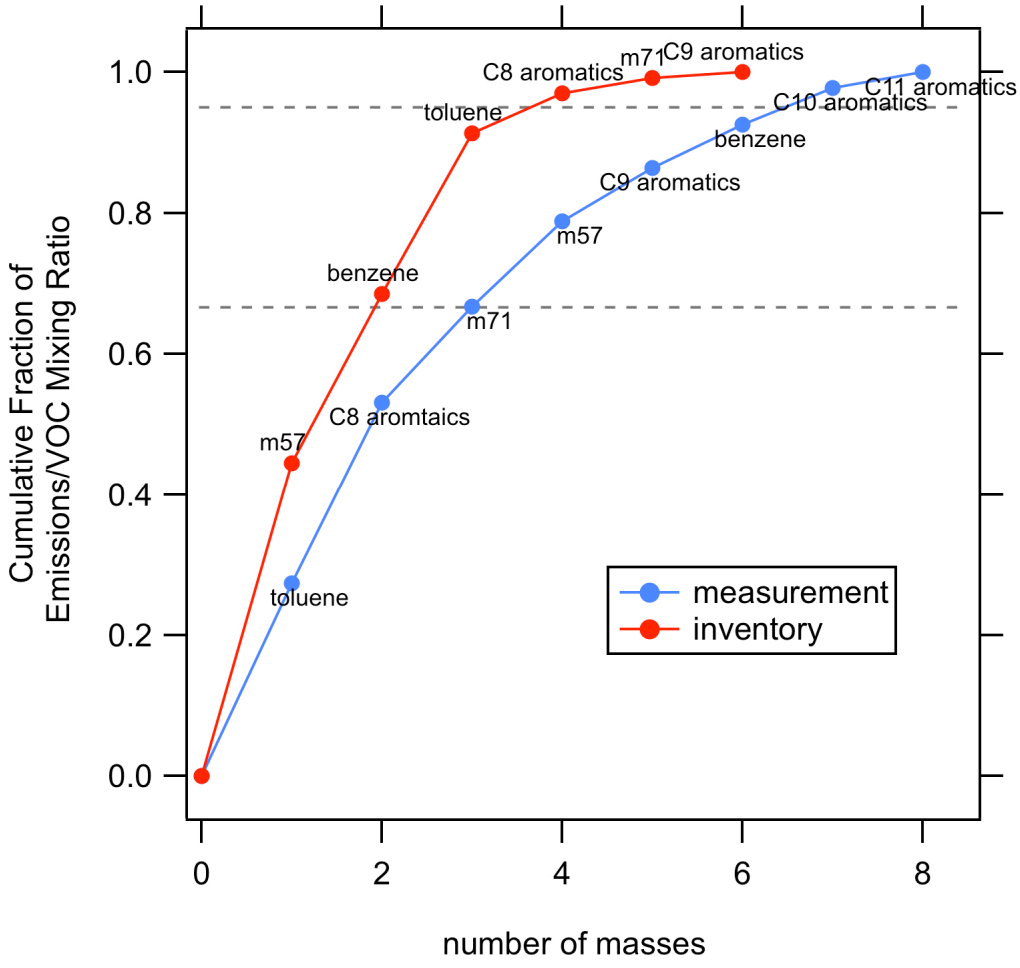

Figure 5.10. Plot of the average complexity metrics MC_{67} (blue) and IC_{67} (red) for two transects of the Houston Ship Channel. The metrics are defined in the text for comparison of PIT-MS instrument measurements with inventory. Results shown here are typical of other plume-inventory comparisons from the TexAQS 2006 campaign.

4.3 Calculation of Flux from Measurements

In the previous section, we compared VOC measurements to inventory values by way of NO_x. In order to determine absolute emission fluxes of VOCs from measurements, we estimate here the emission flux of C8 aromatics at one location along the channel directly from measured mixing ratios. To translate measured mixing ratio to flux estimates we use the following relationship (de Gouw et al., 2009a;White et al., 1976):

$$flux = h \times \int_t \Delta[VOC] \times v \times w \times \sin(\alpha) \times dt \quad (1)$$

where v is the ship speed, w the wind speed, h the mixing height observed by HRDL during the plume, and α the angle between the wind and ship directions. This flux is calculated from measurements of plume HSC2 in both transects and compared to the inventory flux of the most proximate major source of these compounds (Source 190). For comparison purposes, we have also calculated the emission flux of NO_x from measurements.

Measurements of VOC and NO_x occurred from a height of about 20 m and the plume widths were approximately 900m. Mixed layer heights measured by HRDL were 133m and 330m in transects 3 and 4, respectively. Figures 5.7 and 5.8 show the boundaries of source 190. This facility reports 368 individual emission paths in the HGB2K6 inventory. The 5 largest individual inventory emission paths are shown for each aromatic species reported.

The results of the integration are compiled in Table 5.3 and shown visually for transect 4 in Figure 5.11. The NO_x flux observed in the plume was 0.3 and 0.5

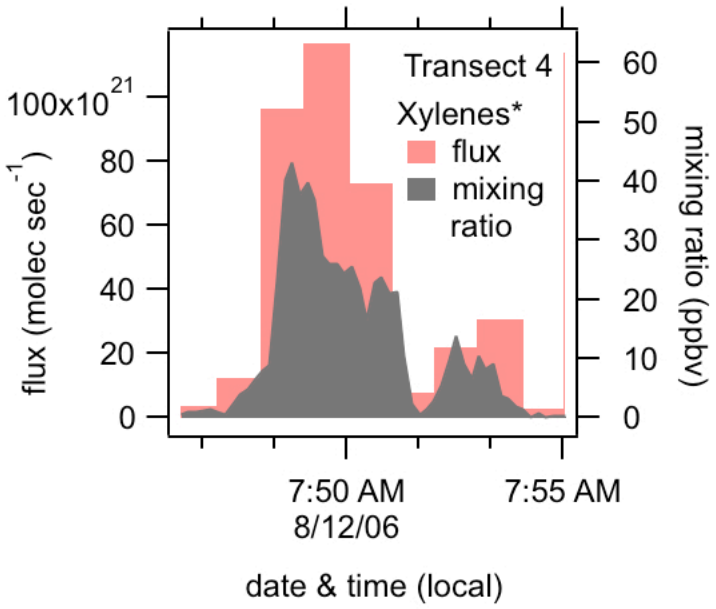

Figure 5.11. Measurements during transect HSC4 of a plume of C8-aromatics near source 190 (grey shaded area) and the instantaneous emission flux calculated from these measurements (red shaded area). Numerical results of this analysis are shown in Table 5.3. The flux calculation is described in the text. Measurements shown on 10s PIT-MS timescale. For Flux calculation, all measurements were averaged to 1 min ship time.

times that listed in the inventory (Table 5.3). In contrast, the C8 aromatic fluxes in the plume were observed to be a factor of about 50 higher than reported in the inventory. The large underestimate of C8-aromatic fluxes in the inventory is consistent with the result obtained from the VOC:NOx ratios in the previous section.

This case study is intended as an order of magnitude exercise that can illustrate for the policy maker the relationship between a measured mixing ratio and an absolute emission flux. Figure 5.12 summarizes the result of this analysis graphically, showing the generalized dependence of observed mixing ratios on the flux given typical ship speed, wind speed for several mixing heights.

5. Conclusions

High time resolution measurements made by the PIT-MS instrument onboard the R/V Ronald H. Brown during the TexAQS 2006 campaign provide valuable insight into the composition and complexity of VOCs emitted near the Houston Ship Channel. VOC measurements made by the PIT-MS instrument supplement the lower time resolution, but more highly speciated measurements made by GC-FID and GC-MS from the same platform in the Houston Ship Channel (Gilman et al., 2009). Chromatograms made by GC-PIT-MS show both the complex nature of industrial VOC plumes and help clarify the interpretation of PIT-MS signals during the TexAQS 2006 campaign, thereby providing a reference point for future measurements by PTR-MS instruments in close proximity to industrial plumes.

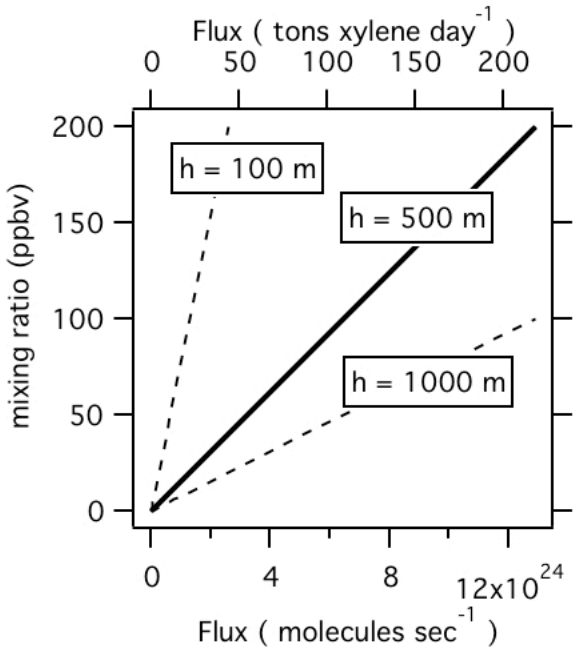

Figure 5.12. The modeled relationship between mixing ratio (ppbv; vertical axis) and fluxes are shown in units of molecules sec^{-1} (bottom) and tons of xylene isomers day^{-1} (top). Assumptions used here are similar to conditions observed during the transects described in the text: plume width = 875 m, time spent in plume = 250 s , cross wind ship speed = 6 m/s, and wind speed 3.5 m/s. The solid black line representing a mixing height of 500 m, is bracketed by values obtained by mixing heights of 100 and 1000 m. Mixing ratios as high as 60-80 ppbv of xylenes were observed in plumes in the HSC area.

Table 5.3. Comparison of VOC and NO_x fluxes calculated from plume VOC mixing ratios to emission inventory fluxes for one particular source (inventory number 190) of VOCs and NO_x in the Houston ship channel.

	Inventory Flux (10^{20} molecules sec^{-1})	Mixing Ratio plume average (ppbv) N=24	(ppbv) N=36	Flux from measurement[a] (10^{20} molecules sec^{-1})		Flux Ratio measured: inventory	
Transect:		3	4	3	4	3	4
total inventory VOC[b]	6423						
ΣC8 xylenes[c]	36	22	17	1931	2422	53	67
NO_x	5862	16	14	1666	3165	0.3	0.5

[a]HRDL BL height transect 3=133 m, transect 4=330 m

[b]Total VOC emissions reported by source 190 in the HGB2K6 inventory. About 5% of this total is reported in the inventory as VOCs detectable by the PIT-MS instrument based on the equivalences defined in Table 1. For speciated emissions see Frost (2009).

[c]Sum of 3 xylene isomers + ethyl benzene

We draw three main conclusions from the analyses presented here. First, many VOC plumes show a variability in composition with time on scales from hours to weeks, which is not described by the emission inventory. Second, VOC composition measured in industrial plumes during the campaign is in many cases inconsistent with the speciated emissions in the inventory. The complexity of VOCs observed in plumes in the area is at least a factor of 2 higher than can the complexity described in the inventory.

Finally, we estimate that industrial emissions of some of the most abundant industrial VOCs (e.g. methanol and benzene) in the Houston area are larger by about a factor of 5 than reported in the inventory based on inventory values for NO_x. For some more highly reactive VOCs with high ozone-formation potentials including xylenes and pentenes, the inventory underestimates emissions by 1-2 orders of magnitude. These results are consistent with previous comparisons of VOC measurements to emissions inventory values in the Houston area.

CHAPTER 6

COLLISION-INDUCED DISSOCIATION OF BIOGENIC VOLATILE ORGANIC COMPOUNDS IN THE LABORATORY AND IN THE FIELD

1. Introduction

Hundreds of individual VOCs and OVOCs are now known to be emitted by plants (Steiner and Goldstein, 2007). The most notable of these compounds is isoprene, a highly reactive C5 diene. Other emissions include alcohols (e.g., methanol, ethanol), monoterpenes and sesquiterpenes. Many species of pine trees emit 2-methyl-3-buten-2-ol (MBO), a C5 alcohol first reported by (Goldan et al., 1993) instead of isoprene. The exact reasons for the emission of these compounds by plants are not known, although in some cases they are thought to play a role in the deterrence of insect herbivory. Because of the quantity of organic carbon emitted into the atmosphere by plants, biogenic VOCs are of great importance to atmospheric scientists.

Biomass burning is another major source of atmospheric VOCs. The combustion of plant material releases a huge diversity of VOCs into the atmosphere (Andreae and Merlet, 2001;Warneke et al., 2011;Yokelson et al., 2008).

Collision-induced dissociation (CID) is a specific type of tandem mass spectrometry (also called MS/MS) where trapped ions are made to collide with an inert buffer gas in order to cause the fragmentation of the ions. Fragmentation

patterns are often different for isomeric and isobaric compounds. As a result, CID can provide valuable chemical information useful in resolving mixtures of compounds. The use of CID in the field is therefore a valuable analytical tool that can be used to resolve complex mixtures of VOCs such as those seen in forests and biomass burning plumes.

CID with the PIT-MS instrument has previously been used to resolve the isobaric carbonyl compounds acetone and propanal in ambient measurements (Warneke et al., 2005a). CID with other ion trap mass spectrometry instruments has been applied in the laboratory to resolve mixtures of monoterpenes (Steeghs et al., 2007) and in the field to discriminate isobaric compounds such as methyl vinyl ketone (MVK) from methacrolein (Mielke et al., 2010), two important oxidation products of isoprene. In this chapter we present laboratory CID measurements of a variety of biogenic compounds. We build on the laboratory measurements to explore the use of CID as a powerful analytic tool to resolve complex VOC mixtures at the Blodgett Research Station near Georgetown, California and in the smoke from biomass burning laboratory experiments at the Fire Sciences Laboratory in Missoula, MT.

2. Methods

CID mode in the PIT-MS instrument was mentioned briefly in Chapter 2 of this thesis and will be discussed in more detail here. CID patterns obtained from product ions of one selected mass, which are collected for several seconds in the ion trap. Other ions are discarded during trapping by a waveform voltage (filtered

noise field or FNF) applied to the endcaps. The resulting electric field is resonant with the motion of all other ions, and ejects them from the trap, except the ions of interest.

After collecting a sufficient number of ions in the trap, an additional FNF is applied to the endcaps that is resonant with the ions of interest to increase their kinetic energy. Collisons of the molecular ions with the helium buffer gas cause the ions to fragment depending on the amplitude of the FNF field. The molecular ions and fragments are ejected from the trap by ramping the amplitude of the radio frequency (RF) trapping voltage and a mass spectrum is recorded with the electron multiplier.

In PIT-MS CID mode, RF frequencies varied from 0.78-0.85 MHz (for m/z 30-100) and 1-1.2 MHz (for m/z > 100) in order to maximize the trapping efficiency of the ions collected. FNF waveform "notches" were set so as to trap ions of a single m/z. Notches can be roughly calculated based on the motion of ions in the trap under the supplied conditions and are dependent on the amplitude of the RF used during trapping. Once notches are calculated, they must be manually adjusted to optimize the trapping of the parent ion of interest and the exclusion of other ions. This process is easiest when a compound with the relevant m/z is available in a calibration standard. For field studies, many of the notches must be calculated in the lab prior to field deployment. In practice, the FNF notches are most efficient at isolating a single m/z at lower masses (33-150 amu).

To obtain a typical CID pattern, 5 trapping sequences at each FNF amplitude are averaged. Ideally, the amplitude of the FNF is increased from 0.0 V to about 0.20

V in steps of 0.02. At 0.00 FNF amplitude, only the parent ion is visible for most VOCs. Fragmentation typically starts at 0.08 V FNF amplitude with maximum fragmentation occurring at about 0.14 V. At field sites where trapping times of 10 seconds are used, this process can take longer than 5 minutes. As a result, larger and fewer FNF steps are often used to reduce the time necessary to collect a CID pattern under field conditions.

2.1 Interpretation of CID measurements

It is not always possible to determine the exact neutral and ionic fragments formed during CID. The determination of thermodynamic activation barriers to possible ionic fragments requires computer modeling or experimentation that is beyond the scope of this work. However, enthalpy of formation (ΔH_f) values for ions are commonly determined based on the proton affinity (PA) of the parent molecule. We will therefore use the proton affinities of the ionic and molecular fragments as a first order thermodynamic approximation to determine the most energetically favorable CID products. Proton affinities and the enthalpies of molecules and ions were obtained from the online NIST database (NIST, 2011) also in thermodynamic reference works (Lias et al., 1988;Hunter and Lias, 1998).

In addition to using proton affinity, I will use the structure of the parent molecular ion to assess possible ionic and neutral fragments, a common practice used in the interpretation of mass spectra. According to this method, we assume that complex rearrangements are less likely than simple bond cleavage and that lost neutral fragments are often identifiable as stable compounds. In gas phase proton-

transfer reactions involving VOCs, protonation occurs in the most electron rich areas of the molecules (e.g., double bonds and carbonyl groups). For molecules with multifunctional groups, protonation can occur at any electron-rich functional group. In a protonated molecule, bonds alpha to the protonation site are more likely to break than bonds further from a functional group. Additional information on the interpretation of fragments in mass spectra can be found elsewhere (McLafferty and Turecek, 1993).

For the discussion that follows, it is useful to distinguish neutral CID fragments (which are not detected) from ion fragments, which are detected after ejection from the trap. We will use the convention of referring to protonated VOCs and ion fragments using an "m" before the atomic mass (e.g., m59, m43, etc.). Neutral fragments lost during CID will be described by atomic mass (e.g., propylene, 42 amu).

2.2 Study Areas

Laboratory Spectra. CID spectra were collected in the laboratory during the summer of 2005 and again in the fall of 2008. Typically, pure compounds were obtained from Sigma-Aldrich, Inc. Bottles of the pure compound were held near the inlet of the PIT-MS and CID spectra were captured using trapping times from 1-10 seconds.

Field CID Spectra. Field data presented here were obtained in the summers of 2005 and 2007 at a forested site in the Sierra Nevada near the University of California's Blodgett Forest Research Station near Georgetown, CA. For the 2005

study, individual representative CID spectra will be presented here. Due to instrument difficulties and low ambient mixing ratios, only campaign sum CID spectra will be shown from the 2007 study.

Plant Enclosures. Studies of ponderosa pine and manzanita branch enclosures were made during the summer of 2005 at Blodgett Forest. Branches were enclosed for about 2 days in a Teflon bag with fittings on either end. Zero air supplemented with CO_2 flowed through the enclosures at a rate of about 4 L min^{-1} and a residence time of about 20 sec. The experimental setup is described in detail elsewhere (Bouvier-Brown et al., 2009b).

An additional enclosure study was made of a ponderosa pine sapling at the NOAA building in Boulder, CO in September 2008. The 40 cm tall sapling was enclosed in a cubical plexiglass chamber with a volume of about 30 L. Lab air was pumped through a catalytic converter and into the chamber at a flow rate of 3.4 L min^{-1}. Positive pressure was maintained in the chamber. The plant enclosure remained outdoors adjacent to the laboratory building for a period of about 1 week.

Fire Laboratory. CID spectra were taken by PIT-MS during the FLAME III study at the Forest Service Fire Sciences Laboratory in Missoula, MT. During a typical experiment, a 100-1000g sample of dried vegetation was burned and the smoke allowed to mix into in a large burn chamber with a volume of ~3000 m^3. The experimental setup is described elsewhere (McKeeking et al., 2009). The PIT-MS instrument operated in an adjacent room and the samples were pumped through a Teflon inlet of length approximately 20m. Trapping times during CID varied from 1-10 sec and 5 samples were averaged at each FNF amplitude.

3. Results and Discussion

3.1 CID patterns of Pure Compounds

Figure 6.1 shows CID spectra for pure standards of 12 biologically relevant compounds obtained in the laboratory. From these spectra it can be seen, especially for alcohols, that a dominant pathway is the loss of a neutral water molecule (18 amu). Hydroxyacetone, 2-methyl-2-buten-2-ol (MBO) and acetoin all contain hydroxy groups and fragment predominantly through this pathway. The dehydration of alcohols is also commonly observed for alcohols (> C2) in the drift tube (non-CID mode) in PTR-MS instruments. During CID, water loss is also common for carbonyl compounds like methyl ethyl ketone (MEK) and its aldehyde isomer n-butanal.

Scheme 1

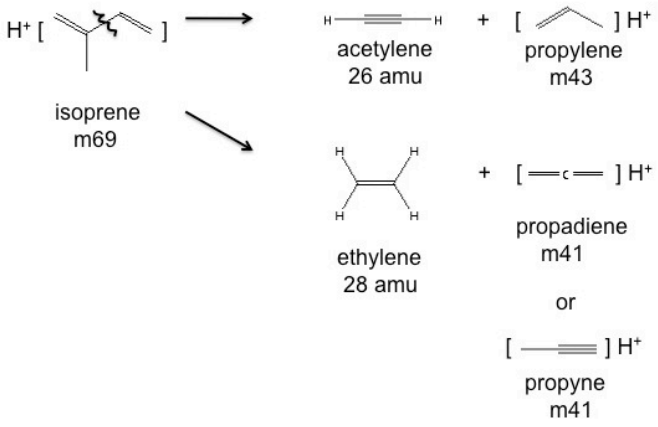

Scheme 1 shows a likely CID fragmentation pattern for isoprene. Many compounds show a CID fragment at m41 ($C_3H_5^+$) and m43 ($C_3H_7^+$ or $C_2H_3O^+$). Fragments at these masses are also commonly observed when parent ions fragment

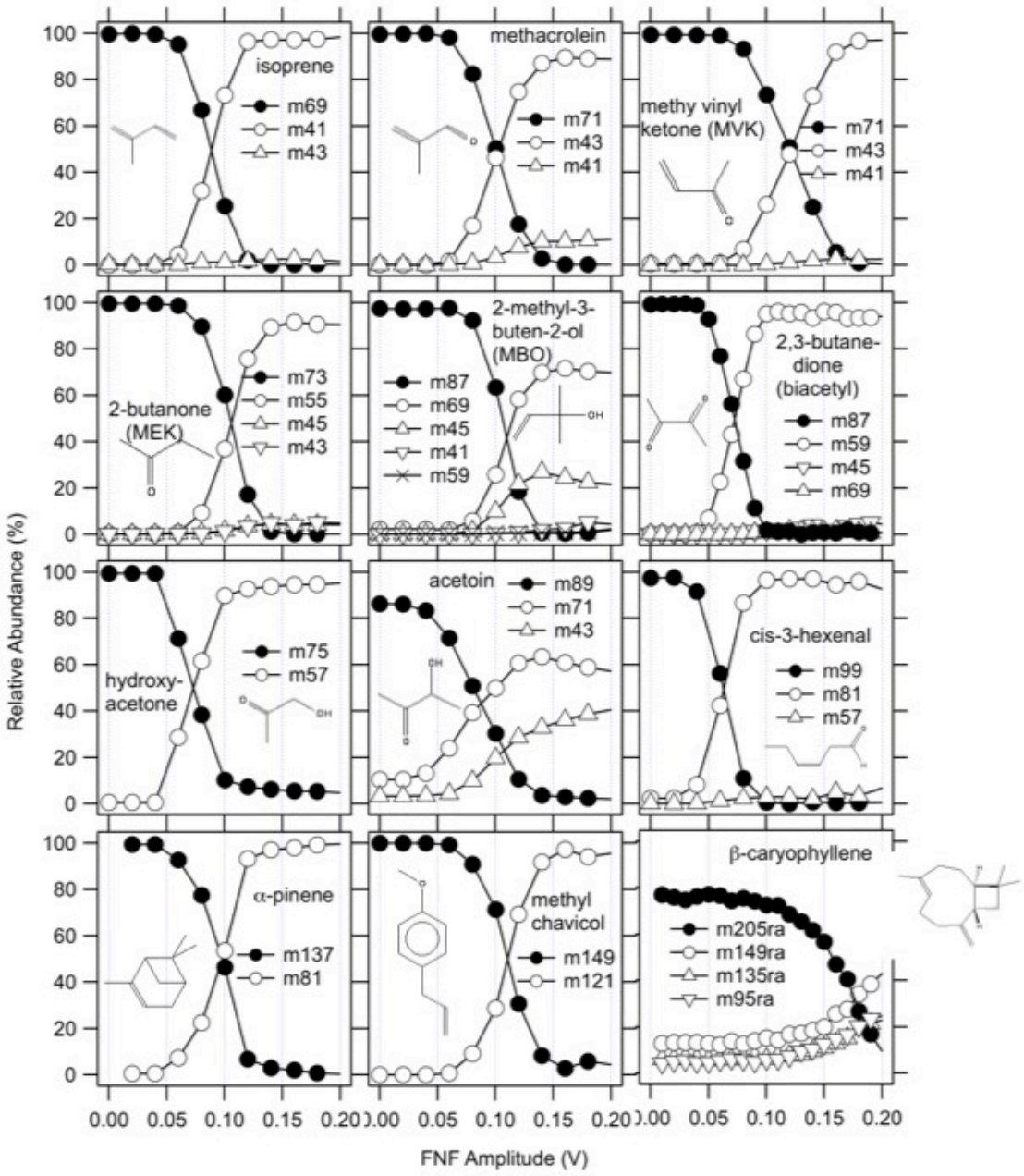

Figure 6.1. CID patterns of some relevant biogenic VOCs using the PIT-MS instrument. CID patterns for individual compounds were consistent over time except for some small variability (<0.05 V) in the FNF amplitude needed to initiate fragmentation.

in normal (non-CID) mode. Isoprene fragments to both m41 and m43 with neutrals lost at 28 and 26 amu. Since no oxygen is involved, the m43 fragment must be $C_3H_7^+$ (protonated propylene, PA=752 kJ/mol) with the corresponding loss of a neutral acetylene (PA=641 kJ/mol). The fragment at m41 requires the loss of a neutral ethylene (PA=680 kJ/mol). By our proton affinity argument, the m41 ion could be either protonated propadiene (PA=775 kJ/mol) or protonated propyne (PA=748 kJ/mol).

Methyl vinyl ketone (MVK) and methacrolein, the first generation oxidation products of isoprene, have a dominant fragment at m43 and a less abundant fragment at m41 (Figure 1). The aldehyde (methacrolein) shows more fragmentation to m41 than the ketone (MVK). Scheme 2 shows the four products possible in the m43 pathway. The two protonated products in this pathway

Scheme 2

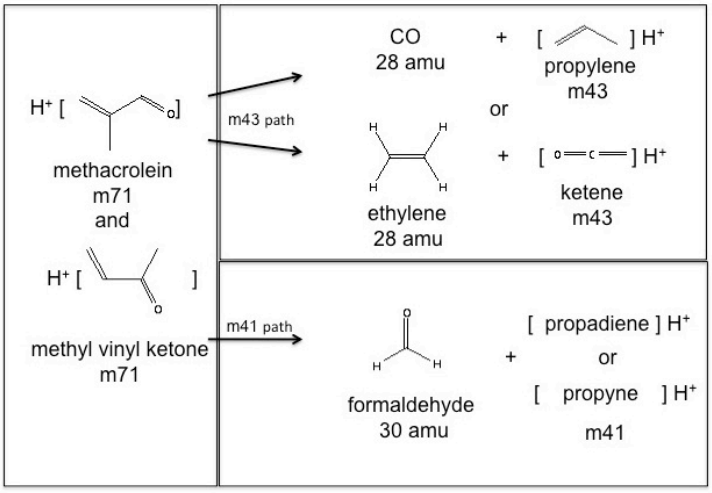

have the highest proton affinities (PA_{ketene}=825 and $PA_{propylene}$=751). By our first order thermodynamic argument, ketene is therefore the most likely product in this

pathway. Because the fragment at m41 is not likely to contain oxygen (it would be a radical), it is most likely that this path involves the loss of a neutral formaldehyde as shown in Scheme 2. In addition, the aldehyde requires little rearrangement to fragment to formaldehyde and we would expect this fragment to be more common in the fragmentation of methacrolein.

Before moving the discussion to the C4 carbonyls, the C3 carbonyls should briefly be discussed. Warneke (2005a) showed that CID spectra of acetone and propanal (both C3 carbonyls) produce fragments at m31 (loss of 28 amu) and m41 (loss of water) but in differing proportions (Scheme 3). For acetone, the dominant

Scheme 3

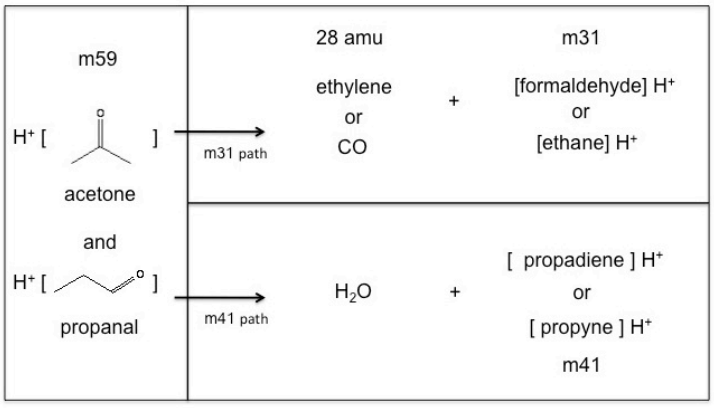

fragment is m31 while propanal more readily loses water. The loss of neutral 28 amu can be either CO or ethylene (C_2H_4). The proton affinity of ethylene (680 kJ/mol) is greater than that of CO (594 kJ/mol) and we can surmise that this is the most likely product. However, the production of either neutral at 28 amu would

require multistep rearrangements. From this, we must conclude that complex rearragments are possible, at least for small molecules like acetone and propanal.

Figure 6.2 shows the CID spectra for protonated methyl ethyl ketone (MEK) and n-butanal (C4 carbonyls). The dominant fragmentation pathways in both cases involve the loss of water, leaving protonated butadiene ($C_4H_7^+$) at m55. MEK also shows low relative abundance fragments at m45 (loss of 28 amu) and m43 (loss of 30 amu) lacking in the pattern of butanal. The most likely neutral lost at 28 amu appears to be ethylene (C_2H_4), which would leave the protonated acetaldehyde ion (m45). The alternative fragmentation, by loss of neutral CO, is less likely because it would require a co-product of protonated propane. Although this second pathway cannot definitively be ruled out, the proton affinity of acetaldehyde (769 kJ/mol) is the greatest of the four possible products and the first pathway also requires few rearrangement steps. The m43 loss pathway from MEK would result in the production of a neutral molecule with a mass of 30 amu, which could be either formaldehyde or ethane. The proton affinity of ethane (596 kJ/mol), formaldehyde (712 kJ/mol) and propylene (750 kJ/mol) are all considerably lower than that of ketene (825 kJ/mol). In this case the m43 fragment again appears most likely to be the oxygenated ion and the neutral lost is most likely ethane.

Figure 6.3 compares the CID spectra of six different compounds observed in PTR-MS at m87: four C5 carbonyl isomers, MBO, and 2,3-butanedione (biacetyl). All m87 isobars showed loss of water during CID except biacetyl. Biacetyl was the only compound with an m59 fragment from CID. This unique fragment from m87 will be discussed in the context of ambient measurements later in this Chapter.

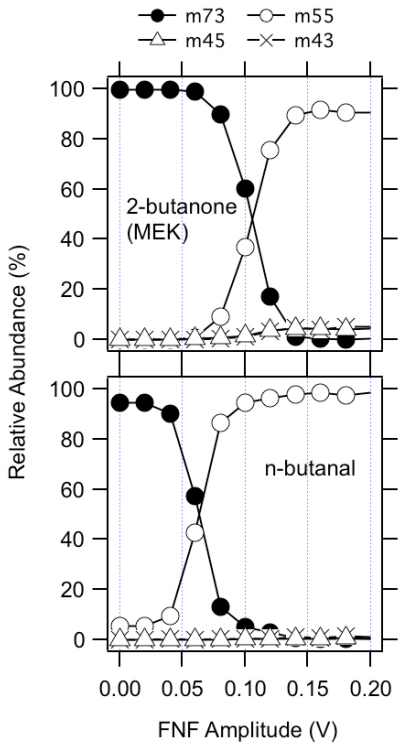

Figure 6.2. Laboratory CID of 2 isomers at m73, methyl ethyl ketone and n-butanal.

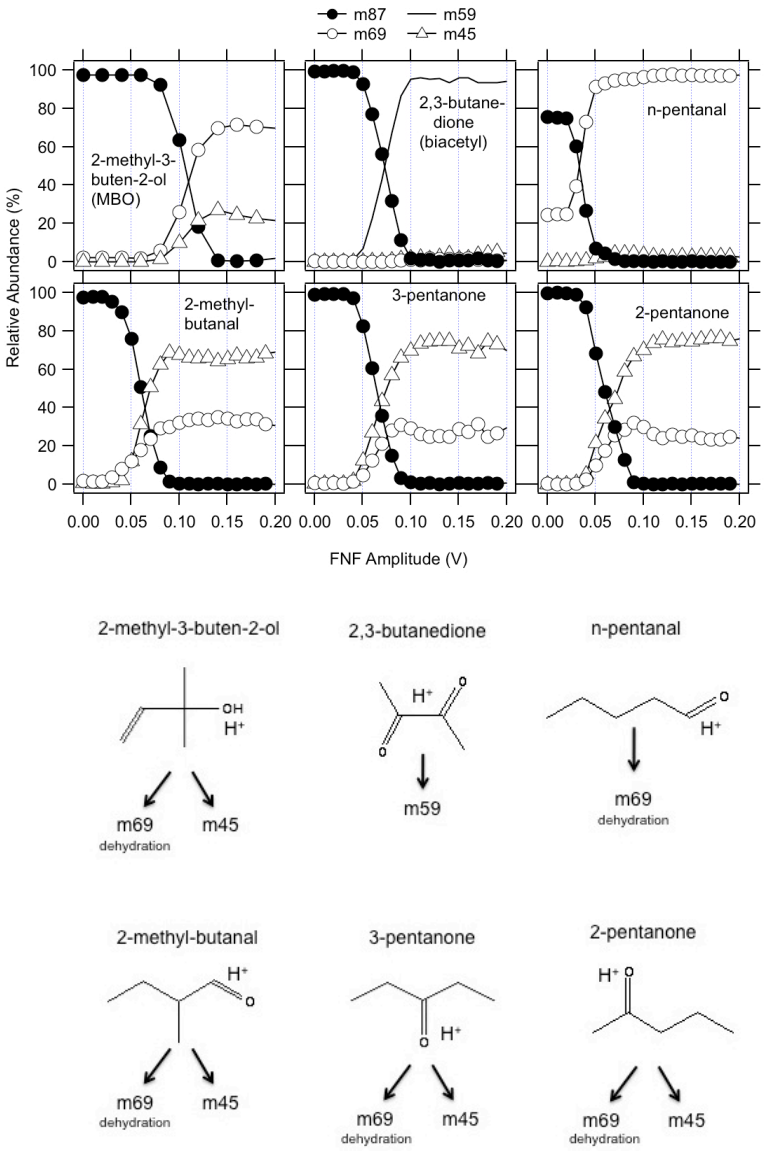

Figure 6.3. Laboratory CID spectra of 6 isobaric compounds at m87. Fragmentation patterns are summarized in the scheme (bottom).

Scheme 4 shows three possible pathways for fragmentation of the alcohol MBO. Dehydration is the primary fragmentation pathway. The production of a fragment at m45 is more difficult to explain as it would require rearrangement of the ion to produce either an oxygenated or non-oxygenated ion at this mass.

Scheme 4

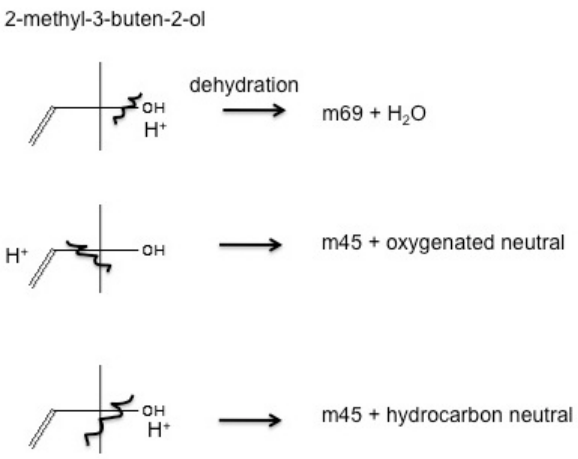

For both MBO and n-pentanal, water loss was the dominant mechanism of fragmentation during CID, while for 2-methyl butanal and the two ketone isomers, m45 was the dominant fragment. The m45 fragment could be protonated acetaldehyde or protonated propane with corresponding losses of neutral propylene or ketene at 42 amu). Of the four possible products, ketene has the highest proton affinity, so in this case the thermodynamic argument does not appear to describe observations. For 2-butanone, fragmentation at the carbon alpha to the carbonyl would produce acetaldehyde as a product, but this is not the case for 2-methyl butanal or 3-butanone. The mechanism that causes these fragmentation

patterns is not obvious and suggests that complex rearrangements can occur during CID fragmentation (as we saw in the case of acetone and propanal described previously). Neither the thermodynamic nor the structural arguments clearly explains all the observed fragmentation patterns.

For n-pentanal, 33% of the ions trapped dehydrate at 0.0 FNF amplitude. In the PIT-MS drift tube the percentage is higher (>45%) even for low E/N values (>110 Td). Clearly for the n-C5 aldehyde, dehydration has very low energy barrier. This does not appear to be the case for the C3 and C4 aldehydes previously discussed, nor is it seen in C5 aldehyde, 2-methyl butanal (CID also shown in Figure 6.3). For the n-C7 aldehyde, discussed in more detail below, there is also some dehydration (~10%) evident at 0.0 FNF amplitude. Substantial fragmentation at 0.0 FNF amplitude can also be seen in the CID pattern of the sesquiterpene β-caryophyllene (Figure 6.1).

Figure 6.1 shows the CID spectra of three higher molecular mass biogenic compounds, α-pinene, methyl chavicol, and β-caryophyllene. The fragmentation of the monoterpene (α-pinene) and the sesquiterpene (β-caryophyllene) show major hydrocarbon fragments at m81 and m149, respectively. These two terpenes were the major representatives of their class in the Blodgett forest studies (Bouvier-Brown et al., 2007) and these fragmentation patterns are typical of other mono- and sesquiterpenes. In ambient air, complex mixtures of these compounds are observed, which are not easily separated by CID (Steeghs et al., 2007). Methyl chavicol (m149) fragments to m121 during CID. From the structure, it is easy to see how an ethylene molecule (28 amu) would be the major neutral lost during CID. It seems likely that

molecules protonated at the double bond would be the most likely to fragment in this way. Protonation at the oxygen appears not to result in fragmentation during CID for this molecule. The CID spectrum of methyl chavicol proved valuable in identification of this molecule in branch enclosures (Bouvier-Brown et al., 2009a).

3.2 Fragmentation from Structure and Functional Group during CID

The CID spectra for 2 different unsaturated aldehydes are shown in Figure 6.4. The spectra of *cis*-3-hexenal and *trans*-2-hexenal both show dehydration fragments at m81. However, the *trans*-2-hexenal spectrum also shows a fragment at m57 (acrolein or a butene isomer). The loss of a neutral at 42 amu could be ketene or propylene. The thermodynamic argument applied to the ionized products suggests that m57 is likely to be protonated acrolein (PA=797 kJ/mol) with a corresponding loss of a neutral propylene (PA=752 kJ/mol) molecule. However, of the four products, ketene has the highest proton affinity and should be protonated (m43 fragment) if proton affinity is the driving factor in product formation. This fragment is not observed in the CID pattern.

Structurally, protonation at the double bond should lead to the m57 fragment while protonation at the terminal carbonyl results in dehydration as shown in the scheme in Figure 6.4. For the *cis*-2-isomer, the production of neutral ethylene (PA=681 kJ/mol) would result in the production of 2-butenal (crotonaldehyde; PA=831 kJ/mol) at m71. This does not appear to occur since the m71 fragment is not observed.

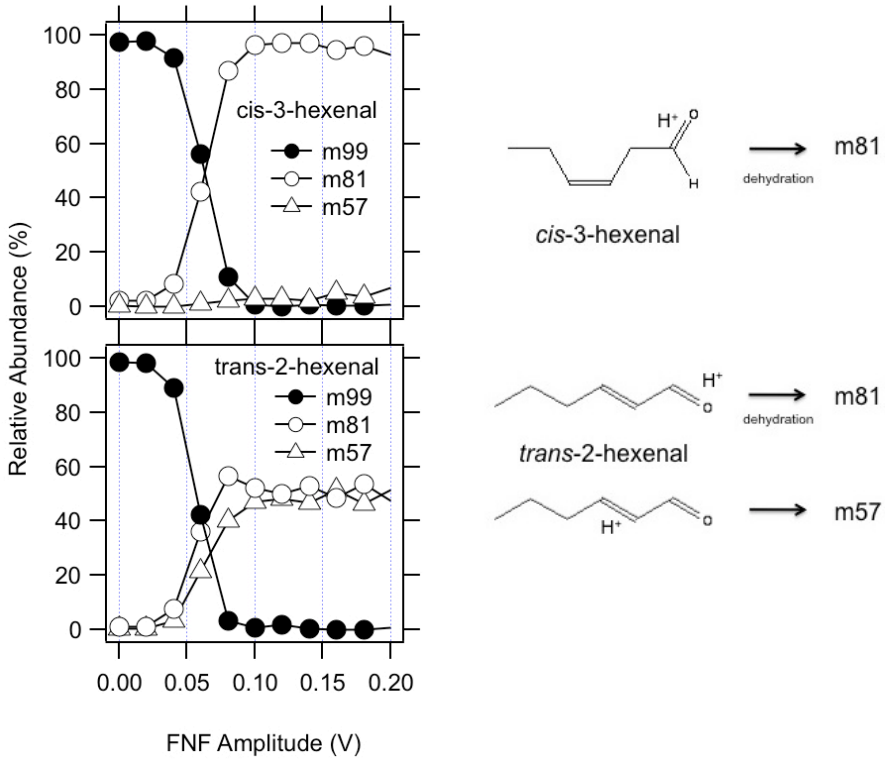

Figure 6.4. Laboratory CID spectra of *cis*-3 and *trans*-2 isomers of hexenal.

In Figure 6.5, the CID spectra of a saturated and unsaturated C7 aldehyde are compared. For both compounds, the loss of water leads to the most abundant fragment. The next most abundant fragment for *trans*-2-heptenal is m57, the equivalent pattern as previously discussed for *trans*-2-hexenal. This fragment is also probably protonated acrolein (PA=797 kJ/mol), which would make the neutral lost butene (C_4H_8 (56 amu), PA≈750 kJ/mol).

3.3 CID of Biogenic Compounds from Field and Enclosure Studies

Figure 6.6 shows select cases where CID provides useful information for compound identification during field measurements. The results in the first column clearly indicate that the compound detected at m99 in the manzanita branch enclosure is cis-2-hexenal (fragment nearly 100% at m81) rather than trans-2-hexenal (~50% of fragments each at m57 and m81). The results from the ponderosa branch enclosure clearly show emissions of monoterpenes, but the CID pattern shows more m95 fragments than the patterns of pure α-pinene (Figure 6.1), β-pinene or 3-carene (Figure 6.6). A similar result is seen in the final column for sesquiterpenes measured during the same enclosure experiment. CID was useful in identifying methyl chavicol emissions from the same branch (Bouvier-Brown et al., 2009).

CID spectra from field and branch enclosure measurements of m71 are compared with laboratory spectra of MVK and methacrolein in Figure 6.7. The branch enclosure CID more closely matches that of methyl vinyl ketone. This

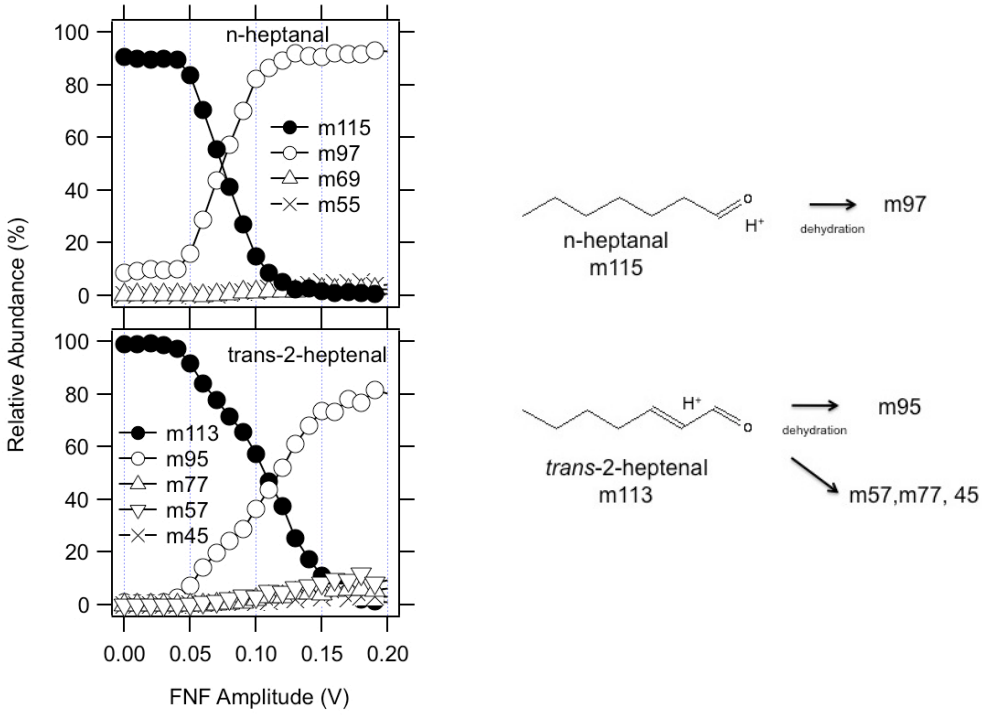

Figure 6.5. Laboratory CID spectra comparing n-heptanal (C7, saturated) with *trans*-2-heptenal (C7, unsaturated).

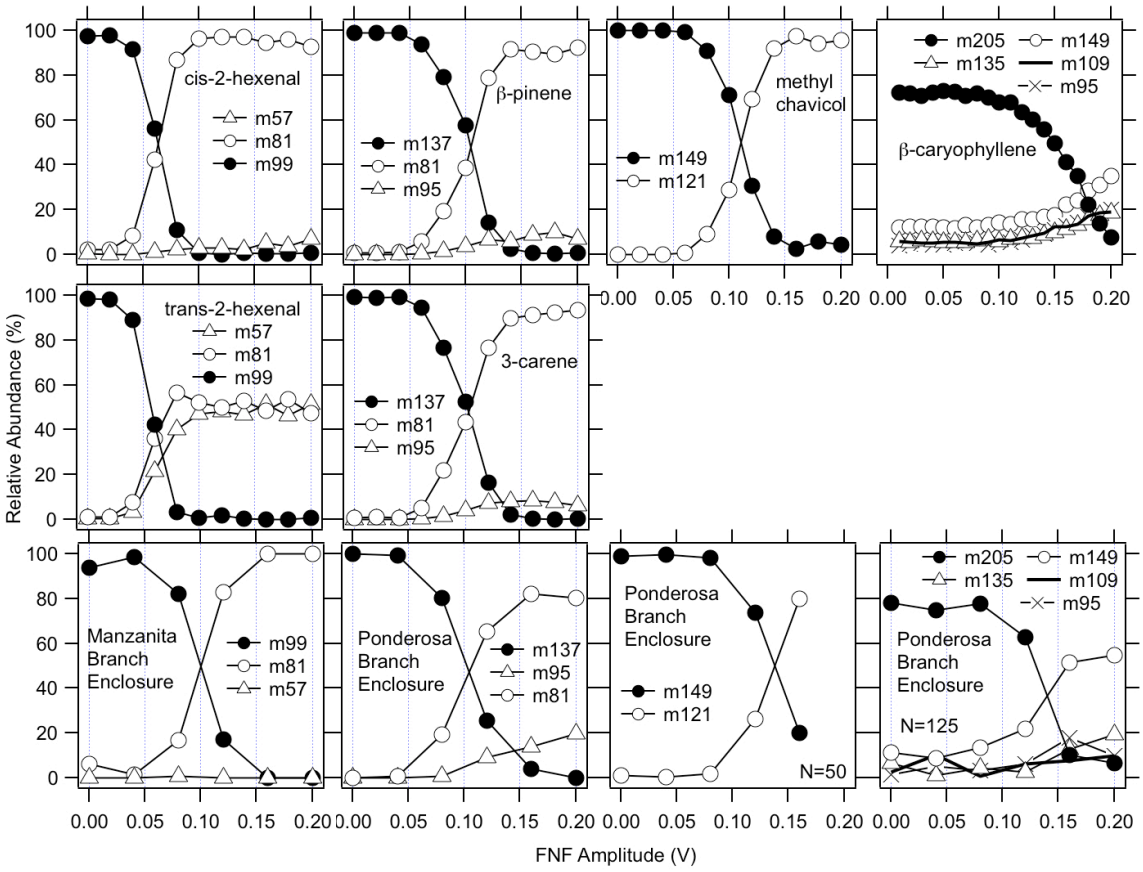

Figure 6.6. Select results from CID on VOCs in 2005 branch enclosures at Blodgett Forest. Rows 1 and 2 show laboratory spectra for comparison with enclosure CID spectra in the bottom row. Each column shows a single m/z.

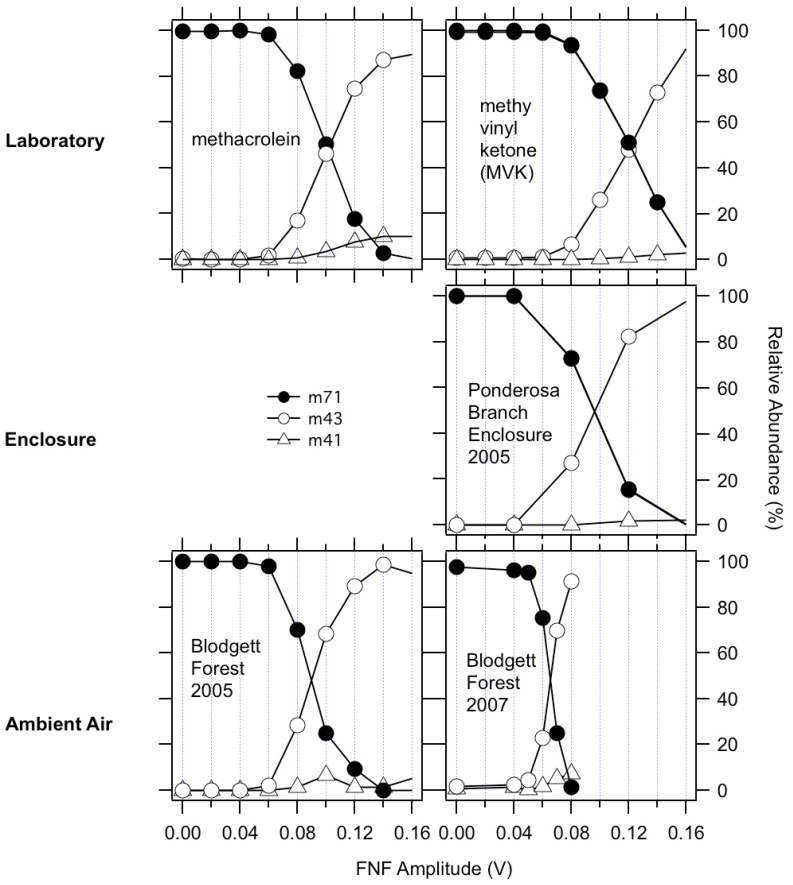

Figure 6.7. Laboratory, ambient and enclosure CID spectra for m71.

compound is not thought to be a primary biogenic emission and was therefore not expected to be present in the branch enclosure. However, many other compounds could be present with this m/z (pentenes, crotonaldehyde, etc.). The m71 trapped could also be fragment of a larger compound (e.g. a m89 alcohol) formed in the drift region of the PIT-MS instrument. Without further information on CID spectra from these other possible signals, we cannot suggest an identification of this emission.

MVK and methacrolein, formed photochemically from isoprene emitted by plants at lower elevations and transported to the study site, are routinely observed at Blodgett Forest (Spaulding et al., 2003). Although considerable effort was made to distinguish the signals from these two compounds based on ambient measurements by PIT-MS in 2005, the precision and repeatability of the CID measurements did not allow a quantitative separation of the two compounds at ambient mixing ratios where CID signals were typically on a few counts per trapping cycle (10s). It is possible that with larger mixing ratios of these compounds or by the dedicated measurement of CID spectra, the two isomers could be distinguished by PIT-MS as they were using CID in a linear ion trap (Muller et al., 2009). This was not attempted, however.

CID patterns of ions at m73 in the 2008 sapling enclosure experiment are compared with laboratory spectra of MEK and n-butanal in Figure 6.8. Direct emission of one of these compounds could contribute to the CID spectrum shown, but the presence of additional CID fragments at m45 and m43 suggests the presence of one or more other compounds. An unsaturated alcohol (e.g. 3-buten-1-ol) might both dehydrate (if protonated at the hydroxy group) and lose a neutral ethylene

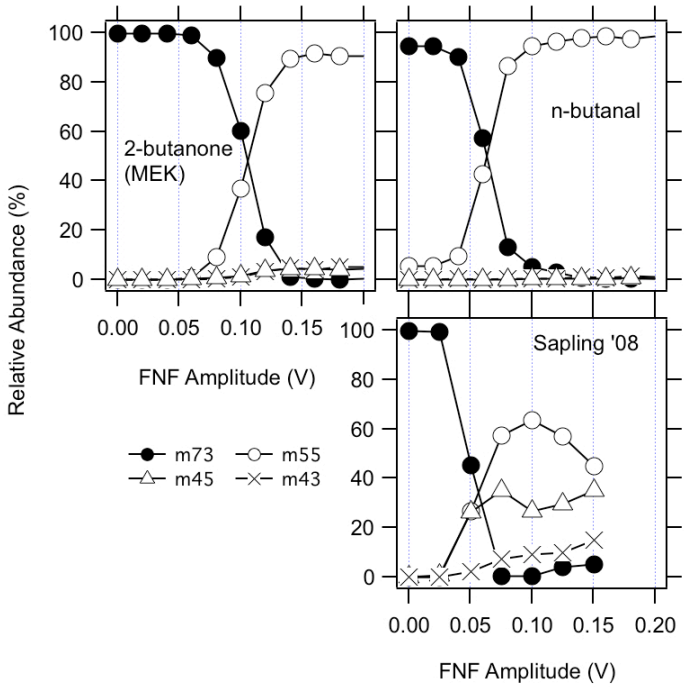

Figure 6.8. Laboratory (top) and enclosure (bottom) CID spectra for m73.

molecule (producing a m45 ion) during CID. This is analogous to what occurs during CID of MBO. Without further data, this remains speculative and compound identification is not possible.

The CID spectra of m87 from field and enclosure studies are compared with laboratory CID of MBO and biacetyl in Figure 6.9. Also shown is the CID spectrum at m87 of a calibration standard containing both MBO and biacetyl (11.0 and 11.3 ppbv, respectively). From Figure 6.3, it appears a fragment at m59 from a parent ion of m87 is a unique characteristic of biacetyl. Although the CID of every possible isomer at m87 was not taken, most other oxygenated compounds would fragment at least partially to m69. In the calibration standard, where MBO:biacetyl ≈ 1, the m59 fragment dominates the CID spectrum (Figure 6.9, top right). The m59 ion appears to be much more efficiently produced than the m69 fragment from MBO by about a factor of 10.

This extreme sensitivity of CID to the presence of biacetyl illustrates the difficulties involved in using CID for quantification of VOCs. The m59 fragment in both branch enclosure studies in 2005 and 2008 and in ambient measurements from Blodgett forest in 2005 and 2007 strongly suggests the presence of biacetyl, possibly at mixing ratios similar to those seen for MBO, making it an important source of the acetyl radical during the daytime due to its short lifetime (~30 min) with respect to photolysis (Kim et al., 2007;Klotz et al., 2001). However, mixing ratios of biacetyl were subsequently measured by GC-MS during the BEARPEX campaign in 2007. Biacetyl was detected in average mixing ratios as high as 60 pptv

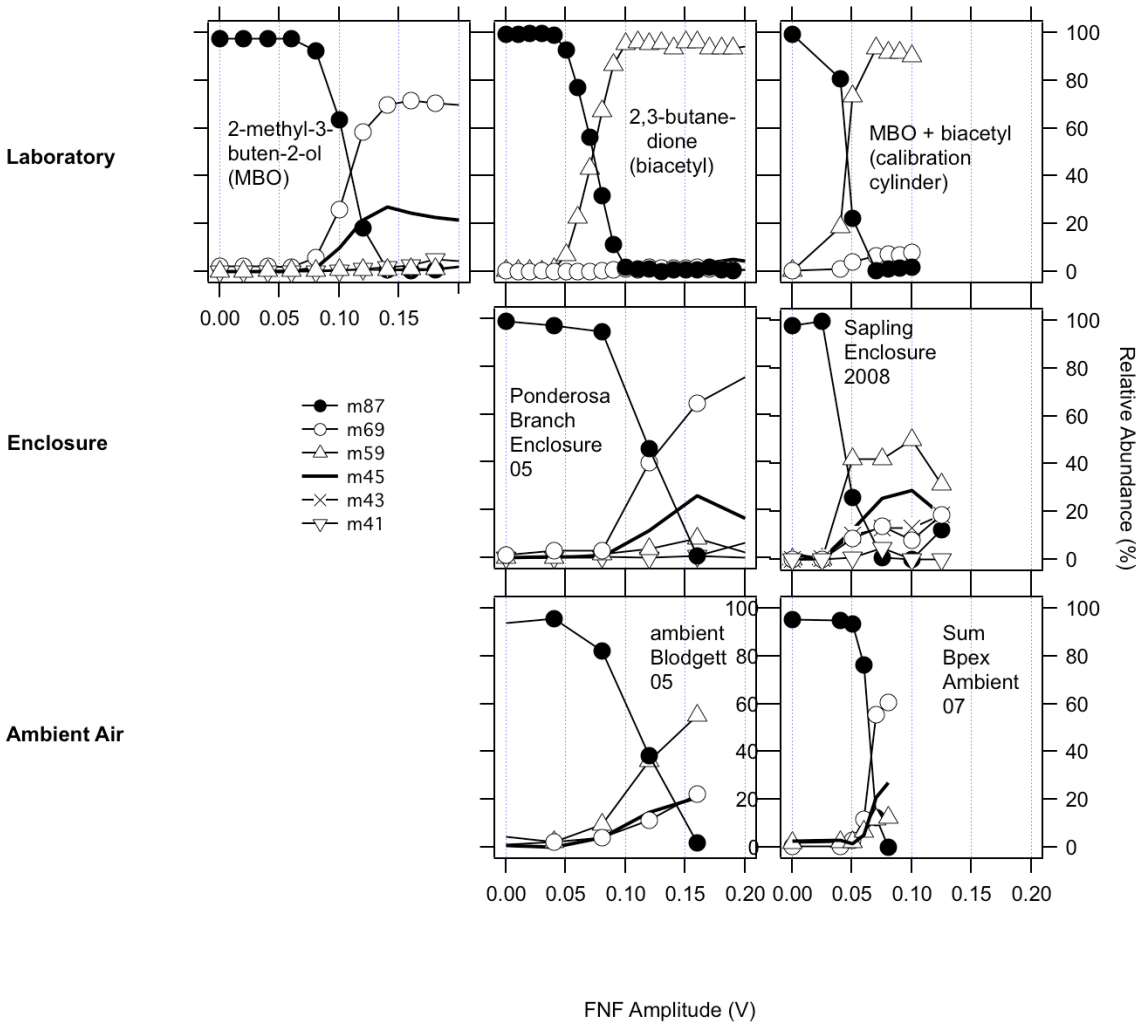

Figure 6.9. Laboratory (top row), enclosure (middle row) and ambient (forest) air CID spectra for m87. The top right CID spectrum was made from a calibration standard containing 11.0 ppm MBO and 11.3 ppm biacetyl. The ambient CID spectrum from 2007 is the normalized sum of multiple individual CID spectra made during the BEARPEX campaign.

during the night, while MBO had daytime averages of about 5 ppbv during the same period with nighttime minima of about 1 ppbv.

A typical CID of m87 from the 2005 ambient measurement (Figure 6.9, bottom left) shows the m59 fragment larger than that of the m69 fragments. The campaign average CID from 2007 shows more of the m69 fragment. This result suggests that there may have been more biacetyl present during the 2005 campaign, but because there were no measurements made by GC-FID/MS in 2005, this can not be verified. The presence of the m59 fragment in CID spectra of m87 during enclosure studies of ponderosa pine from 2005 and 2008 (Figure 6.9, middle row) support the hypothesis that biacetyl is a primary biogenic emission but more work is required to show this definitively.

One important oxidation product unique to MBO is 2-hydroxy-2-methyl propanal (HMPr) (Alvarado et al., 1999;Spaulding et al., 2003). Hydroxy aldehydes and ketones cannot be measured by the NOAA GC-MS but are detectable using the proton-transfer reaction method. HMPr is not stable and cannot be purchased and therefore, no laboratory CID spectrum is available. However, HMPr has been reported at m89 using PTR-MS (Kim et al., 2010). As an alcohol, HMPr (and all other C4 hydroxy carbonyls) would be expected to have a dehydration fragment in CID at m71. One biogenic isomer of HMPr that is stable is acetoin, which is a common product in bacterial fermentation (Cheng, 2010). The CID spectrum of acetoin (Figure 6.10, top) shows the alcohol dehydration fragment at m71 and another fragment at m43. These fragments are also observed in the CID spectrum shown from the 2005 ponderosa branch enclosure.

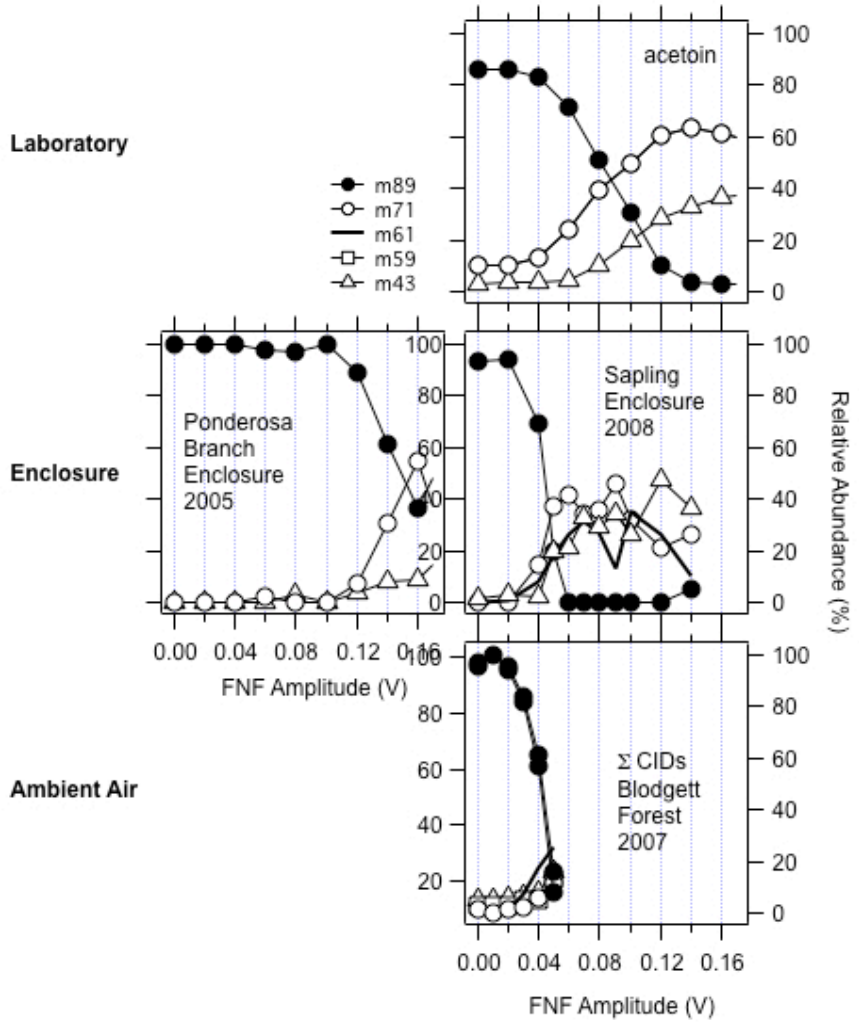

Figure 6.10. CID spectra of m89 from the laboratory (top), enclosure studies (middle row) and ambient (forest) air. The ambient CID is the normalized sum of multiple individual CID spectra made during the 2007 BEARPEX campaign.

HMPr would not be expected as a direct emission from ponderosa pine. Fragments are observed at m71, m61 and m43 in m89 CID spectra from the ponderosa sapling enclosure in 2008 and in ambient CIDs at Blodgett Forest in 2007, this suggests the presence of another compound at m89. The m61 CID fragment requires the loss of a neutral of 28 amu (ethylene). Based on the laboratory CID spectra of 5 isomers at m87 (Section 3.1), the loss of a neutral alkene is more likely for a protonated ketone. The protonated C4 hydroxyketone 1-hydroxy-2-butanone would have the right molecular mass and might split off an ethylene molecule during CID. Obviously, a definitive identification of the parent molecule cannot be made based on CID alone. However, CID spectra do suggest that another compound might be present at m89.

3.4 CID from Biomass Burning Experiments

CID spectra were also made during the FLAME III biomass burning experiment and will be briefly discussed here. Hundreds of individual compounds were observed by PIT-MS during a similar burn experiment (Warneke et al., 2011). Multiple compounds contributed to the signal at many different product ion mass signals, especially at higher molecular masses. Figure 6.11 shows CID spectra from the smoke from 3 different fuel types burned during the study at masses 87, 89, 125, 153 and 157. During the combustion of ponderosa pine, CID spectra at m87 show fragments at m59 and m69. Based on the previous discussion of CID at this mass, it seems likely that at least two compounds contribute to the signal observed at m87.

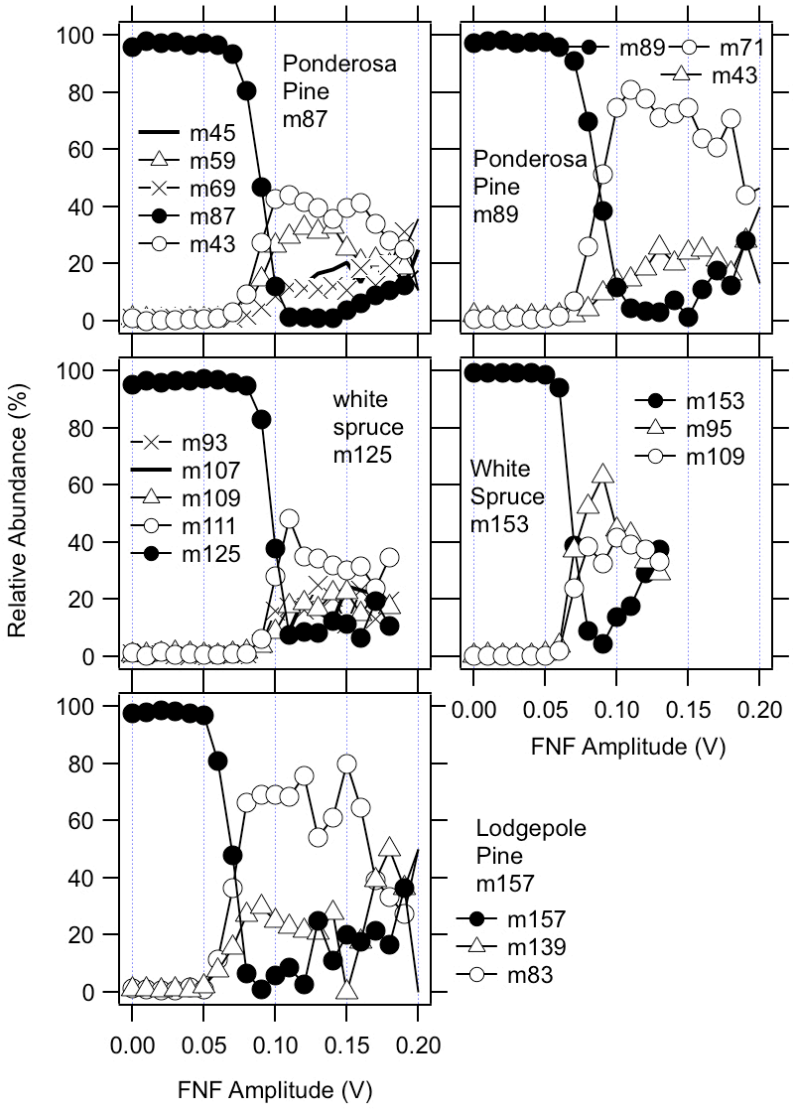

Figure 6.11. CID spectra made from smoke generated from biomass burning during the FLAME III study for three different fuel types.

The presence of biacetyl is strongly suggested by the CID. Because the fuel was ponderosa pine, it seems likely that MBO also contributes to the signal observed here, but CID cannot confirm or refute this identification.

The CID of m89 made during the same burn reveals the likely presence of a C4 hydroxycarbonyl because of the m71 fragment. The spectrum is similar to that of acetoin, but definitive identification is not possible due to the large number of possible isomers at this m/z.

Two CID spectra are shown in Figure 6.11 from a burn of white spruce. The first CID, that of m125, shows fragments from the loss of 14, 16, 18 and 32 amu. The identity of this compound or compounds is not evident from the CID, nor is the fragmentation pattern similar to any previous CID spectrum.

The CID at m153 taken during the same burn shows fragments at m109 and m95 (loss of neutrals at 44 (e.g., propane or acetaldehyde) and 58 amu (e.g., butane or acetone)). A CID pattern of this product ion mass was also taken during the 2008 sapling enclosure experiment (Figure 6.12). It is interesting that both CID spectra show the same two fragments at m108 and m95. During the sapling enclosure study, signal at this mass correlated well with MBO. An additional fragment at m125 was observed in the CID from the sapling experiment. A likely neutral lost from m153 is therefore ethylene and this would be consistent with previous losses of neutral ethylene during CID. Oxygenated monoterpenes and methyl salicylate have been identified by PTR-MS at this mass in ponderosa pine forests (Kim et al., 2010) and in a walnut plantation (Karl et al., 2008) respectively. However, there are so many possible isobaric compounds at this mass that identification is not possible

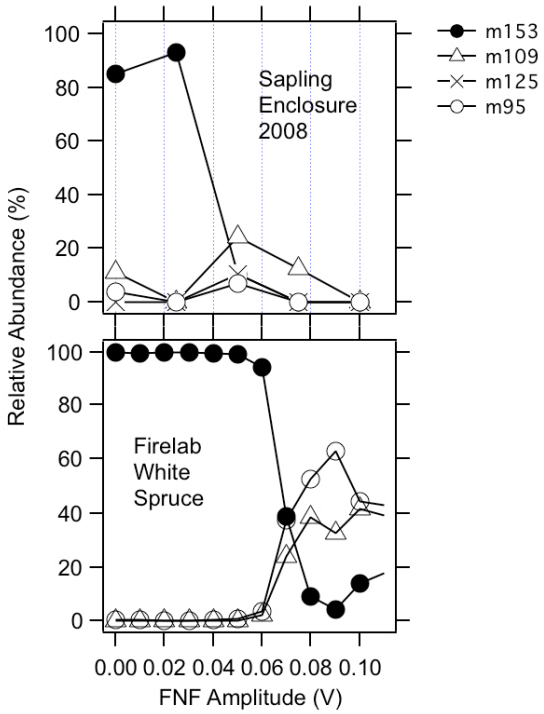

Figure 6.12. CID spectra of m153 observed in the 2008 sapling enclosure study and from smoke analyzed during the FLAME III study.

from either CID spectrum.

Finally, a CID spectrum is shown in Figure 6.11 for m157 from a burn of lodgepole pine. Signal at this mass was common in burns during the FLAME III study. Fragments are seen at m139 (loss of water) and m83 (loss of 74). The loss of water implies an oxygenated molecule. Few hydrocarbons containing only carbon and hydrogen can have a molecular mass of 74 so it seems likely that we observe the first loss of an oxygenated neutral (e.g., butanol) during CID. However, diamine compounds (e.g. 1,2-propanediamine) can have a molecular mass of 74 amu. Nitrogenated compounds are thought to be common in wood smoke, so it is possible that a diamine could contribute to signal at this mass. Again, CID spectra provide hints of a compound's structure but are not sufficient for identification by themselves.

4. Conclusions

In this Chapter, we have examined CID spectra taken by PIT-MS over the period of four years in the laboratory, in field studies, branch enclosures and in the smoke from biomass burning experiments. During CID, protonated VOCs fragment to both charged species that can be detected and neutral fragments that cannot be detected.

We find that the most common fragments observed in CID spectra of oxygenates are the result of the dehydration of compounds including alcohols, ketones and aldehydes. Protonation at a terminal oxygen molecule or on any hydroxy functional group often appears to result in dehydration. Neutral losses of

ethylene (28 amu), propylene (42 amu), alkanes and even formaldehyde (30 amu) were observed during CID.

The hypothesis that the structure of fragments is often driven by the proton affinity of the possible ions and neutral compounds produced often does not agree with experimental results. In many cases, the ionized fragments observed are neutral compounds with higher proton affinities than the neutrals lost. Molecular rearrangements appear common and result in fragments that might be difficult to predict from first principles.

CID provides valuable information that can distinguish some isomers and isobaric compounds and supplement other measurement methods (e.g., PTR-MS or GC-MS). In some cases, CID has been useful for the identification of unknown compounds (e.g., methyl chavicol). The CID method works best for compounds where there are unique fragment ions. However, there can be considerable variability in the efficiency of production of fragment ions (e.g., MBO and biacetyl) that complicates measurements of compound mixtures, which are common in ambient measurements. Discrimination of isomers like MVK and methacrolein using PIT-MS CID should be possible because the m41 and m43 have different relative abundances during CID. However, efforts to distinguish these isomers were not successful due to low ambient mixing ratios (< 1 ppbv). PIT-MS CID should be able to resolve these compounds at higher mixing ratios, or in the case of a dedicated continuous measurement, which could be done in a future study.

CHAPTER 7

CONCLUSIONS

The PIT-MS instrument was designed to enhance the capabilities of the proton-transfer-reaction method for identification and speciation of complex VOC mixtures in ambient air. The coupling of a PTR ion source to an ion trap mass spectrometer was undertaken to provide two main capabilities not available in the commercial PTR-MS instrument. First, the ability of the PIT-MS instrument to perform full range mass scans of 180+ masses allows the routine monitoring of signals not normally monitored using the commercial instruments which typically monitor 10-15 masses during field studies. Second, the PIT-MS instrument has the capability to operate in CID mode, which is not possible in the commercial instrument. In addition, the PIT-MS instrument has been operated several times in the field and coupled to a GC-separation system to provide chemical speciation beyond that offered by PTR-based instruments alone. While this latter application is not unique to the PIT-MS instrument, it has been useful in speciating (but not quantifying) isobaric mixtures of organic compounds under field conditions.

In this thesis, we have discussed results from the PIT-MS instrument over the period from 2004-2008 in both the field and the laboratory. In Chapters 2 and 3, I discussed the measurements made by the PIT-MS instrument in a subtropical megacity during the MILAGRO campaign in 2006. Measurements made during the campaign have produced scientifically interesting results related to the

photochemical processing of VOCs (de Gouw et al., 2009b) and VOC source apportionment (Bon et al., 2011). PIT-MS data were used to calculate Emission Ratios that should be useful to policy makers, regulators and atmospheric modelers. In addition, the GC-PIT-MS results from the MILAGRO study presented in Chapter 3 supplement our understanding of VOC source apportionment and signal assignment by PTR-MS and PIT-MS in heavily populated urban areas (Chapters 3-4).

We have also discussed the results of ship based PIT-MS measurements in the heavily industrialized areas near Houston, Texas made later in 2006. In this environment, the high time resolution and full mass range of the instrument was very useful in resolving the highly complex and variable VOC mixtures in industrial plumes. Data from the PIT-MS instrument were used to evaluate an industrial emission inventory, providing valuable information for policy makers and regulators trying to understand the sources of the area's high ozone. Again during the TexAQS 2006 campaign, the use of GC-PIT-MS helped identify and speciate PIT-MS measurements and increased our understanding and ability to interpret PTR-MS measurements in industrialized areas.

The deployment of the PIT-MS instrument in the forested environment near the Blodgett Forest Research Station in 2004 and 2007, successfully demonstrated the use of CID to identify and resolve complex VOC mixtures while still providing on-line ambient VOC measurements. Field (2004) and laboratory (2008) studies of plant enclosures also extended our understanding of PTR-MS measurements made in forested environments.

Finally, the PIT-MS was deployed twice to the Fire Sciences Laboratory (FSL) in Missoula, MT in 2009 to characterize the smoke from biomass burning experiments. The first deployment (not discussed here) was useful in identifying and characterizing VOCs in biomass burning emissions by region. GC-PIT-MS chromatograms and emission factors calculated from PIT-MS instrument measurements can be found in the literature (Warneke et al., 2011). During the second deployment of the PIT-MS instrument to FSL, the CID capabilities of the PIT-MS instrument were used. Some of the results of this second deployment are presented here in Chapter 6.

One major motivation in deploying the PIT-MS in field campaigns was to provide the standard suite of PTR-MS online measurements of aromatics and OVOCs. The success at this is shown here in Chapters 3 and 5 where PIT-MS measurements are compared with VOC data from other instruments. It is interesting to note both the success of these measurements (e.g., toluene measurements) and the places where it was not particularly successful (e.g., benzene measurements). Hopefully the work presented here will be used to validate future PIT-MS measurements and also serve as a motivation for the continued improvement of this unique instrument.

The use of CID, GC-PIT-MS and careful comparison of PIT-MS measurements to GC-FID/MS measurements revealed that some common signal attributions of PTR-MS were not appropriate in one or more of the locations. For example, the PTR-MS signal at m69 is commonly interpreted as biogenic isoprene. However, in pine forests, m69 is a common fragment of MBO, another biogenic VOC. In Houston,

signal at m69 was indicative of industrial process involving isoprene as well as other compounds. And in Mexico City, m69 correlated well with vehicular tracers.

In this thesis, I have demonstrated the use of PIT-MS instrument in both laboratory and field settings to the analysis of complex VOC mixtures in ambient air. The high time-resolution, full range mass scans and capability for CID of the PIT-MS instrument all provided capabilities needed during field campaigns at Blodgett Forest, Mexico City and in Houston, TX. The PIT-MS was used to provide not just routine on-line VOC measurements, but to validate and refine our interpretation and understanding of PTR-MS measurements through the application of both CID and GC-PIT-MS.

BIBLIOGRAPHY

Alvarado, A., Tuazon, E. C., Aschmann, S. M., Arey, J., and Atkinson, R.: Products and mechanisms of the gas-phase reactions of oh radicals and o-3 with 2-methyl-3-buten-2-ol, Atmospheric Environment, 33, 2893-2905, 1999.

Andreae, M. O., and Merlet, P.: Emission of trace gases and aerosols from biomass burning, Glob. Biogeochem. Cycle, 15, 955-966, 2001.

Apel, E. C., Calvert, J. G., and Fehsenfeld, F. C.: The nonmethane hydrocarbon intercomparison experiment (nomhice) - task-1 and task-2, J. Geophys. Res.-Atmos., 99, 16651-16664, 1994.

Apel, E. C., Emmons, L. K., Karl, T., Flocke, F., Hills, A. J., Madronich, S., Lee-Taylor, J., Fried, A., Weibring, P., Walega, J., Richter, D., Tie, X., Mauldin, L., Campos, T., Weinheimer, A., Knapp, D., Sive, B., Kleinman, L., Springston, S., Zaveri, R., Ortega, J., Voss, P., Blake, D., Baker, A., Warneke, C., Welsh-Bon, D., de Gouw, J., Zheng, J., Zhang, R., Rudolph, J., Junkermann, W., and Riemer, D. D.: Chemical evolution of volatile organic compounds in the outflow of the mexico city metropolitan area, Atmospheric Chemistry and Physics, 10, 2353-2375, 2010.

Atkinson, R., and Arey, J.: Atmospheric degradation of volatile organic compounds, Chemical Reviews, 103, 4605-4638, 2003.

Baker, A. K., Beyersdorf, A. J., Doezema, L., Katzenstein, A., Meinardi, S., Simpson, I., Blake, D. R., and Rowland, F. S.: Measurements of nonmethane hydrocarbons in 28 united states cities, Atmospheric Environment, 42, 170-182, 10.1016/j.atmosenv.2007.09.007, 2008.

Baker, J., Arey, J., and Atkinson, R.: Rate constants for the gas-phase reactions of oh radicals with a series of hydroxyaldehydes at 296 +/- 2 k, Journal Of Physical Chemistry A, 108, 7032-7037, 10.1021/jp048979o, 2004.

Ban-Weiss, G. A., McLaughlin, J. P., Harley, R. A., Kean, A. J., Grosjean, E., and Grosjean, D.: Carbonyl and nitrogen dioxide emissions from gasoline- and diesel-powered motor vehicles, Environmental Science & Technology, 42, 3944–3950, 10.1021/es8002487 2008.

Blake, D. R., and Rowland, F. S.: Urban leakage of liquefied petroleum gas and its impact on mexico-city air-quality, Science, 269, 953-956, 1995.

Blake, R. S., Monks, P. S., and Ellis, A. M.: Proton-transfer reaction mass spectrometry, Chem. Rev., 109, 861-896, 10.1021/cr800364q, 2009.

Bon, D. M., Ulbrich, I. M., de Gouw, J. A., Warneke, C., Kuster, W. C., Alexander, M. L., Baker, A., Beyersdorf, A. J., Blake, D., Fall, R., Jimenez, J. L., Herndon, S. C., Huey, L. G., Knighton, W. B., Ortega, J., Springston, S., and Vargas, O.: Measurements of volatile organic compounds at a suburban ground site (t1) in mexico city during the milagro 2006 campaign: Measurement comparison, emission ratios, and source attribution, Atmos. Chem. Phys., 11, 2399-2421, 10.5194/acp-11-2399-2011, 2011.

Bouvier-Brown, N. C., Holzinger, R., Palitzsch, K., and Goldstein, A. H.: Quantifying sesquiterpene and oxygenated terpene emissions from live vegetation using solid-phase microextraction fibers, J. Chromatogr. A, 1161, 113-120, 10.1016/j.chroma.2007.05.094, 2007.

Bouvier-Brown, N. C., Goldstein, A. H., Worton, D. R., Matross, D. M., Gilman, J. B., Kuster, W. C., Welsh-Bon, D., Warneke, C., de Gouw, J. A., Cahill, T. M., and Holzinger, R.: Methyl chavicol: Characterization of its biogenic emission rate, abundance, and oxidation products in the atmosphere, Atmospheric Chemistry and Physics, 9, 2061-2074, 2009a.

Bouvier-Brown, N. C., Holzinger, R., Palitzsch, K., and Goldstein, A. H.: Large emissions of sesquiterpenes and methyl chavicol quantified from branch enclosure measurements, Atmospheric Environment, 43, 389-401, 10.1016/j.atmosenv.2008.08.039, 2009b.

Brown, S. G., Frankel, A., and Hafner, H. R.: Source apportionment of vocs in the los angeles area using positive matrix factorization, Atmospheric Environment, 41, 227-237, 2007.

Brunekreef, B., and Forsberg, B.: Epidemiological evidence of effects of coarse airborne particles on health, Eur. Resp. J., 26, 309-318, 2005.

Buzcu, B., and Fraser, M. P.: Source identification and apportionment of volatile organic compounds in houston, tx, Atmospheric Environment, 40, 2385-2400, 10.1016/j.atmosenv.2005.12.020, 2006.

Cheng, H. F.: Volatile flavor compounds in yogurt: A review, Crit. Rev. Food Sci. Nutr., 50, 938-950, 10.1080/10408390903044081, 2010.

Collins, W. J., Derwent, R. G., Johnson, C. E., and Stevenson, D. S.: The oxidation of organic compounds in the troposphere and their global warming potentials, Clim. Change, 52, 453-479, 2002.

Colman, J. J., Swanson, A. L., Meinardi, S., Sive, B. C., Blake, D. R., and Rowland, F. S.: Description of the analysis of a wide range of volatile organic compounds in whole air samples collected during pem-tropics a and b, Analytical Chemistry, 73, 3723-3731, 2001.

Curtius, J., Froyd, K. D., and Lovejoy, E. R.: Cluster ion thermal decomposition (i): Experimental kinetics study and ab initio calculations for hso4-(h2so4)(x)(hno3)(y), J. Phys. Chem. A, 105, 10867-10873, 10.1021/jp0124950, 2001.

de Gouw, J., and Jimenez, J. L.: Organic aerosols in the earth's atmosphere, Environ. Sci. Technol., 43, 7614-7618, 10.1021/es9006004, 2009.

de Gouw, J. A., Goldan, P. D., Warneke, C., Kuster, W. C., Roberts, J. M., Marchewka, M., Bertman, S. B., Pszenny, A. A. P., and Keene, W. C.: Validation of proton transfer reaction-mass spectrometry (ptr-ms) measurements of gas-phase organic compounds in the atmosphere during the new england air quality study (neaqs) in 2002, Journal of Geophysical Research-Atmospheres, 108, 4682, 10.1029/2003JD003863, 2003.

de Gouw, J. A., Cooper, O. R., Warneke, C., Hudson, P. K., Fehsenfeld, F. C., Holloway, J. S., Hubler, G., Nicks, D. K., Nowak, J. B., Parrish, D. D., Ryerson, T. B., Atlas, E. L., Donnelly, S. G., Schauffler, S. M., Stroud, V., Johnson, K., Carmichael, G. R., and Streets, D. G.: Chemical composition of air masses transported from asia to the u. S. West coast during itct 2k2: Fossil fuel combustion versus biomass-burning signatures, J. Geophys. Res.-Atmos., 109, D23S20, doi:10.1029/2003JD004202, 2004.

de Gouw, J. A., Middlebrook, A. M., Warneke, C., Goldan, P. D., Kuster, W. C., Roberts, J. M., Fehsenfeld, F. C., Worsnop, D. R., Canagaratna, M. R., Pszenny, A. A. P., Keene, W. C., Marchewka, M., Bertman, S. B., and Bates, T. S.: Budget of organic carbon in a polluted atmosphere: Results from the new england air quality study in 2002, Journal of Geophysical Research-Atmospheres, 110, D16305, doi:10.1029/2004JD005623, 2005.

de Gouw, J. A., and Warneke, C.: Measurements of volatile organic compounds in the earth's atmosphere using proton-transfer-reaction mass spectrometry, Mass Spectrometry Reviews, 26, 223-257, 2007.

de Gouw, J. A., Hekkert, S. T. L., Mellqvist, J., Warneke, C., Atlas, E. L., Fehsenfeld, F. C., Fried, A., Frost, G. J., Harren, F. J. M., Holloway, J. S., Lefer, B., Lueb, R., Meagher, J. F., Parrish, D. D., Patel, M., Pope, L., Richter, D., Rivera, C., Ryerson, T. B., Samuelsson, J., Walega, J., Washenfelder, R. A., Weibring, P., and Zhu, X.: Airborne measurements of ethene from industrial sources using laser photo-acoustic spectroscopy, Environ. Sci. Technol., 43, 2437-2442, 10.1021/es802701a, 2009a.

de Gouw, J. A., Welsh-Bon, D., Warneke, C., Kuster, W. C., Alexander, L., Baker, A. K., Beyersdorf, A. J., Blake, D. R., Canagaratna, M., Celada, A. T., Huey, L. G., Junkermann, W., Onasch, T. B., Salcido, A., Sjostedt, S. J., Sullivan, A. P., Tanner, D. J., Vargas, O., Weber, R. J., Worsnop, D. R., Yu, X. Y., and Zaveri, R.: Emission and chemistry of organic carbon in the gas and aerosol phase at a sub-urban

site near mexico city in march 2006 during the milagro study, Atmospheric Chemistry And Physics, 9, 3425-3442, 2009b.

de Gouw, J. A., Middlebrook, A. M., Warneke, C., Ahmadov, R., Atlas, E. L., Bahreini, R., Blake, D. R., Brock, C. A., Brioude, J., Fahey, D. W., Fehsenfeld, F. C., Holloway, J. S., Le Henaff, M., Lueb, R. A., McKeen, S. A., Meagher, J. F., Murphy, D. M., Paris, C., Parrish, D. D., Perring, A. E., Pollack, I. B., Ravishankara, A. R., Robinson, A. L., Ryerson, T. B., Schwarz, J. P., Spackman, J. R., Srinivasan, A., and Watts, L. A.: Organic aerosol formation downwind from the deepwater horizon oil spill, Science, 331, 1295-1299, 10.1126/science.1200320, 2011.

Diaz, L., Schifter, I., Lopez-Salinas, E., Gamas, E., Rodriguez, R., and Avalos, S.: Optimizing automotive lpg blend for mexico city, Fuel, 79, 79-88, 2000.

Edgerton, S. A., Bian, X., Doran, J. C., Fast, J. D., Hubbe, J. M., Malone, E. L., Shaw, W. J., Whiteman, C. D., Zhong, S., Arriaga, J. L., Ortiz, E., Ruiz, M., Sosa, G., Vega, E., Limon, T., Guzman, F., Archuleta, J., Bossert, J. E., Elliot, S. M., Lee, J. T., McNair, L. A., Chow, J. C., Watson, J. G., Coulter, R. L., Doskey, P. V., Gaffney, J. S., Marley, N. A., Neff, W., and Petty, R.: Particulate air pollution in mexico city: A collaborative research project, J. Air Waste Manage. Assoc., 49, 1221-1229, 1999.

Engel-Cox, J. A., and Weber, S. A.: Compilation and assessment of recent positive matrix factorization and unmix receptor model studies on fine particulate matter source apportionment for the eastern united states, Journal Of the Air & Waste Management Association, 57, 1307-1316, 10.3155/1047-3289.57.11.1307, 2007.

Fast, J., Aiken, A. C., Allan, J., Alexander, L., Campos, T., Canagaratna, M. R., Chapman, E., DeCarlo, P. F., de Foy, B., Gaffney, J., de Gouw, J., Doran, J. C., Emmons, L., Hodzic, A., Herndon, S. C., Huey, G., Jayne, J. T., Jimenez, J. L., Kleinman, L., Kuster, W., Marley, N., Russell, L., Ochoa, C., Onasch, T. B., Pekour, M., Song, C., Ulbrich, I. M., Warneke, C., Welsh-Bon, D., Wiedinmyer, C., Worsnop, D. R., Yu, X. Y., and Zaveri, R.: Evaluating simulated primary anthropogenic and biomass burning organic aerosols during milagro: Implications for assessing treatments of secondary organic aerosols, Atmospheric Chemistry And Physics, 9, 6191-6215, 2009.

Fast, J. D., de Foy, B., Rosas, F. A., Caetano, E., Carmichael, G. R., Emmons, L., McKenna, D., Mena, M., Skamarock, W., Tie, X., Coulter, R. L., Barnard, J. C., Wiedinmyer, C., and Madronich, S.: A meteorological overview of the milagro field campaigns, Atmospheric Chemistry And Physics, 7, 2233-2257, 2007.

Field, F. H.: The early days of chemical ionization - a reminiscence, J. Am. Soc. Mass Spectrom., 1, 277-283, 1990.

Finlayson-Pitts, B. J.: Tropospheric air pollution: Ozone, airborne toxics, polycyclic aromatic hydrocarbons, and particles, Science, 276, 1045-1051, 10.1126/science.276.5315.1045, 1997.

Finlayson-Pitts, B. J., and Pitts, J. N.: Chemistry of the upper and lower atmosphere, Academic Prss, San Diego, 2000.

Fortner, E. C., and Knighton, W. B.: Quantitatively resolving mixtures of isobaric compounds using chemical ionization mass spectrometry by modulating the reactant ion composition, Rapid Communications in Mass Spectrometry, 22, 2597-2601, 10.1002/rcm.3645, 2008.

Fortner, E. C., Zheng, J., Zhang, R., Knighton, W. B., Volkamer, R. M., Sheehy, P., Molina, L., and Andre, M.: Measurements of volatile organic compounds using proton transfer reaction - mass spectrometry during the milagro 2006 campaign, Atmospheric Chemistry And Physics, 9, 467-481, 2009.

Frost, G.J., Revised TexAQS2K6 HGB point source emission inventory: http://www.esrl.noaa.gov/csd/2006/fieldops/emission.html, 2009.

Gilman, J. B., Kuster, W. C., Goldan, P. D., Herndon, S. C., Zahniser, M. S., Tucker, S. C., Brewer, W. A., Lerner, B. M., Williams, E. J., Harley, R. A., Fehsenfeld, F. C., Warneke, C., and de Gouw, J. A.: Measurements of volatile organic compounds during the 2006 texaqs/gomaccs campaign: Industrial influences, regional characteristics, and diurnal dependencies of the oh reactivity, J. Geophys. Res.-Atmos., 114, 17, D00f0610.1029/2008jd011525, 2009.

Goldan, P. D., Kuster, W. C., Fehsenfeld, F. C., and Montzka, S. A.: The observation of a c5 alcohol emission in a north-american pine forest, Geophys. Res. Lett., 20, 1039-1042, 1993.

Goldan, P. D., Parrish, D. D., Kuster, W. C., Trainer, M., McKeen, S. A., Holloway, J., Jobson, B. T., Sueper, D. T., and Fehsenfeld, F. C.: Airborne measurements of isoprene, co, and anthropogenic hydrocarbons and their implications, Journal of Geophysical Research-Atmospheres, 105, 9091-9105, 2000.

Goldan, P. D., Kuster, W. C., Williams, E., Murphy, P. C., Fehsenfeld, F. C., and Meagher, J.: Nonmethane hydrocarbon and oxy hydrocarbon measurements during the 2002 new england air quality study, J. Geophys. Res.-Atmos., 109, D2130910.1029/2003jd004455, 2004.

Goldstein, A. H., and Galbally, I. E.: Known and unexplored organic constituents in the earth's atmosphere, Environmental Science & Technology, 41, 1514-1521, 2007.

Graus, M., Muller, M., and Hansel, A.: High resolution ptr-tof: Quantification and formula confirmation of voc in real time, J. Am. Soc. Mass Spectrom., 21, 1037-1044, 10.1016/j.jasms.2010.02.006, 2010.

Green, T. J., Reeves, C. E., Fleming, Z. L., Brough, N., Rickard, A. R., Bandy, B. J., Monks, P. S., and Penkett, S. A.: An improved dual channel perca instrument for atmospheric measurements of peroxy radicals, J. Environ. Monit., 8, 530-536, 10.1039/b514630e, 2006.

Guenther, A., Hewitt, C. N., Erickson, D., Fall, R., Geron, C., Graedel, T., Harley, P., Klinger, L., Lerdau, M., McKay, W. A., Pierce, T., Scholes, B., Steinbrecher, R., Tallamraju, R., Taylor, J., and Zimmerman, P.: A global model of natural volatile organic compound emissions, Journal of Geophysical Research-Atmospheres, 100, 8873-8892, 1995.

Guenther, A., Karl, T., Harley, P., Wiedinmyer, C., Palmer, P. I., and Geron, C.: Estimates of global terrestrial isoprene emissions using megan (model of emissions of gases and aerosols from nature), Atmospheric Chemistry And Physics, 6, 3181-3210, 2006.

Hallquist, M., Wenger, J. C., Baltensperger, U., Rudich, Y., Simpson, D., Claeys, M., Dommen, J., Donahue, N. M., George, C., Goldstein, A. H., Hamilton, J. F., Herrmann, H., Hoffmann, T., Iinuma, Y., Jang, M., Jenkin, M. E., Jimenez, J. L., Kiendler-Scharr, A., Maenhaut, W., McFiggans, G., Mentel, T. F., Monod, A., Prevot, A. S. H., Seinfeld, J. H., Surratt, J. D., Szmigielski, R., and Wildt, J.: The formation, properties and impact of secondary organic aerosol: Current and emerging issues, Atmospheric Chemistry And Physics, 9, 5155-5236, 2009.

Harley, R. A., Hannigan, M. P., and Cass, G. R.: Respeciation of organic gas emissions and the detection of excess unburned gasoline in the atmosphere, Environ. Sci. Technol., 26, 2395-2408, 1992.

Hayward, S., Hewitt, C. N., Sartin, J. H., and Owen, S. M.: Performance characteristics and applications of a proton transfer reaction-mass spectrometer for measuring volatile organic compounds in ambient air, Environmental Science & Technology, 36, 1554-1560, 10.1021/es0102181, 2002.

Heald, C. L., Goldstein, A. H., Allan, J. D., Aiken, A. C., Apel, E., Atlas, E. L., Baker, A. K., Bates, T. S., Beyersdorf, A. J., Blake, D. R., Campos, T. L., Coe, H., Crounse, J. D., DeCarlo, P. F., de Gouw, J. A., Dunlea, E. J., Flocke, F. M., Fried, A., Goldan, P. D., Griffin, R. J., Herndon, S. C., Holloway, J. S., Holzinger, R., Jimenez, J. L., Junkermann, W., Kuster, W. C., Lewis, A. C., Meinardi, S., Millet, D. B., Onasch, T., Polidori, A., Quinn, P., Riemer, D. D., Roberts, J. M., Salcedo, D., Sive, B. C., Swanson, A. L., Talbot, R. W., Warneke, C., Weber, R. J., Weibring, P., Wennberg, P. O., Worsnop, D. R., Wittig, A. E., Zhang, R., Zheng, J., and Zheng, W.: Total observed organic carbon (tooc) in the atmosphere: A synthesis of

north american observations, Atmospheric Chemistry And Physics, 8, 2007-2025, 2008.

Herndon, S. C., Onasch, T. B., Wood, E. C., Kroll, J. H., Canagaratna, M. R., Jayne, J. T., Zavala, M. A., Knighton, W. B., Mazzoleni, C., Dubey, M. K., Ulbrich, I. M., Jimenez, J. L., Seila, R., de Gouw, J. A., de Foy, B., Fast, J., Molina, L. T., Kolb, C. E., and Worsnop, D. R.: Correlation of secondary organic aerosol with odd oxygen in mexico city, Geophysical Research Letters, 35, L15804, doi:10.1029/2008GL034058, 2008.

Huey, L. G.: Measurement of trace atmospheric species by chemical ionization mass spectrometry: Speciation of reactive nitrogen and future directions, Mass Spec. Rev., 26, 166-184, 10.1002/mas.20118, 2007.

Hunter, E. P. L., and Lias, S. G.: Evaluated gas phase basicities and proton affinities of molecules: An update, J. Phys. Chem. Ref. Data, 27, 413-656, 1998.

Jacob, D. J.: Global budget of methanol: Constraints from atmospheric observations, Journal of Geophysical Research, 110, 17, 10.1029/2004JD005172, 2005.

Jobson, B. T., Berkowitz, C. M., Kuster, W. C., Goldan, P. D., Williams, E. J., Fesenfeld, F. C., Apel, E. C., Karl, T., Lonneman, W. A., and Riemer, D.: Hydrocarbon source signatures in houston, texas: Influence of the petrochemical industry, J. Geophys. Res.-Atmos., 109, D2430510.1029/2004jd004887, 2004.

Karl, T.: Use of proton-transfer-reaction mass spectrometry to characterize volatile organic compound sources at the la porte super site during the texas air quality study 2000, J. Geophys. Res., 108, 15, doi:10.1029/2002JD003333, 2003.

Karl, T., Guenther, A., Turnipseed, A., Patton, E. G., and Jardine, K.: Chemical sensing of plant stress at the ecosystem scale, Biogeosciences, 5, 1287-1294, 2008.

Karl, T., Apel, E., Hodzic, A., Riemer, D. D., Blake, D. R., and Wiedinmyer, C.: Emissions of volatile organic compounds inferred from airborne flux measurements over a megacity, Atmospheric Chemistry and Physics, 9, 271-285, 2009.

Kim, D., Loughner, C. P., Wetzel, M. A., Goliff, W. S., and Stockwell, W. R.: A comparison of photolysis rate parameters estimated from measured and simulated actinic flux for wintertime conditions at storm peak laboratory, colorado, J. Atmos. Chem., 57, 59-71, 10.1007/s10874-007-9061-2, 2007.

Kim, E., Brown, S. G., Hafner, H. R., and Hopke, P. K.: Characterization of non-methane volatile organic compounds sources in houston during 2001 using positive matrix factorization, Atmospheric Environment, 39, 5934-5946, 10.1016/j.atmonsenv.2005.06.045, 2005.

Kim, S., Karl, T., Guenther, A., Tyndall, G., Orlando, J., Harley, P., Rasmussen, R., and Apel, E.: Emissions and ambient distributions of biogenic volatile organic compounds (bvoc) in a ponderosa pine ecosystem: Interpretation of ptr-ms mass spectra, Atmospheric Chemistry and Physics, 10, 1759-1771, 2010.

Kleinman, L. I., Daum, P. H., Lee, Y. N., Nunnermacker, L. J., Springston, S. R., Weinstein-Lloyd, J., and Rudolph, J.: A comparative study of ozone production in five u.S. Metropolitan areas, J. Geophys. Res.-Atmos., 110, 20, D0230110.1029/2004jd005096, 2005.

Kleinman, L. I., Springston, S. R., Daum, P. H., Lee, Y. N., Nunnermacker, L. J., Senum, G. I., Wang, J., Weinstein-Lloyd, J., Alexander, M. L., Hubbe, J., Ortega, J., Canagaratna, M. R., and Jayne, J.: The time evolution of aerosol composition over the mexico city plateau, Atmospheric Chemistry And Physics, 8, 1559-1575, 2008.

Klotz, B., Graedler, F., Sorensen, S., Barnes, I., and Becker, K. H.: A kinetic study of the atmospheric photolysis of alpha-dicarbonyls, Int. J. Chem. Kinet., 33, 9-20, 2001.

Krupa, S., McGrath, M. T., Andersen, C. P., Booker, F. L., Burkey, K. O., Chappelka, A. H., Chevone, B. I., Pell, E. J., and Zilinskas, B. A.: Ambient ozone and plant health, Plant Dis., 85, 4-12, 2001.

Kuster, W. C., Jobson, B. T., Karl, T., Riemer, D., Apel, E., Goldan, P. D., and Fehsenfeld, F. C.: Intercomparison of volatile organic carbon measurement techniques and data at la porte during the texaqs2000 air quality study, Environ. Sci. Technol., 38, 221-228, 10.1021/es034710r, 2004.

Lanz, V. A., Hueglin, C., Buchmann, B., Hill, M., Locher, R., Staehelin, J., and Reimann, S.: Receptor modeling of c2–c7 hydrocarbon sources at an urban background site in zurich, switzerland: Changes between 1993–1994 and 2005–2006, Atmospheric Chemistry And Physics, 8, 2313-2332, 2008.

Legreid, G., Loov, J. B., Staehelin, J., Hueglin, C., Hill, M., Buchmann, B., Prevot, A. S. H., and Reimann, S.: Oxygenated volatile organic compounds (ovocs) at an urban background site in zurich (europe): Seasonal variation and source allocation, Atmospheric Environment, 41, 8409-8423, 2007.

Lerner, B. M., Murphy, P. C., and Williams, E. J.: Field measurements of small marine craft gaseous emission factors during neaqs 2004 and texaqs 2006, Environ. Sci. Technol., 43, 8213-8219, 10.1021/es901191p, 2009.

Lias, S. G., Barmess, J. E., Liebman, J. F., Holmes, J. L., Levin, R. D., and Mallard, W. G.: Gas-phase ion and neutral thermochemistry, J. Phys. Chem. Ref. Data, 17, Supplement 1, 1988.

Lindinger, W., Hansel, A., and Jordan, A.: On-line monitoring of volatile organic compounds at pptv levels by means of proton-transfer-reaction mass spectrometry (ptr-ms) - medical applications, food control and environmental research, Int. J. Mass Spectrom., 173, 191-241, 1998.

Lovejoy, E. R., and Wilson, R. R.: Kinetic studies of negative ion reactions in a quadrupole ion trap: Absolute rate coefficients and ion energies, J. Phys. Chem. A, 102, 2309-2315, 1998.

McLafferty, F. W., and Turecek, F.: Interpretation of mass spectra, 4th ed., University Science Books, Sausalito, CA, 1993.

McMeeking, G. R., Kreidenweis, S. M., Baker, S., Carrico, C. M., Chow, J. C., Collett, J. L., Jr., Hao, W. M., Holden, A. S., Kirchstetter, T. W., Malm, W. C., Moosm¸ller, H., Sullivan, A. P., and Wold, C. E.: Emissions of trace gases and aerosols during the open combustion of biomass in the laboratory, J. Geophys. Res., 114, D19210, 10.1029/2009jd011836, 2009.

Mellqvist, J., Samuelsson, J., Johansson, J., Rivera, C., Lefer, B., Alvarez, S., and Jolly, J.: Measurements of industrial emissions of alkenes in texas using the solar occultation flux method, J. Geophys. Res.-Atmos., 115, 13, D00f1710.1029/2008jd011682, 2010.

Mielke, L. H., Pratt, K. A., Shepson, P. B., McLuckey, S. A., Wisthaler, A., and Hansel, A.: Quantitative determination of biogenic volatile organic compounds in the atmosphere using proton-transfer reaction linear ion trap mass spectrometry, Anal. Chem., 82, 7952-7957, 10.1021/ac1014244, 2010.

Millet, D. B., Goldstein, A. H., Holzinger, R., Williams, B. J., Allan, J. D., Jimenez, J. L., Worsnop, D. R., Roberts, J. M., White, A. B., Hudman, R. C., Bertschi, I. T., and Stohl, A.: Chemical characteristics of north american surface layer outflow: Insights from chebogue point, nova scotia, J. Geophys. Res.-Atmos., 111, 15, doi:D23s5310.1029/2006jd007287, 2006.

Millet, D. B., Jacob, D. J., Custer, T. G., de Gouw, J. A., Goldstein, A. H., Karl, T., Singh, H. B., Sive, B. C., Talbot, R. W., Warneke, C., and Williams, J.: New constraints on terrestrial and oceanic sources of atmospheric methanol, Atmospheric Chemistry And Physics, 8, 6887-6905, 2008.

Molina, L. T., Kolb, C. E., de Foy, B., Lamb, B. K., Brune, W. H., Jimenez, J. L., Ramos-Villegas, R., Sarmiento, J., Paramo-Figueroa, V. H., Cardenas, B., Gutierrez-Avedoy, V., and Molina, M. J.: Air quality in north america's most populous city - overview of the mcma-2003 campaign, Atmospheric Chemistry And Physics, 7, 2447-2473, 2007.

Molina, L. T., Madronich, S., Gaffney, J. S., Apel, E., de Foy, B., Fast, J., Ferrare, R., Herndon, S., Jimenez, J. L., Lamb, B., Osornio-Vargas, A. R., Russell, P., Schauer,

J. J., Stevens, P. S., Volkamer, R., and Zavala, M.: An overview of the milagro 2006 campaign: Mexico city emissions and their transport and transformation, Atmospheric Chemistry and Physics, 10, 8697-8760, 2010.

Muller, M., Mielke, L. H., Breitenlechner, M., McLuckey, S. A., Shepson, P. B., Wisthaler, A., and Hansel, A.: Ms/ms studies for the selective detection of isomeric biogenic vocs using a townsend discharge triple quadrupole tandem ms and a ptr-linear ion trap ms, Atmos. Meas. Tech., 2, 703-712, 2009.

Nist chemistry webbook database: http://webbook.nist.gov/chemistry/, 2011.

Olivier, J. G. J., Van Aardenne, J. A., Dentener, F. J., Ganzeveld, L., and Peters, J. A. H. W.: Recent trends in global greenhouse gas emissions: Regional trends and spatial distribution of key sources, in: Non-co 2 greenhouse gases (ncgg-4), ed., edited by: van Amstel, A., Millpress, Rotterdam, 325-330, 2005.

Paatero, P., and Tapper, U.: Positive matrix factorization: A non-negative factor model with optimal utilization of error estimates of data values, Environmetrics, 5, 111-126, 1994.

Paatero, P.: Least squares formulation of robust non-negative factor analysis, Chemometr. Intell. Lab., 37, 23-35, 1997.

Paatero, P., and Hopke, P. K.: Discarding or downweighting high-noise variables in factor analytic models, Analytica Chimica Acta, 490, 277-289, 10.1016/s0003-2670(02)01643-4, 2003.

Paatero, P., and Hopke, P. K.: Rotational tools for factor analytic models, J. Chemometr., 23, 91-100, 10.1002/cem.1197, 2009.

Parrish, D. D., Holloway, J. S., and Fehsenfeld, F. C.: Routine, continuous measurement of carbon-monoxide with parts-per-billion precision, Environmental Science & Technology, 28, 1615-1618, 1994.

Parrish, D. D., Allen, D. T., Bates, T. S., Estes, M., Fehsenfeld, F. C., Feingold, G., Ferrare, R., Hardesty, R. M., Meagher, J. F., Nielsen-Gammon, J. W., Pierce, R. B., Ryerson, T. B., Seinfeld, J. H., and Williams, E. J.: Overview of the second texas air quality study (texaqs ii) and the gulf of mexico atmospheric composition and climate study (gomaccs), J. Geophys. Res.-Atmos., 114, 28, D00f1310.1029/2009jd011842, 2009.

Prazeller, P., Palmer, P. T., Boscaini, E., Jobson, T., and Alexander, M.: Proton transfer reaction ion trap mass spectrometer, Rapid Commun. Mass Spectrom., 17, 1593-1599, 10.1002/rcm.1088, 2003.

Reff, A., Eberly, S. I., and Bhave, P. V.: Receptor modeling of ambient particulate matter data using positive matrix factorization: Review of existing methods, Journal Of the Air & Waste Management Association, 57, 146-154, 2007.

Reimann, S., and Lewis, A. C.: Anthropogenic vocs, in: Volatile organic compounds in the atmosphere, 1st ed., edited by: Koppman, R., Blackwell Publishing Ltd., Oxford, UK, 2007.

Rogers, T., Grimsrud, E., Herndon, S. C., Jayne, J., Kolb, C. E., Allwine, E., Westberg, H., Lamb, B. K., Zavala, M., and Molina, L. T.: On-road measurements of volatile organic compounds in the mexico city metropolitan area using proton transfer reaction mass spectrometry, International Journal of Mass Spectrometry, 252, 26-37, 10.1016/j.ijms.2006.01.027, 2006.

Ryerson, T. B., Trainer, M., Angevine, W. M., Brock, C. A., Dissly, R. W., Fehsenfeld, F. C., Frost, G. J., Goldan, P. D., Holloway, J. S., Hubler, G., Jakoubek, R. O., Kuster, W. C., Neuman, J. A., Nicks, D. K., Parrish, D. D., Roberts, J. M., and Sueper, D. T.: Effect of petrochemical industrial emissions of reactive alkenes and nox on tropospheric ozone formation in houston, texas, J. Geophys. Res.-Atmos., 108, 424910.1029/2002jd003070, 2003.

Shaw, W. J., Pekour, M. S., Coulter, R. L., Martin, T. J., and Walters, J. T.: The daytime mixing layer observed by radiosonde, profiler, and lidar during milagro, Atmos. Chem. Phys. Discuss., 7, 15025-15065, 2007.

Shindell, D. T., Faluvegi, G., Koch, D. M., Schmidt, G. A., Unger, N., and Bauer, S. E.: Improved attribution of climate forcing to emissions, Science, 326, 716-718, 10.1126/science.1174760, 2009.

Slowik, J. G., Vlasenko, A., McGuire, M., Evans, G. J., and Abbatt, J. P. D.: Simultaneous factor analysis of organic particle and gas mass spectra: Ams and ptr-ms measurements at an urban site, Atmospheric Chemistry And Physics, 10, 1969-1988, 2010.

Solomon, S., Qin, D., Manning, M., Alley, R. B., Berntsen, T., Bindoff, N. L., Chen, Z., Chidthaisong, A., Gregory, J. M., Hegerl, G. C., Heimann, M., Hewitson, B., Hoskins, B. J., Joos, F., Jouzel, J., Kattsov, V., Lohmann, U., Matsuno, T., Molina, M., Nicholls, N., Overpeck, J., Raga, G., Ramaswamy, V., M. Rusticucci, J. R., Somerville, R., Stocker, T. F., Whetton, P., Wood, R. A., and Wratt, D.: Technical summary, in: Climate change 2007: The physical science basis. Contribution of working group i to the fourth assessment report of the intergovernmental panel on climate change, edited by: Solomon, S., Qin, D., Manning, M., Chen, Z., Marquis, M., Averyt, K. B., Tignor, M., and Miller, H. L., Cambridge University Press, Cambridge, United Kingdom and New York, NY, USA., 2007.

Song, Y., Shao, M., Liu, Y., Lu, S. H., Kuster, W., Goldan, P., and Xie, S. D.: Source apportionment of ambient volatile organic compounds in beijing, Environ. Sci. Technol., 41, 4348-4353, 2007.

Spaulding, R. S., Schade, G. W., Goldstein, A. H., and Charles, M. J.: Characterization of secondary atmospheric photooxidation products: Evidence for biogenic and anthropogenic sources, J. Geophys. Res., 108, 4247, 10.1029/2002jd002478, 2003.

St Clair, J. M., McCabe, D. C., Crounse, J. D., Steiner, U., and Wennberg, P. O.: Chemical ionization tandem mass spectrometer for the in situ measurement of methyl hydrogen peroxide, Rev. Sci. Instrum., 81, 6, 09410210.1063/1.3480552, 2010.

Steeghs, M. M. L., Crespo, E., and Harren, F. J. M.: Collision induced dissociation study of 10 monoterpenes for identification in trace gas measurements using the newly developed proton-transfer reaction ion trap mass spectrometer, Int. J. Mass Spectrom., 263, 204-212, 10.1016/j.ijms.2007.02.011, 2007.

Steiner, A., and Goldstein, A.: Biogenic vocs, in: Volatile organic compounds in the atmosphere, 1st ed., edited by: Koppman, R., Blackwell Publishing Ltd., Oxford, UK, 82-128, 2007.

Takegawa, N., Kondo, Y., Koike, M., Chen, G., Machida, T., Watai, T., Blake, D. R., Streets, D. G., Woo, J. H., Carmichael, G. R., Kita, K., Miyazaki, Y., Shirai, T., Liley, J. B., and Ogawa, T.: Removal of nox and noy in asian outflow plumes: Aircraft measurements over the western pacific in january 2002, J. Geophys. Res.-Atmos., 109, 16, doi:D23s0410.1029/2004jd004866, 2004.

Thornberry, T., Murphy, D. M., Thomson, D. S., de Gouw, J., Warneke, C., Bates, T. S., Quinn, P. K., and Coffman, D.: Measurement of aerosol organic compounds using a novel collection/thermal-desorption ptr-itms instrument, Aerosol Sci. Technol., 43, 486-501, 10.1080/02786820902763132, 2009.

Tucker, S. C., Banta, R. M., Langford, A. O., Senff, C. J., Brewer, W. A., Williams, E. J., Lerner, B. M., Osthoff, H. D., and Hardesty, R. M.: Relationships of coastal nocturnal boundary layer winds and turbulence to houston ozone concentrations during texaqs 2006, J. Geophys. Res.-Atmos., 115, 17, D1030410.1029/2009jd013169, 2010.

Ulbrich, I. M., Canagaratna, M. R., Zhang, Q., Worsnop, D. R., and Jimenez, J. L.: Interpretation of organic components from positive matrix factorization of aerosol mass spectrometric data, Atmospheric Chemistry And Physics, 9, 2891-2918, 2009.

van Zelm, R., Huijbregts, M. A. J., den Hollander, H. A., van Jaarsveld, H. A., Sauter, F. J., Struijs, J., van Wijnen, H. J., and van de Meent, D.: European characterization

factors for human health damage of pm10 and ozone in life cycle impact assessment, Atmospheric Environment, 42, 441-453, 2008.

Vay, S. A., Tyler, S. C., Choi, Y., Blake, D. R., Blake, N. J., Sachse, G. W., Diskin, G. S., and Singh, H. B.: Sources and transport of δ14c in co2 within the mexico city basin and vicinity, Atmospheric Chemistry And Physics, 9, 4973-4985, 10.5194/acp-9-4973-2009, 2009.

Vega, E., Mugica, V., Carmona, R., and Valencia, E.: Hydrocarbon source apportionment in mexico city using the chemical mass balance receptor model, Atmospheric Environment, 34, 4121-4129, 2000.

Velasco, E., Lamb, B., Westberg, H., Allwine, E., Sosa, G., Arriaga-Colina, J. L., Jobson, B. T., Alexander, M. L., Prazeller, P., Knighton, W. B., Rogers, T. M., Grutter, M., Herndon, S. C., Kolb, C. E., Zavala, M., de Foy, B., Volkamer, R., Molina, L. T., and Molina, M. J.: Distribution, magnitudes, reactivities, ratios and diurnal patterns of volatile organic compounds in the valley of mexico during the mcma 2002 & 2003 field campaigns, Atmospheric Chemistry and Physics, 7, 329-353, 2007.

Veres, P., Roberts, J. M., Warneke, C., Welsh-Bon, D., Zahniser, M., Herndon, S., Fall, R., and de Gouw, J.: Development of negative-ion proton-transfer chemical-ionization mass spectrometry (ni-pt-cims) for the measurement of gas-phase organic acids in the atmosphere, Int. J. Mass Spectrom., 274, 48-55, 2008.

Volkamer, R., Jimenez, J. L., San Martini, F., Dzepina, K., Zhang, Q., Salcedo, D., Molina, L. T., Worsnop, D. R., and Molina, M. J.: Secondary organic aerosol formation from anthropogenic air pollution: Rapid and higher than expected, Geophysical Research Letters, 33, 4, 10.1029/2006GL026899, 2006.

Warneke, C., van der Veen, C., Luxembourg, S., de Gouw, J. A., and Kok, A.: Measurements of benzene and toluene in ambient air using proton-transfer-reaction mass spectrometry: Calibration, humidity dependence, and field intercomparison, Int. J. Mass Spectrom., 207, 167-182, 2001.

Warneke, C., de Gouw, J. A., Kuster, W. C., Goldan, P. D., and Fall, R.: Validation of atmospheric voc measurements by proton-transfer-reaction mass spectrometry using a gas-chromatographic preseparation method, Environ. Sci. Technol., 37, 2494-2501, 2003.

Warneke, C., de Gouw, J. A., Lovejoy, E. R., Murphy, P. C., Kuster, W. C., and Fall, R.: Development of proton-transfer ion trap-mass spectrometry: On-line detection and identification of volatile organic compounds in air, J. Am. Soc. Mass Spectrom., 16, 1316-1324, 2005a.

Warneke, C., Kato, S., De Gouw, J. A., Goldan, P. D., Kuster, W. C., Shao, M., Lovejoy, E. R., Fall, R., and Fehsenfeld, F. C.: Online volatile organic compound

measurements using a newly developed proton-transfer ion trap mass spectrometry instrument during new england air quality study - intercontinental transport and chemical transformation 2004: Performance, intercomparison, and compound identification, Environmental Science & Technology, 39, 5390-5397, 2005b.

Warneke, C., Mckeen, S. A., de Gouw, J. A., Goldan, P. D., Kuster, W. C., Holloway, J. S., Williams, E. J., Lerner, B. M., Parrish, D. D., Trainer, M., Fehsenfeld, F. C., Kato, S., Atlas, E. L., Baker, A. K., and Blake, D. R.: Determination of urban volatile organic compound emission ratios and comparison with an emissions database, Journal of Geophysical Research, 112, 13, 10.1029/2006JD007930, 2007.

Warneke, C., Roberts, J. M., Veres, P., Gilman, J., Kuster, W. C., Burling, I., Yokelson, R., and de Gouw, J. A.: Voc identification and inter-comparison from laboratory biomass burning using ptr-ms and pit-ms, Int. J. Mass Spectrom., In Press, Corrected Proof, 2011.

Washenfelder, R. A., Trainer, M., Frost, G. J., Ryerson, T. B., Atlas, E. L., de Gouw, J. A., Flocke, F. M., Fried, A., Holloway, J. S., Parrish, D. D., Peischl, J., Richter, D., Schauffler, S. M., Walega, J. G., Warneke, C., Weibring, P., and Zheng, W.: Characterization of nox, so2, ethene, and propene from industrial emission sources in houston, texas, J. Geophys. Res.-Atmos., 115, 14, D1631110.1029/2009jd013645, 2010.

Wert, B. P., Trainer, M., Fried, A., Ryerson, T. B., Henry, B., Potter, W., Angevine, W. M., Atlas, E., Donnelly, S. G., Fehsenfeld, F. C., Frost, G. J., Goldan, P. D., Hansel, A., Holloway, J. S., Hubler, G., Kuster, W. C., Nicks, D. K., Neuman, J. A., Parrish, D. D., Schauffler, S., Stutz, J., Sueper, D. T., Wiedinmyer, C., and Wisthaler, A.: Signatures of terminal alkene oxidation in airborne formaldehyde measurements during texaqs 2000, J. Geophys. Res.-Atmos., 108, 14, 410410.1029/2002jd002502, 2003.

White, W. H., Anderson, J. A., Blumenthal, D. L., Husar, R. B., Gillani, N. V., Husar, J. D., and Wilson, W. E.: Formation and transport of secondary air-pollutants: Ozone and aeosols in the st. Louis urban plume, Science, 194, 187-189, 1976.

Williams, J., and Koppmann, R.: Volatile organic compounds in the atmosphere: An overview, in: Volatile organic compounds in the atmosphere, 1st ed., edited by: Koppman, R., Blackwell Publishing Ltd., Oxford, UK, 1-32, 2007.

Xie, Y. L., and Berkowitz, C. M.: The use of positive matrix factorization with conditional probability functions in air quality studies: An application to hydrocarbon emissions in houston, texas, Atmospheric Environment, 40, 3070-3091, 10.1016/j.atmosenv.2005.12.065, 2006.

Yokelson, R. J., Christian, T. J., Karl, T. G., and Guenther, A.: The tropical forest and fire emissions experiment: Laboratory fire measurements and synthesis of campaign data, Atmospheric Chemistry And Physics, 8, 3509-3527, 2008.

Zhao, W. X., Hopke, P. K., and Karl, T.: Source identification of volatile organic compounds in houston, texas, Environmental Science & Technology, 38, 1338-1347, 10.1021/es034999c, 2004.